1 Table of Contents

1 ANIMALS

All animal handling and surgical procedures were reviewed and approved by the University of Texas at El Paso Institutional Animal Care and Use Committee (IACUC; protocol # 24-10-043), Intramural Research Program (IRP)-NIDA IACUC (#23-BNRB-204) and Icahn School of Medicine at Mount Sinai (#IPROTO202600000015). Both Long-Evans rats and transgenic CRISPR-based Oprm1-Cre knock-in rats were used across experiments (see **Fig. 3A** for validation)[1].

Rats were maintained on a 12:12 h light/dark cycle unless otherwise noted. Breeding rats were housed on a standard light cycle, while rats used for behavioral experiments were maintained on a reversed light cycle. Rats were housed either individually or in pairs depending on experimental requirements. Experiments were conducted across five distinct animal colonies. First, Long-Evans rats (purchased from Envigo at 4 weeks of age) were used for behavioral characterization and IBU manipulation studies, as well as for histological dilution experiments (**Fig. 1-2**). Second, an initial colony of 24 Oprm1-Cre rats (Cre: n=11; WT: n=13) was obtained from the breeding program of IRP-NIDA at 3–5 months of age. These rats were used for a subset of excitatory DREADD experiments. Third, this initial cohort was used to establish a breeding colony at UTEP. Offspring derived from this colony were used for most of the subsequent experiments, including all inhibitory DREADD manipulations and in vivo calcium imaging experiments using the Inscopix system (**Fig. 3-4**). Finally, Tyrosine Hydroxylase (TH)-Cre (breeding program of IRP-NIDA) rats were used for rabies-based circuit tracing experiments performed in parallel studies at NIDA (**fig. S9**).

1.1 Breeding

From the 24 Oprm1-Cre rats received from NIDA, six breeding pairs were established. Pairings were arranged to maximize genetic heterogeneity and avoid inbreeding; no half-sibling pairings were permitted. Each breeding pair consisted of one Wild-type (WT) and one heterozygous Oprm1-Cre parent. Pairs were housed together for two weeks in a dedicated breeding room maintained on a 12:12 hour light/dark cycle and were monitored daily for signs of aggression or pregnancy. If aggression was observed, pairs were separated immediately. After the two-week pairing period, all rats were single-housed. Once pups were born, they underwent daily monitoring. At three weeks of age, pups were weaned and moved to the experimental holding room. During weaning rats were genotyped by hole-punching either the left or right ear (done in a manner to distinguish double-housed cage mates from each other) and samples were sent to Transnetyx for genotyping for the *Oprm1-iCre* gene. Rats were habituated shortly after weaning to minimize stress and fear.

1.2 Rigor and reproducibility

All in vivo experiments were designed, conducted, analyzed, and reported in accordance with the ARRIVE 2.0 (Animal Research: Reporting of In Vivo Experiments) guidelines. To maximize rigor and reproducibility, key findings were independently replicated using complementary experimental approaches, independent animal cohorts, technical replicates, and separate experimenters.

Behavioral findings were reproduced across two independent rat strains (Long–Evans and Oprm1-WT) to ensure that observed effects reflected GHSR activation rather than strain-specific characteristics. Behavioral outcomes were compared between strains and showed no significant strain-dependent differences. Animals were randomly assigned to treatment groups while

maintaining balanced representation of males and females. Behavioral experiments were conducted under blinded conditions whenever possible. One team (A.Y.M. and S.A.B.) prepared and administered injections, whereas a separate team (C.N.H., A.C.M.-D., C.N.O., and M.M.) performed behavioral testing without knowledge of treatment assignment. Automated tracking software quantified animal position and entries within behavioral zones. Feeding experiments were independently replicated by two separate research teams using independent animal cohorts and both rat strains. One set of experiments was performed by A.A.S. and N.F.R., whereas an independent replication was performed by A.Y.M., S.A.B., C.N.H., A.C.M.-D., C.N.O., and M.M., yielding consistent behavioral outcomes across investigators and cohorts.

Histological findings were independently reproduced by two laboratories. Initial experiments were performed at UTEP (A.A.S. and N.F.R.), and the main finding that GHSR activation selectively increased striosomal cFos expression was independently replicated at NIDA (K.N. and H.-L. W.) using a separate animal cohort and an independent rat strain, providing biological replication across laboratories. Within UTEP, each immunohistochemical experiment was repeated in at least three independent staining runs, and quantitative analyses were performed only after confirming consistent labeling across technical replicates. Control and treatment groups were processed in parallel under identical conditions. Image quantification was performed using standardized automated image-processing pipelines with predefined thresholding and segmentation parameters applied uniformly across all samples, minimizing experimenter bias.

The histological observation of GHSR-mediated striosomal activation was further validated using an orthogonal experimental approach through in vivo calcium imaging, demonstrating that the same neuronal population exhibited dose-dependent functional activation in awake behaving animals.

Motor behavioral analyses were independently performed by two investigators (D.W.B. and A.G.), producing consistent results across analyses. Whenever feasible for in vivo experiments, treatment administration and experimental testing were performed by different investigators to maintain blinding throughout data collection.

Finally, experimental findings were validated through computational modeling. D.W.B. developed a mathematical model based on the experimentally measured biological data, which confirmed the observed dose-dependent effects of GHSR activation on striosomal circuit activity and conflict-based decision-making.

Finally, but importantly, the study benefited from integrating the expertise of senior authors across disciplines. I.R.W is an expert in virology, Y.S. and T.M.M. are experts in behavioral neuroscience and neurobiology; K.A.G. expert in endocrinology and circuit physiology, and A.F. is an expert in striosomal circuit physiology, behavioral, and computational neuroscience.

Together, these practices, including randomization, blinding, independent biological and technical replication, orthogonal validation, automated quantitative analyses, and predefined inclusion criteria, were incorporated throughout the study to maximize rigor and reproducibility.

2 SURGERY

2.1 Animal allocations for surgical procedures

All surgical procedures were performed in rats that had reached a minimum weight of 250-300 g and were at least 8 weeks of age at the time of surgery. Oprm1-Cre rats were used for both chemogenetic manipulation and calcium imaging experiments. For DREADD-based studies, rats were assigned to either an inhibitory or an excitatory group, and all underwent stereotaxic intracranial viral injections as described below. In addition, a separate cohort of Oprm1-Cre rats received a Cre-dependent calcium indicator (pGP-AAV-syn-FLEX-GCaMP7f-WPRE) followed by GRIN lens implantation for in vivo calcium imaging. Wild-type litter mates served as surgical controls and underwent the same stereotaxic procedures as experimental rats, including intracranial viral delivery, to control for surgical and viral exposure. Behavioral and imaging results are presented in **Fig. 3-4** and **fig. S5-8**, **S13**.

2.2 Surgical procedure

All Oprm1-Cre rats described above underwent stereotaxic surgery for intracranial viral delivery and, in a subset of rats, miniscope implantation. These rats received Cre-dependent viral constructs, including the calcium indicator pGP-AAV-syn-FLEX-GCaMP7f-WPRE for imaging experiments and chemogenetic vectors encoding excitatory (hM3Dq) or inhibitory (hM4Di) DREADD for functional manipulation. Viral expression and striosomal specificity were validated using immunohistochemistry (IHC) see section 5.4.5. Stereotaxic coordinates for each procedure are described in detail below. All reagents used are listed in detail in table S2.

2.2.1 ANESTHESIA AND ANALGESIA

All surgical procedures were performed under isoflurane anesthesia (induction at 3%, maintenance initially at 2%, oxygen flow rate 2–2.5 L/min). Due to increased sensitivity to isoflurane in this Oprm1-Cre strain, rats were continuously monitored throughout the procedure for respiratory rate and depth. To stabilize anesthesia and reduce isoflurane requirements, rats received an intramuscular injection of ketamine (0.1 mL) prior to the start of surgery, after which isoflurane levels were reduced to ~1% for the remainder of the procedure. For surgeries exceeding 2 hours, an additional ketamine dose (0.1 mL, IM) was administered in the contralateral hindlimb.

At the start of surgery, rats received a bupivacaine injection (0.1ml subcutaneous, SQ) near incision site and a second SQ injection near abdomen of 5 mL Ringer's solution containing a half-dose of meloxicam (0.5 mg/kg). Body temperature was continuously monitored and maintained at ~37 °C using a heating pad. A reversal agent (atipamezole; Revertidine) was kept readily available throughout all procedures. In the event of respiratory suppression, rats were immediately removed from isoflurane and administered atipamezole (0.1 mL, IM), resulting in rapid recovery of respiration and stabilization prior to resuming monitoring.

For post-operative care, rats received meloxicam (1 mg/kg, SQ) and enrofloxacin (5 mg/kg, SQ) once daily for 3 days, including the day of surgery. These were administered in Ringer's solution, with additional subcutaneous fluids provided as needed to support recovery. Rats were monitored continuously during recovery until the return of the righting reflex and were assessed daily thereafter to ensure proper healing.

2.2.2 STEREOTAXIC PREPARATION AND SURGICAL SETUP

Following induction of anesthesia, rats were shaved and positioned in a stereotaxic frame (Kopf Instruments, Model 942) and secured using ear bars. The surgical site was sterilized using alternating applications of alcohol and iodine (3x). Ophthalmic ointment (Puralube; MWI, cat#027505) was applied to both eyes to prevent corneal drying during the procedure.

Once fully secured and prepared, a midline anterior–posterior incision was made along the scalp to expose the skull. The overlying connective tissue was carefully removed, and the skull surface was cleaned using sterile saline or hydrogen peroxide to improve visualization. Rats were positioned in a flat skull configuration by aligning bregma and lambda along both anterior-posterior and medial-lateral axes, and all stereotaxic coordinates were determined relative to bregma.

2.3 DREADD virus injections

Oprm1-Cre rats described above underwent stereotaxic DREADD viral injections for causal manipulation of striosomal activity (**Fig. 4**, **fig. S6-8, S13**). For inhibitory manipulations, Oprm1-Cre rats and Wild-type rats received a Cre-dependent inhibitory DREADD virus (pAAV-hSyn-DIO-HA-hM4D(Gi)-IRES-mCitrine; Addgene #50455), prepared at an initial titer of 1×10^{13} vg/mL and diluted 1:1 in sterile saline prior to injection. For excitatory manipulations, a separate cohort of Oprm1-Cre rats and Wild-type received a Cre-dependent excitatory DREADD virus (AAV8-hSyn-DIO-hM3D(Gq)-mCherry; Addgene #44361), prepared at an initial titer of 4×10^{12} vg/mL and similarly diluted 1:1 in sterile saline.

Following stereotaxic preparation described in section 2.2.1 bilateral viral injections were performed targeting the anterior dorsal striatum (AP +1.28 mm, ML ±1.8 mm, DV −3.7 mm relative to Bregma). Small craniotomies were made at the designated coordinates, and the dura mater was carefully removed to allow for viral delivery. Cre-dependent DREADD viral constructs encoding either excitatory (hM3Dq) or inhibitory (hM4Di) receptors were delivered bilaterally using a microsyringe. For each hemisphere, the injection needle was first lowered slightly beyond the target depth (DV −3.8 mm) and then raised to verify no obstruction by expelling a small volume of virus (“bubble check”) to ensure the needle was not clogged. The needle was then reinserted and positioned at the final injection depth (DV −3.7 mm), and 1 µL of virus was infused at a rate of 0.1 µL/min. Following infusion, the needle was left in place for 10 min to allow for viral diffusion and to minimize backflow, after which it was slowly withdrawn. The same procedure was repeated for the contralateral hemisphere.

Following completion of viral injections, craniotomy sites were sealed using silicone elastomer (Kwik-Sil™, World Precision Instruments). The incision was closed using 5-0 sutures. Rats received SQ administration of Ringer’s solution (10 mL) containing meloxicam (1 mg/kg) and enrofloxacin (5 mg/kg) to support recovery.

Rats were maintained on a heating pad and closely monitored until the return of the righting reflex. Recovery times were modestly prolonged due to ketamine administration. Rats were monitored daily for 5 days following surgery to ensure proper healing and recovery. A minimum of 4 weeks was allowed for viral expression prior to the start of behavioral experiments, as described in section 4. All rats underwent perfusion and IHC to verify injection, as described in section 5.

2.4 Surgery for GCaMP injection and in-vivo calcium imaging

2.4.1 GCaMP VIRUS INJECTION

A subset of the Oprm1-Cre rats underwent a modified surgical procedure for in vivo calcium imaging. These rats received bilateral injections of a Cre-dependent calcium indicator virus (pGP-AAV-syn-FLEX-GCaMP7f-WPRE-GCaMP7f; Addgene #104492) targeting the anterior dorsal striatum. The virus was prepared at an initial titer of 1×10^{13} vg/mL and diluted 1:8 in sterile saline prior to injection. An initial concertation curve was performed to identify ideal concentration, as described in section 6.1.

Prior to performing any craniotomies, the skull surface was lightly scored in a cross-hatch pattern to improve adhesion, and 5–6 flat-top stainless steel screws were inserted epidurally to provide structural support for headcap fixation. Following this, bilateral viral delivery was performed targeting the anterior dorsal striatum (AP +1.5 mm, ML ±2.0 mm, DV −3.6 mm relative to bregma) using a microsyringe. For each hemisphere, the injection needle was first lowered slightly beyond the target depth (DV −3.7 mm) and then raised to verify no needle obstruction by expelling a small volume of virus ("bubble check") to ensure the needle was not clogged. The needle was then reinserted and positioned at the final injection depth (DV −3.6 mm), and 1 µL of virus was infused at a rate of 0.1 µL/min. Following infusion, the needle was left in place for 10 min to allow for viral diffusion and to minimize backflow, after which it was slowly withdrawn. The same procedure was repeated for the contralateral hemisphere.

2.4.2 GRIN LENS IMPLANTATION

Following bilateral viral injections, a larger craniotomy was expanded over the right injection site to accommodate GRIN lens implantation. Dura mater was carefully removed under a surgical microscope. Exposed tissue was kept moist using sterile saline to maintain visibility. A sterile flat 18-gauge needle was used to create a tract for lens placement. The needle was slowly lowered through the cortex until reaching striatum, identified by gray matter.

The GRIN lens (Inscopix, ProView Integrated Lens, 1.0 mm x 9.0 mm; cat#1050-00416) was sterilized, mounted on a custom holder, and positioned over the craniotomy. The lens was slowly lowered to a final depth approximately 100 µm dorsal to the viral injection site (DV −3.5 mm relative to dura) at a controlled rate (~1 mm per 5 min). Once in position, the craniotomy was sealed using silicone elastomer (Kwik-Sil™, World Precision Instruments) to stabilize the implant. The GRIN lens and skull screws were then secured using dental cement (Metabond). An initial thin layer of liquid Metabond quick base (Patterson Dental, #NC1013606) was applied across the skull surface to promote adhesion, followed by additional layers mixed with Metabond tooth powder (Patterson Dental, #NC0877382) to build a stable headcap around the lens base and screws. Care was taken to avoid covering functional components of the implant during headcap construction, and the cement was allowed to fully cure. Excess skin surrounding the implant was trimmed as needed, and the remaining incision margins were closed using 5-0 sutures. The surgical site was treated with topical antibiotic ointment prior to recovery.

Rats received the same post-operative care described in the anesthesia and analgesia section 2.2.1 and were allowed to recover for 5 days prior to further handling. After recovery, rats were monitored regularly, and imaging sessions were initiated approximately 4 weeks post-surgery to allow for sufficient viral expression. Imaging was performed every few days until stable calcium activity was observed. Rats were approximately 7 weeks post-surgery at the start of IBU imaging experiments, described in section 4.5.4.

3 PRE-EXPERIMENTAL PROCEDURES

3.1 Reagents and preparation

3.1.1 IBUTAMOREN MESYLATE PREPARATION AND STORAGE

Ibutamoren mesylate (IBU; MedChemExpress, HY-50844 table S2), a growth hormone secretagogue receptor (GHSR; ghrelin receptor) agonist with a prolonged half-life relative to endogenous ghrelin, was used to enable sustained modulation of ghrelin signaling during behavioral experiments. Stock powder was stored at −80 °C until use.

For experiments, IBU was reconstituted in sterile saline to generate working solutions ranging from 0.5 to 10 mg/mL, where solution concentration (mg/mL) matched the intended dose (mg/kg). For clarity, concentrations were expressed using an “x” notation, where 1x corresponds to 1 mg/mL (1 mg/kg) and 10x corresponds to 10 mg/mL (10 mg/kg).

This approach allowed injection volume (mL) to scale directly with body weight (kg) (i.e., 1 mL/kg). For example, a 300 g rat received 0.3 mL, whereas an 800 g rat received 0.8 mL. Behavioral experiments primarily utilized 2x (2 mg/mL; 2 mg/kg) and 10x (10 mg/mL; 10 mg/kg) conditions, while histological analyses incorporated the full range of concentrations.

Fresh working solutions were maintained at 4 °C during the day of use and kept cold throughout experimental procedures. For longer-term storage, reconstituted aliquots were stored at −20 °C for up to one month.

3.1.2 CLOZAPINE-N-OXIDE

Clozapine-N-oxide (CNO) (Medchem HY-17366, table S2) powder was stored at −20 °C. For preparation, 75 mg of CNO was first dissolved in 2.5 mL of 100% dimethyl sulfoxide (DMSO) (Sigma D8418) and then diluted in 22.5 mL of sterile saline. The solution was vortexed until fully mixed, protected from light, and used within 5 days of preparation. For DREADD experiments, CNO (3 mg/kg) was administered to activate Cre-dependent viral constructs in Oprm1-Cre rats and was also administered to Wild-type rats to control for nonspecific effects. Solution was stored at room temperature for up to 5 days, covered in foil.

3.1.3 HUMAN ACYL-GHRELIN

To compare the effects of IBU with endogenous ghrelin signaling, acyl-ghrelin (Bachem, H-6795, table S2) was used. Acyl-ghrelin powder was stored at −80 °C for long-term storage. For experimental use, the peptide was reconstituted in 1 mL of Milli-Q water, aliquoted, and stored at −80 °C. A fresh aliquot was thawed and used for each testing day to maintain peptide stability.

Acyl-ghrelin was administered via intraperitoneal (IP) injection at doses ranging from 4.3 to 125 ug/kg, with injection volumes adjusted based on body weight. These doses were selected to enable comparison with the longer-acting GHSR agonist IBU across a range of physiologically relevant concentrations.

3.2 Drug administration

Injections were performed using sterile 1 mL syringes fitted with 26G needles. Drug volumes were adjusted based on body weight, and rats were weighed at least once per week to ensure accurate

dosing. Behavioral experiments were carried out 2 hours after IBU and/or CNO administration, and 15 mins post acyl-ghrelin injection. Perfusions for IHC were conducted 3.5 hours post IBU injections.

3.3 **Animal acclimation to experimental setting**

Before behavioral and in-vivo calcium imaging experiments, rats were transferred from the holding room to the experimental room using transport carts. Upon arrival, rats remained in their home cages for 3 minutes to acclimate to the environment. For behavioral experiments described in section 4, rats were placed into one of four behavioral arenas and allowed to acclimate for an additional 5 minutes prior to the start of the experiment. All behavioral trials were conducted in darkness.

4 DECISION MAKING TASK BATTERY

4.1 Experimental task set up

For all behavioral experiments, animals were randomly assigned to treatment groups before testing, with group allocations balanced to include comparable numbers of males and females when possible. Behavioral testing was performed under blinded conditions. On each day of testing, one team handled animals and administered injections, while a separate team ran behavioral tasks, without knowledge of the treatment condition. In addition, animal tracking and scoring of entries into reward zones were performed using automated tracking software. Lastly, on each day of testing, half of the animal received saline while the other half received treatment, and conditions were reversed after a 2-day washout period. This design ensured that saline and treatment groups were both tested on each experimental day, controlling for day-to-day variability in behavioral performance.

4.1.1 ANIMAL TRACKING

Rats were run on behavior tasks in an open field arena. Behavior within the arena was captured using a Basler GenICam (Basler acA1300-60, table S2) mounted above the maze that recorded at a resolution of 720x576 at 25 frames per second and Noldus EthoVision XT 16 software; used to track movements/spatial location of the rats during task performance. To minimize distractions from external stimuli and contain the rats, the arenas are surrounded by walls made from polyvinyl chloride sheets (75cm x 64.5cm x 0.32cm). The maze floor was 3D printed with four different floor patterns (Radial, Horizontal, Grid, and Diagonal) as described in our previous publication [2]. Depending on task conditions, the available stimulus/stimuli were either placed in a corner or in the center of the arena. A region of interest (ROI) was created around the stimulus or stimuli for determining whether the rat interacted with/showed interest in the available factors across conditions. ROIs were set using the arena settings within the Noldus EthoVision XT version 16.0 tracking software. For tasks which had a stimulus in the center of the arena, the ROI was set as a 4x4 square (each side measuring approximately 15.5cm), when the stimulus was placed in the corner, the ROI was defined by a curved section with a diameter of 15cm. The tracking software recorded animal entries into this region, and the data output (frequency of entries to the defined ROI) was analyzed to assess behavior.

4.1.2 DECISION MAKING TASK BATTERY SET UP

Rats were habituated to an empty, unlit arena and to the experimenters for two weeks prior to task execution. Depending on the experimental condition, the stimulus or stimuli were then added to the maze. Rats were placed in the center of the arena, and their nose, center, and tail points

were identified using Noldus EthovisionXT tracking software. Each trial lasted 20 minutes, during which rats were allowed to freely move. Stimuli (see sections 4.2-4.3 below) were secured to the maze with zip ties at the predetermined region of interest (ROI). Two types of flooring were used, depending on the rat strain. Long Evans rats were tested on a 3D-printed floor with four different patterns that were spray-painted green using Rust-Oleum Gloss Neon Green lacquer paint to improve detection. In contrast, Oprm1-Cre rats were tested on alternative flooring of similar texture but darker in color, which provided better contrast for tracking. For tasks involving light, a lamp was clamped to a corner of the arena and encased in aluminum foil to focus on the defined region of interest (ROI). Light intensity in this ROI was measured at 500 lux (2335 lumens) using an Amprobe Light Meter for all light-based tasks. For food-based tasks, all rats regardless of strain were exposed to the food in their home cage for at least three days prior to testing. All toy-based tasks were designed to assess responses to novelty. Therefore, rats were not pre-exposed to the object. The object was a rodent stick chew toy purchased at PetSmart.

4.2 Non-conflict decision making tasks procedures

To determine the effects of IBU on decision-making processes, non-conflict tasks were designed to independently assess exploratory behavior, food-directed motivation, novelty-seeking, and avoidance behavior in the absence of competing stimuli or behavioral conflict.

4.2.1 FOOD ALONE TASK

A slice of apple, an appetitive food reward, was zip-tied to the center of the maze with no additional stimuli present. Apples were weighed before and after each session, and a fresh slice was used at the start of each new session. This task was performed across multiple experiments to assess the effects of IBU on approach and consumption behaviors.

SAL v 2x IBU: Data are available at https://doi.org/10.7910/DVN/DCB1IH.
SAL v 10x IBU: Data are available at https://doi.org/10.7910/DVN/OE73LI
Striosomal manipulations: Data are available at https://doi.org/10.7910/DVN/NTB2PG.

4.2.2 TOY ALONE TASK

A novel toy was zip-tied to a corner of the maze with no additional stimuli present. This task was performed across multiple experiments to assess the effects of IBU on approach and exploratory behaviors in the context of novelty.

SAL v 2x IBU: Data are available at https://doi.org/10.7910/DVN/YMYXO0.
SAL v 10x IBU: Data are available at https://doi.org/10.7910/DVN/OE73LI.
Striosomal manipulations: Data are available at https://doi.org/10.7910/DVN/NTB2PG

4.2.3 LIGHT ALONE TASK

A corner of the maze was illuminated by a lamp held in place with a clamp on the wall of the maze. Light was directed to the region of interest (ROI) using aluminum foil as a cost, and no additional stimuli was present. This task was performed across multiple experiments to assess the effects of IBU on cost-avoidance behaviors.

SAL v 2x IBU: Data are available at https://doi.org/10.7910/DVN/JW2C3Q.
SAL v 10x IBU: Data are available at https://doi.org/10.7910/DVN/OE73LI.
Striosomal manipulations: Data are available at https://doi.org/10.7910/DVN/NTB2PG.

4.2.4 MAZE ALONE TASK

To establish a baseline measure of approach behavior in the absence of external stimuli, rats were allowed to freely explore an unlit open-field arena with no additional stimuli present during the Maze Alone task. A randomly selected corner of the arena was designated as the region of interest (ROI) for behavioral tracking. The purpose of this task was to quantify baseline approach rates toward a neutral location and compare them to approach rates observed when a single stimulus was present during the simple behavioral tasks (Food alone, Toy alone, and Light alone). Approach rates across tasks were compared using a one-way ANOVA (fig. S1A; SAL: rats = 9, 5 males and 4 females).

Data are available at https://doi.org/10.7910/DVN/OE73LI

4.3 Conflict DM task procedures

To evaluate the effects of IBU on conflict-based decision-making, conflict tasks were designed to determine whether IBU altered behavioral choice and approach behavior under conditions requiring motivational tradeoff between reward-seeking and avoidance of an aversive stimulus.

4.3.1 FOOD+LIGHT

To test the effect of IBU on food-cost tradeoff, an apple slice was zip-tied to the corner of the maze while simultaneously being illuminated by an aversive light (15 lux). Apples were weighed before and after each session, and a fresh slice was used at the start of each new session. The lamp was held in place by a clamp on the wall of the maze, and aluminum foil was used to direct the light toward the ROI.

SAL v 2x IBU: Data are available at https://doi.org/10.7910/DVN/0V6WKG.
SAL v 10x IBU: Data are available at https://doi.org/10.7910/DVN/OE73LI.
Striosomal manipulations: Data are available at https://doi.org/10.7910/DVN/NTB2PG.

4.3.2 TOY+LIGHT TASK

To test the effect of IBU on novelty-cost tradeoff, a novel toy was zip-tied to the corner of the maze, which was simultaneously illuminated by an aversive light (15 lux). The lamp was held in place by a clamp on the wall of the maze, and aluminum foil was used to direct the light toward the region of interest.

SAL v 2x IBU: Data are available at https://doi.org/10.7910/DVN/ZUH9YY.
SAL v 10x IBU: Data are available at https://doi.org/10.7910/DVN/OE73LI.
Striosomal manipulations: Data are available at https://doi.org/10.7910/DVN/NTB2PG.

4.4 Food consumption task

To confirm that IBU produced its expected effects, food consumption tasks were performed under both home cage and task-based conditions. These experiments were designed to specifically assess the effects of IBU on consummatory feeding behavior independent of exploratory behavior, novelty-seeking, or conflict-based decision-making processes.

4.4.1 FOOD CONSUMPTION TASK PROCEDURE

At the beginning of each session, the standard chow (Teklad Global Irradiated 18% protein rodent diet provided Laboratory Animal Resources Center) was removed from the home cage and replaced with 40 grams of pre-weighed chow. Food consumption was measured over a four-hour

period, with chow being re-weighed at hourly intervals. The difference between the initial chow weight and the chow remaining at each time point was recorded to determine cumulative intake across the session. This task was conducted under 2x IBU, 10x IBU, aGHR conditions, as described below.

IBU Food consumption in home cage: https://doi.org/10.7910/DVN/GFLZYM.
aGHR Food consumption in homecage: Data is available athttps://doi.org/10.7910/DVN/US8QTS
Food alone task: Data are available at https://doi.org/10.7910/DVN/GFLZYM
Food+light task: https://doi.org/10.7910/DVN/GFLZYM

4.5 Behavioral experimental designs

4.5.1 Exp. 1: Evaluate DM with 2x IBU manipulation

Frist, to determine whether administration of 2x IBU altered performance across five behavioral tasks, including both simple and conflict-based paradigms with varying levels of conflict, using the same rats across all tasks. The full behavioral battery was independently replicated in two cohorts: Long-Evans rats (LE: rats=11–16 per group) and Oprm1-WT rats (SAL: rats=14; 2x IBU: rats=14), with each experimental group containing equal numbers of males and females (**Fig. 1C-D**). A crossover design was used in which half of the cohort initially received 2x IBU and half received saline. Following a minimum 2-day washout period, rats were re-tested under the opposite condition. This design minimized inter-animal variability, enabled direct within-animal comparisons across treatment conditions, and ensured that both treatment and control conditions were represented on each testing day. For each behavioral task, raw non-normalized data were initially analyzed independently using paired t-tests comparing SAL and 2x IBU conditions (**fig. S1**). To enable comparisons across behavioral tasks with different measurement scales and ranges, data were subsequently normalized using min-max normalization prior to cross-task analyses (see 4.7 below; **Fig. 1C-D**).

Data are available at https://doi.org/10.7910/DVN/OE73LI.

4.5.2 Exp. 2: Evaluate DM with 10x IBU manipulation

In Exp. 1, we found that 2x IBU selectively altered performance during conflict-based tasks, with little effect on simple tasks. To determine whether a higher dose of IBU produced broader behavioral effects, a separate cohort of rats was tested under SAL (rats = 9; 5 males and 4 females) and 10x IBU conditions (rats = 10; 6 males and 4 females). Raw non-normalized behavioral data were analyzed using two-sample t-tests to assess group differences (**fig. S2**). And normalized data was used to compare across all tasks (**Fig. 1H**).

4.5.3 Exp. 3: Feeding consumption in home cage and conflict tasks

To determine changes in feeding behavior, food consumption experiments were conducted with rats undergoing 2x and 10x IBU in their home cage and in conflict-based tasks. For home cage feeding behavior, in the 2x IBU (**Fig. 1E**) and 10x IBU experiments (**fig. S2H;** SAL: rats=19; 2x IBU: rats=19; 10X IBU: rats=19), a paired t-test was used to assess differences in home cage food consumption between saline and 2x or 10x IBU rats. Values for the saline control group are the same as those shown in **Fig. 1E**. To compare feeding behavior across different aGHR concentrations, a one-way ANOVA was used to assess (**fig. S5F;** WT rats = 6-8) food

consumption under aGHR in home cage. Under 2x and 10x IBU conditions, a two-way ANOVA (**fig S5G;** WT-SAL rats=8-19) was used to compare feeding behavior across different IBU and aGHR doses.
Food consumption in home cage IBU: https://doi.org/10.7910/DVN/GFLZYM.
Food consumption in home cage IBU: Data is available at https://doi.org/10.7910/DVN/US8QTS

Food consumed during the light alone task was also measured where the weight (grams) of the apple was measured during the tasks and analyzed using unpaired t-tests in both 2x (**Fig. 1F**) and 10x (**fig. S2I**) IBU conditions (SAL: rats = 9-14; 2xIBU: rats = 14;10x IBU: rats= 10) Food consumed during the Food+ light task was also measured and analyzed using unpaired t-tests in both 2x (**Fig. 1G**) and 10x IBU (**fig. S2J**) experiments (SAL: rats = 9-14; 2x IBU: rats = 14; 10x IBU: rats = 10).

4.5.4 Exp. 4: DREADD Manipulations

Lastly, we examined whether striosomal manipulation altered decision-making performance across the five behavioral tasks. Oprm1-Cre rats used for behavioral testing were divided into four experimental groups: 1) CNO saline (CNO SAL; rats = 14), 2) WT 2x IBU (CNO IBU; rats = 14), 3) inhibitory hM4D(Gi) (Inh; rats = 15), and 4) excitatory hM3D(Gq) (Exc; rats = 7–13) groups (**Fig. 4B**). All rats, including Oprm1-WT littermates, underwent stereotaxic surgery for viral targeting of striosomal neurons as described in Section 2.3. During behavioral testing, all experimental groups received CNO to control for nonspecific effects, in combination with either saline or 2x IBU treatment depending on the experimental condition. Wild-type rats were analyzed using a between-subjects design, whereas inhibitory and excitatory rats were tested twice under both saline and 2x IBU conditions while receiving CNO during all sessions. Raw behavioral data for each task were initially analyzed independently using two-sample (unpaired) t-tests to compare performance across experimental conditions (**fig. S7B-C**). To allow comparisons across behavioral tasks with different measurement scales, behavioral data were subsequently normalized prior to cross-task analyses (**Fig. 4D-E**). Full statistical results are provided in the Statistical Depository.

Data are available at https://doi.org/10.7910/DVN/NTB2PG.

4.6 Data processing for behavioral tasks

The Noldus EthoVision software generated a 20-minute-long video (the duration of the task), along with raw data and statistics during the task. In the Export tab, both the raw data and statistics files were exported and saved to the appropriate folder on the computer. After saving the data, the Trial List in EthoVisionXT was reset in preparation for the next trial session. The statistics data included "Frequency" data, which represented the number of entries into the ROI, tracked by the system based on the rat's center point. This frequency data was then input into an Excel spreadsheet, where results from each group were compared.

When multiple rats were running in parallel, video files were split using a Python script (https://github.com/atanugiri/DLC-Jupyter-Notebooks/blob/main/Python scripts/split videos with ffmpeg.py). This process facilitated analysis of individual rats within each arena. The script generates four separate videos, one for each rat. These videos were manually checked and analyzed using Noldus EthoVision. Data was saved and input into an Excel spreadsheet for further analysis.

README and analysis for Non-conflict tasks, Conflict tasks, and food consumption experiments available at https://doi.org/10.7910/DVN/KJAMMP

4.7 Data normalization

In order to compare tasks on the same scale, we normalized data using min–max normalization to rescale values to a common range between 0 and 1 according to the formula x'= x - min(x)/ max(x) - min(x), where x represents the original value and x' represents the normalized value. This approach was used to standardize behavioral measures across all non-conflict tasks (Food alone, Toy alone, and Light alone), which differed in their reward and cost parameters. Normalization enabled direct comparison across tasks by minimizing scale-dependent differences while preserving relative behavioral variation.

5 IMMUNOHISTOCHEMISTRY FOLLOWING GHSR-ACTIVATION

5.1 Histological quality control

Rats were randomly assigned to experimental groups, and both male and female rats were included in all experiments. Tissue collection and quantitative analysis were performed blinded to treatment whenever possible. All staining experiments were independently repeated at least three times to ensure reproducibility. Each experimental run included both control and treatment groups processed in parallel under identical conditions. For each region of interest (ROI), multiple sections were analyzed per animal, and representative images were selected only after confirming consistency across replicates. We ensured that all rats that were included in analysis had good perfusion and immunolabeling.

5.2 General tissue preparation, immunolabeling and microscopy

Rats were deeply anesthetized with Isoflurane and transcardially perfused with 0.9% saline followed by 4% (w/v) paraformaldehyde in 0.01 M phosphate-buffered saline (PBS), pH 7.4. Brains were dissected, post-fixed overnight at 4°C, then transferred to a 30% (w/v) sucrose sinking solution overnight at 4°C. Coronal sections (30 µm) were collected using a sliding microtome and stored in cryoprotectant solution (ethylene glycol and glycerol in 0.05 M phosphate buffer) at −20°C until further processing.

Briefly, all IHC experiments followed a standardized protocol below, for detailed IHC staining and imaging protocols: see section 5.5 Detailed immunohistochemical protocols. Free-floating sections were rinsed in Tris-buffered saline (TBS) (5 washes, 5 mins each) and blocked in 1x TBS containing 0.1% Triton X-100 and 4% normal donkey serum (NDS) for 2 hours at room temperature with gentle agitation. Unless otherwise specified, all wash steps consisted of five washes in TBS (5 min each). Sections were incubated with primary antibodies (table S2) diluted in blocking solution overnight at 4°C on a shaker. Following primary incubation, sections were rinsed in TBS and incubated with species-appropriate Alexa Fluor-conjugated secondary antibodies (table S2) diluted in blocking solution for 5 hours at room temperature. All antibodies were diluted in a carrier solution consisting of TBS, 0.1% Triton X-100, and with 4% NDS, and incubations with fluorescent antibodies were performed protected from light. Following secondary incubation, sections were rinsed with TBS and incubated with NeuroTrace Blue (NT) for somatic counterstaining (1:500 in TBS). Sectioned were then rinsed with TBS, mounted on to glass slides

(Fisher, 22-03448), and coverslipped using a glycerol-based antifade mounting medium with #1.5 glass coverslips (VWR, 16004-312). Slides were imaged withing 48 hours of coverslipping.

Imaging was performed using a Zeiss LSM 900 confocal microscope (Carl Zeiss) in standard confocal mode (non-Airyscan). Diode lasers at 405, 488, 561, and 640 nm were used for excitation of fluorescent signals. Images were acquired using a 20x objective for most experiments (unless otherwise stated), and a 60x oil immersion objective (1.4 NA) for high-resolution imaging of GHSR labeling. Slides were first screened using a low-magnification preview scan (2.5x) to identify regions of interest (ROIs) for subsequent imaging. Optical sectioning parameters were optimized using Zeiss acquisition software. Laser power, gain, and offset settings were held constant across all sections within each staining experiment but were adjusted between experiments as needed based on fluorophore signal intensity. All images were acquired as single optical sections (no z-stacks). Tiled images were collected to capture entire regions of interest and exported as TIFF files without downsampling.

5.3 Image processing and analysis

All image processing and quantification were performed using ImageJ (Fiji). Background subtraction and linear contrast adjustments were applied uniformly across images for presentation purposes only and did not affect quantitative analyses. Raw image files were exported as TIFF images and analyzed in ImageJ using standardized processing workflows, described below. Figures were assembled using Adobe Illustrator.

5.3.1 NEUROANATOMICAL PARCELLATION USING NEUROTRACE

Neuroanatomical regions were identified using NeuroTrace (NT) fluorescent Nissl staining, which provided visualization of neuron cell bodies and cytoarchitectural boundaries. For each section, NT labeling was used in conjunction with anatomical landmarks and Paxinos and Watson's *The Rat Brain in Stereotaxic Coordinates* atlas to identify regions of interest (ROIs). ROIs were manually delineated in ImageJ using the polygon selection tool. ROIs were then added to the ImageJ ROI Manager and applied to the corresponding protein of interest mask for subsequent quantification. For analyses involving striosomes, NT-based boundaries were supplemented with μ-opioid receptor (MOR) immunolabeling to distinguish striosome and matrix compartments. All ROI definitions were performed prior to quantitative analysis and were applied uniformly across experimental groups.

5.3.2 STRIATAL SUBDIVISION INTO 4 COMPARTMENTS

For striatal analyses, the dorsal striatum was subdivided into 4 regions, dorsal medial (DMS), dorsal lateral (DLS), ventral dorsomedial (vDMS), and ventral dorsolateral (vDLS) compartments using a standardized geometric parcellation scheme based on anatomical landmarks [3] (**fig. S3E**).

The dorsal and ventral striatum (AcbC) were first delineated using a horizontal line (#1) drawn from the dorsal tip of the anterior commissure to the lateral boundary of the striatum. A diagonal line (#2) was then extended from the dorsal tip of the nucleus accumbens shell, intersecting line #1. To generate dorsoventral subdivisions, a second horizontal line (#3), was drawn across the dorsal extent of the striatum. A vertical line (#4) was drawn from the dorsal tip of the nucleus accumbens shell to intersect line #3. A diagonal line (#5), parallel to line #2, was drawn from the midpoint of line #4 to the lateral boundary of the striatum. To generate mediolateral subdivisions, a final diagonal line (#6) connecting the midpoints of lines #2 and #5 to the dorsal boundary of

the striatum was drawn. These boundaries separated the striatum into four regions: DMS, DLS, vDMS, and vDLS. The same parcellation scheme was applied to all sections and experimental groups, and resulting ROIs were stored in the ImageJ ROI Manager for subsequent analyses.

5.3.3 STRIOSOMES AND MATRIX SEGMENTATION USING MOR IMMUNOREACTIVITY

Striosomes were identified using MOR immunoreactivity and segmented using a standardized image-processing workflow in ImageJ (**fig. S3F-Q**). The MOR channel was converted to 8-bit grayscale and pre-processed to remove isolated overexposed pixels using the Remove Outliers function (radius=5 pixels). Background fluorescence was subtracted using a rolling-ball radius of 50 pixels, and a Gaussian blur filter (radius=2-3 pixels) was applied to reduce image noise and improve compartment boundaries. Thresholding was then performed to isolate MOR-positive regions and generate binary masks. Unless otherwise noted, masks were generated using the Triangle auto-threshold algorithm. In sections exhibiting excessive signal intensity, threshold parameters were adjusted to capture the upper 1-3% of MOR signal while preserving anatomical compartment boundaries. Resulting binary masks were converted to ROIs and added to the ImageJ ROI Manager. MOR-defined ROIs were then intersected with striatal subdivisions generated as described in section 5.3.2 to create compartment-specific ROIs (e.g., MOR^+ DMS, MOR^+ DLS, MOR^+ vDMS, and MOR^+ vDLS). These ROIs were used for all subsequent striosomal analyses.

For quantification of proteins of interest, positive cells or puncta were identified using marker-specific processing pipelines described below. Total counts were obtained for each striatal subdivision, and striosomal counts were isolated using MOR-defined ROIs. Matrix values were calculated by subtracting striosomal counts from total counts within the corresponding striatal subdivision. Counts were normalized to the ROI area and reported as density measurements.

5.3.4 CFOS (MAKER FOR NEURONAL ACTIVITY) QUANTIFICATION

cFos-positive nuclei were quantified using a standardized image-processing workflow in ImageJ. As illustrated in **fig. S3F-Q**, the cFos channel was converted to 8-bit grayscale. Images were despeckled to remove overexposed pixels, and background signal was subtracted using a rolling-ball radius of 50 pixels. A median filter (radius=2-3 pixels) was then applied to reduce image noise. Thresholding was performed using the upper 0.10% of pixel intensities to isolate cFos-positive nuclei and generate binary masks. Threshold parameters were held constant across all sections within a staining experiment. Watershed segmentation was used to separate clustered cells prior to automated quantification. Cell counts were obtained using the ImageJ Particle Analyzer with circularity constraints of 0.8-1.0 to identify individual nuclei. Quantification was performed within anatomically defined ROIs generated as described in section 5.3.1-5.3.3. Cell counts were normalized to the ROI area and reported as cFos-positive cells per mm2.

5.3.5 PPDH (MAKER FOR NEURONAL INACTIVITY) QUANTIFICATION

Phosphorylated pyruvate dehydrogenase (pPDH) immunoreactivity was quantified as an inverse marker of cellular activity. Quantification was performed within the same anatomically defined ROIs used for cFos analyses. The pPDH channel was converted to 8-bit grayscale, processed using background subtraction (rolling-ball radius=50 pixels), and despeckled to reduce noise. No additional filtering was applied. Thresholding was performed using the upper 5% of pixel intensities to isolate pPDH-positive signal and generate binary masks.

Because pPDH labeling is not restricted to the nucleus, pPDH-positive cells were manually identified based on colocalization with NT-positive neurons to ensure cellular localization. Only pPDH signal overlapping with NT-labeled cell bodies was included in the analysis, thereby excluding non-cellular labeling or glial processes. Positive cells were quantified within each ROI and normalized to area. For striatal analyses, pPDH-positive cells were additionally separated into striosome and matrix compartments using MOR-defined ROIs as described in Section 5.3.3. In dopaminergic regions, including the substantia nigra pars compacta (daSNc), pPDH quantification was combined with tyrosine hydroxylase (TH) labeling to restrict analysis to dopaminergic neurons.

5.3.6 TH QUANTIFICATION AND DOPAMINERGIC SNC SEGMENTATION

The substantia nigra pars compacta (SNc) was first distinguished from the adjacent substantia nigra pars reticulata (SNr) using anatomical landmarks and NT-defined cytoarchitecture. Dopaminergic neurons of the SNc (daSNc) were identified based on tyrosine hydroxylase (TH) immunoreactivity. To generate daSNc ROIs, the TH channel was converted to 8-bit grayscale, processed using background subtraction (rolling-ball radius=50 pixels), and despeckled to reduce image noise. Thresholding was then applied to isolate TH-positive cell bodies and generate binary masks of dopaminergic neurons. TH-derived masks were spatially restricted to the anatomically defined SNc ROI, yielding a final ROI corresponding to the daSNc. These daSNc ROIs were used for all analyses of dopaminergic neuron activity. For cFos and pPDH analyses, only signal colocalized with TH-positive neurons within the daSNc ROI was included in quantification.

5.3.7 GHSR QUANTIFICATION: LOCALIZATION OF THE GROWTH HORMONE SECRETAGOGUE RECEPTOR

GHSR expression was quantified within striosome and matrix compartments using MOR-defined ROIs generated as described in section 5.3.3. Images were converted to 8-bit grayscale and preprocessed using background subtraction and despeckling prior to threshold-based segmentation. Binary masks were generated using a fixed intensity threshold corresponding to the upper 0.1% of pixel intensities. GHSR-positive puncta were then identified using the ImageJ Particle Analyzer with size constraints of 3.0×10^{-8} to 1.0×10^{-5} mm^2 and circularity constraints of 0.8-1.0 to exclude background fluorescence and non-specific artifacts. Puncta counts were normalized to ROI area and reported as puncta density (puncta/mm^2). All image-processing parameters described were held constant within each GHSR staining experiment.

5.3.8 BIOTINYLATED GHRELIN (BGHR) QUANTIFICATION

Biotinylated ghrelin (BGHR) binding was quantified within striosome and matrix compartments using MOR-defined ROIs generated as described in section 5.3.3. Images were converted to 8-bit grayscale and preprocessed using background subtraction and despeckling prior to threshold-based segmentation. To isolate high-intensity ligand signal, a fixed threshold corresponding to the upper 0.1% of pixel intensities was applied uniformly across all images to generate binary masks of BGHR-positive puncta. BGHR-positive puncta were identified using the ImageJ Particle Analyzer with size constraints of $5.0 \times 10^{-7}$to 9.0×10^{-6} mm^2 and circularity constraints of 0.9-1.0 to exclude background fluorescence and non-specific artifacts. Puncta counts were normalized to ROI area and reported as puncta density (puncta/mm^2). All image-processing parameters

788 described were held constant within each BGHR staining experiment.
789

790 *5.3.9 IDENTIFICATION / SEGMENTATION OF DREADD VIRUS IN STRIATUM*

791 For analyses restricted to DREADD-expressing neurons, viral reporter expression (HA, mCitrine,
792 or RFP) was used to generate virus-positive ROIs. Reporter channels were converted to 8-bit
793 grayscale, despeckled, and processed using the Remove Outliers function to eliminate isolated
794 overexposed pixels. A Gaussian blur filter (radius=3-5 pixels) was applied to smooth signal
795 boundaries prior to thresholding. Binary masks were generated using a fixed threshold
796 corresponding to the upper 10% of pixel intensities, selected to capture the full extent of reporter
797 expression while minimizing background fluorescence.

798 For striosomal analyses, virus-derived masks were combined with MOR-defined striosome masks
799 to generate intersection ROIs corresponding to DREADD-expressing striosomal neurons
800 (MOR+/virus+). These intersection ROIs were used for all subsequent analyses of DREADD-
801 mediated effects.

802 **5.4 Histological experimental design**

803 *5.4.1 EXP 5: WHOLE-BRAIN MAPPING OF IBU INDUCED ACTIVITY*

804 To identify brain regions responsive to ghrelin receptor activation, cFos immunolabeling was
805 quantified across approximately 50 anatomically defined regions of interest (ROIs) (**fig. S3A-R**;
806 table S4). Adult rats (n=7-10 per group) received intraperitoneal (IP) injections of either SAL or
807 IBU (1 mg/kg) and were perfused 3.5 hours following treatment.

808 Anatomically defined regions spanning cortical, striatal, thalamic, hypothalamic, and midbrain
809 structures were quantified using NT-based parcellation as described in section 5.3.1. ROIs were
810 selected within ±1 mm of the designated bregma coordinate for each anatomical region (table
811 S4). Images were acquired at 10x magnification (0.4 NA) using a Zeiss LSM 900 confocal
812 microscope. Tissue processing and immunolabeling were performed using two parallel staining
813 pipelines. For regions outside the striatum, sections were processed for cFos
814 immunohistochemistry alone as described in section 5.5.2. For sections containing the striatum,
815 MOR and cFos were co-labeled as described in section 5.5.3 to enable compartment-specific
816 quantification of striosome and matrix activity.

817 To assess region-specific effects of IBU, cFos density was compared between SAL and IBU
818 groups within each anatomical region using unpaired two-tailed t-tests. To facilitate cross-region
819 comparisons, cFos densities were additionally normalized across ROIs using z-score
820 transformation. Resulting z-score values for each region are reported in **fig. S3R**.

821 Raw image datasets, detailed image-processing workflows, and binary masks are publicly
822 available at DOI: https://doi.org/10.7910/DVN/DTXBD5
823 https://doi.org/10.7910/DVN/EI60AH
824 https://doi.org/10.7910/DVN/PYW4WW
825

5.4.2 *Exp 6: Dose-dependent effects of IBU on striatal activity*

To assess compartment-specific dynamics of neuronal activation and inactivity within the striatum following GHSR activation, sections were co-labeled for cFos, pPDH, NT, and MOR (**Fig. 2A-C**; **fig. S3S-T**). Rats (n=6-8 per group) received IP injections of SAL or IBU (0.5x, 1x, 2x, or 10x) and were perfused 3.5 hours post-injection. For detailed staining and imaging protocols, see section 5.5.4. Sections were imaged at 20x and exported as TIFF files: merged and individual. cFos and pPDH counts were obtained within striosome and matrix compartments for DMS and DLS (**fig. S14C-E**). cFos quantification was restricted to MOR+ regions as described in sections 5.3.3 to 5.3.4 and pPDH quantification was restricted to NT-defined somas and MOR+ regions ROIs as described in section 5.3.5.

For cFos and pPDH analyses, a two-way ANOVA was used to assess the effects of treatment (SAL vs IBU) and compartment (striosome vs matrix), followed by Tukey's multiple-comparisons tests. Additional three-way ANOVAs were performed to evaluate the effects of region (DMS vs DLS), treatment (SAL vs IBU), and compartment (DMS vs DLS; **fig. S14H)**.

Raw image datasets are publicly available at DOI: https://doi.org/10.7910/DVN/KRAGMO. Detailed image-processing workflows and binary masks used for quantitative analyses are available at DOI: https://doi.org/10.7910/DVN/NEVZXF.

5.4.3 *Exp 7: Dose-dependent effects of IBU on LHb, ARC, and daSNc*

To assess dose-dependent effects of IBU throughout the broader ghrelin-responsive circuit, cFos expression was quantified within the lateral habenula (LHb; **Fig. 3J-K**) and arcuate nucleus (ARC; **fig. S4G**), while cFos and pPDH expression were quantified within TH-positive neurons of daSNc (**Fig. L-M**). Rats (rats=5-8 per group) received SAL, 0.5x, 1x, 2x, or 10x IBU and were perfused 3.5 h following treatment. Tissue was processed using region-specific staining protocols as described in sections 5.3. cFos quantification was restricted to NT-defined LHb and ARC ROIs. daSNc ROIs generated as described in section 5.3.6 was used for cFos and pPDH quantitation.

For all analyses, treatment groups were compared using one-way ANOVA followed by Tukey's multiple-comparisons tests.

Raw image datasets are publicly available:
LHb DOI: https://doi.org/10.7910/DVN/D5BCOY)
ARC DOI: https://doi.org/10.7910/DVN/WANMCY)
daSNc DOI: https://doi.org/10.7910/DVN/AVMV9E)

All Image-processing workflows and binary masks are available at DOI: https://doi.org/10.7910/DVN/JWSLB

5.4.4 *Exp 8: GHSR expression and biotinylated ghrelin (BGHR) binding within striatum*

To determine whether ghrelin signaling is preferentially associated with striosomes, two complementary approaches were used to assess receptor localization and ligand binding within striatal compartments.

First, GHSR expression was evaluated in saline-treated rats (n=7). Rats received SAL injections IP and were perfused 3.5 h later. Sections were co-labeled for GHSR and MOR (**Fig. 2D-F;** see section 5.5.5 for detailed staining protocls), imaged at 63x magnification, and GHSR puncta density was quantified within MOR-defined striosome and matrix compartments as described above (striosomes: sections 5.3.2-5.3.3; GHSR: 5.3.7). Comparisons between compartments were performed using paired two-tailed t-tests.

To validate receptor localization, additional sections were labeled for GHSR, MOR, and biotinylated ghrelin (BGHR) to assess the spatial relationship between receptor expression and ligand binding within striosome and matrix compartments (**Fig. 2G;** see section 5.5.6 for staining procedures).

Finally, BGHR binding was quantified across the IBU dose-response cohort (SAL, 0.5x, 1x, 2x, and 10x IBU; n=6–8/group) to determine whether prior IBU exposure altered ligand binding and receptor availability (**Fig. 2H; fig. S3W;** see section 5.5.4 for detailed staining protocols). BGHR puncta density was quantified within MOR-defined striosome and matrix compartments as described above (striosomes: sections 5.3.2-5.3.3; BGHR: 5.3.8). Statistical comparisons were performed using two-way ANOVA to assess the effects of treatment and striatal compartment, followed by Tukey's multiple-comparisons tests.

Raw image datasets are publicly available:
GHSR DOI: https://doi.org/10.7910/DVN/UHTDDW
bGHR DOI: https://doi.org/10.7910/DVN/KRAGMO)

All Image-processing workflows and binary masks are available at DOI: https://doi.org/10.7910/DVN/SNSRF4.

5.4.5 *Exp 9: DREADD manipulations*

To determine whether IBU-induced changes in neural activity and behavior depend on striosomal activity, Oprm1-Cre rats received Cre-dependent inhibitory hM4D(Gi) or excitatory hM3D(Gq) DREADD targeting striosomal neurons. Oprm1-Cre and Wild-type rats underwent stereotaxic viral injections as described in section 2.3. Following a 4-week recovery period, rats underwent behavioral testing for 4-6 months as described in section 4. The same cohort was subsequently used for immunohistochemical analyses. A schematic of the experimental timeline is shown in **Fig. 4A**.

For IHC analysis, Wild-type cohorts received SAL alone, IBU alone, or CNO+SAL treatment. Rats expressing inhibitory DREADD received either CNO+SAL (Inh SAL) or CNO+IBU (Inh IBU), whereas rats expressing excitatory DREADD received either CNO+SAL (Exc SAL) or CNO+IBU (Exc IBU). An additional inhibitory cohort received IBU in the absence of CNO (Cre+IBU) to control

for viral expression and ensure comparable experimental handling across groups. Detailed group assignments are shown in **Fig. 4B**. On day of testing, rats (rats=6-8/group) received an initial CNO injection concurrent with SAL or IBU administration, followed by a second CNO injection 1.5 h later to maintain receptor activation throughout the experimental window. Rats were perfused 3.5 h following the initial injection.

First, to validate selective targeting of striosomal neurons, the Cre + IBU (no CNO) cohort was used exclusively to assess viral targeting specificity. Sections were labeled for MOR and viral reporters (HA and mCitrine). Virus-positive cells were quantified within MOR-defined striosome and matrix compartments as described in Sections 5.5.5, and targeting specificity was assessed by comparing the proportion of virus-positive cells localized to each compartment using paired two-tailed t-tests (**Fig. 3A-B;** see section 5.5.10-5.5.11 for detailed staining protocols).

Second, determine how striosomal activity influences neuronal activation, cFos and pPDH expression were quantified following inhibitory and excitatory DREADD-mediated manipulation of striosomal neurons (**Fig. 4C; fig. S6; fig. S8A-D**). Brains were processed for MOR, cFos, pPDH, and viral reporter expression as described above. To restrict analyses to DREADD-expressing striosomal neurons, MOR-defined striosome masks were combined with virus-derived masks (HA or RFP), generating intersection ROIs corresponding to MOR+/virus+ cells. cFos and pPDH expression were quantified within these ROIs using the methods described in sections 5.3. Statistical comparisons among experimental groups were performed using one-way ANOVA followed by Tukey's multiple-comparisons tests.

Lastly, to determine whether striosomal manipulation altered activity within downstream circuit regions, cFos expression was quantified in the LHb, while cFos and pPDH expression were quantified in TH-positive neurons of the daSNc using tissue from the experimental groups described above (**Fig. 4D-I**). Quantification was performed using the methods described in Sections 5.3.4-6. Statistical comparisons among experimental groups were conducted using one-way ANOVA followed by Tukey's multiple-comparisons tests.

Raw image datasets are publicly available:
Striatum DOI: https://doi.org/10.7910/DVN/WHLWVB)
LHb DOI: https://doi.org/10.7910/DVN/CT9ATL)
daSNc DOI: https://doi.org/10.7910/DVN/O5GNIF)

All Image-processing workflows and binary masks are available at DOI: https://doi.org/10.7910/DVN/QLVA4X

5.5 Detailed immunohistochemical protocols

5.5.1 PERFUSION

1. Deeply anesthetize rats with isoflurane.
2. Transcardially perfuse with 0.9% saline, followed by 4% paraformaldehyde (PFA) in PBS.
3. Extract brains and post-fix overnight in 4% PFA at 4 °C.
4. Transfer brains to 30% sucrose in PBS for ~48 hours (or until fully sunk).
5. Section coronally at 30 µm on a sliding microtome.
6. Store sections in cryoprotectant (25% (v/v) ethylene glycol and 25% (v/v) glycerol in 0.05 M phosphate buffer (0.2M Sodium Phosphate Buffer Monobasic + 0.2M Sodium phosphate buffer dibasic) at –20 °C until staining.

5.5.2 cFOS IMMUNOHISTOCHEMISTRY ACROSS 50 BRAIN REGIONS (EXCLUDING STRIATUM)

Experimental procedure for cFos analysis

1. Inject rats with 1 mg/kg Ibutamoren (IBU; 1x dose) via IP injection.
2. Return rats to their home cage with ad libitum access to food and water.
3. Allow rats to remain undisturbed for 3.5 hours post-injection.
4. Following the 3.5-hour incubation period, perform transcardial perfusion as described in Section 5.5.1.
5. Section brains coronally (30 µm) and store tissue in cryoprotectant at −20°C until processing.

Section retrieval and washes (5 x 5 min)

1. Remove free-floating sections from cryoprotectant and transfer into 1x Tris-buffered saline (TBS).
2. Select sections corresponding to target anatomical regions within ±0.5 mm of the following bregma coordinates:
    - Prefrontal cortex: +3.24 mm
    - Rostral thalamus and GPe/GPi: −1.56 mm
    - Thalamus: -3.24
    - Hypothalamus: −3.0 mm
    - Amygdala: −3.0 mm
    - Midbrain regions: −5.16 mm
3. Wash sections 5 times for 5 minutes each in fresh 1x TBS with gentle agitation.

Blocking (2 hours, room temperature)

1. Prepare blocking solution with the following:
    - 1x TBS
    - 0.1% Triton X-100
    - 4% normal donkey serum (NDS)
2. Incubate sections in blocking solution for 2 hours at room temperature.
3. Maintain gentle agitation throughout incubation.

cFos Primary antibody incubation (48 hours, 4°C)

1. Prepare primary antibody solution by diluting mouse anti-cFos (1:2000; Santa Cruz, sc-272343) in same blocking solution prepared above.
2. Incubate sections in primary antibody solution for 48 hours at 4°C, maintaining gentle agitation on an orbital shaker.
3. Ensure sections are fully submerged and evenly spaced.
4. Following primary incubation, wash sections 5 x 5 in fresh TBS

Secondary antibody incubation (5 hours, room temperature)

1. Prepare secondary antibody solution by diluting donkey anti-mouse Alexa Fluor647 (1:1000; Jackson ImmunoResearch, 715-605-151) in the same blocking solution prepared above.
2. Incubate sections for 5 hours at room temperature, maintaining gentle agitation on an orbital shaker.
3. Following secondary incubation, wash sections 5 times in fresh TBS, for 5 mins

Nissl counterstaining (NT Blue)

1. Incubate sections in NT (1:500 in TBS) for 10 minutes at room temperature.
2. Maintain gentle agitation on the orbital shaker and protect from light.
3. Wash sections 5 x 5 minutes in fresh 1x TBS.

Mounting and storage

1. Mount sections onto glass slides
2. Allow excess buffer to drain without drying tissue.
3. Coverslip using glycerol-based antifade mounting medium and #1.5 glass coverslips.
4. Store slides at 4°C protected from light.
5. Image slides within 48 hours of coverslipping.

cFos Imaging across 50 brain regions

1. Perform imaging using a Zeiss LSM 900 confocal microscope.
2. Acquire tiled images at 10x magnification (0.4 NA) to capture full regions of interest.
3. Use 4x line averaging to improve signal-to-noise ratio.
4. Perform an initial low-magnification preview scan to identify regions of interest prior to acquisition.
5. Acquire tiled images covering the full region of interest and fuse tiles using microscope software to remove stitching artifacts.
6. Export final images as TIFF files without downsampling.
7. Image processing and analysis described in section 5.3.

5.5.3 cFOS IHC IN STRIOSOME AND MATRIX COMPARTMENTS

Experimental procedure for cFos analysis in striatum

1. Inject rats with either saline or 1x IBU (1 mg/kg) via IP injection (n = 10-12 rats per condition).
2. Return rats to their home cage with ad libitum access to food and water.
3. Allow rats to remain undisturbed for 3.5 hours post-injection.
4. Following the 3.5-hour incubation period, perform transcardial perfusion as described in Section 5.5.1.
5. Section brains coronally (30 µm) and store tissue in cryoprotectant at −20°C until processing.

Striatum section selection and washes

1. Remove free-floating sections from cryoprotectant and transfer into 1x TBS

2. Select sections corresponding to anterior dorsal striatum within ±0.5 mm of bregma +1.8 mm.
3. Wash sections 5 times for 5 minutes each in fresh 1x TBS with gentle agitation.

Blocking (2 hours, room temperature)

1. Prepare blocking solution with the following:
    - 1x TBS
    - 0.1% Triton X-100
    - 4% normal donkey serum (NDS)
2. Incubate sections in blocking solution for 2 hours at room temperature.
3. Maintain gentle agitation throughout incubation.

cFos and MOR primary antibody incubation (48 hours, 4°C)

1. Mix primary antibodies in blocking solution prepared above
    - mouse anti-cFos (1:2000; Santa Cruz, sc-272343) and
    - rabbit anti-μ-opioid receptor (MOR) (1:5000; ImmunoStar, 24216)
2. Incubate sections in primary antibody solution for 48 hours at 4°C, maintaining gentle agitation on an orbital shaker.
3. Following primary incubation, wash sections 5 x 5 in fresh TBS

Secondary antibody incubation (5 hours, room temperature)

1. Mix secondaries antibodies in blocking solution
    - cFos: donkey anti-mouse Alexa Fluor 647 (1:1000; Jackson ImmunoResearch, 715-605-151)
    - MOR: donkey anti-rabbit Alexa Fluor 555 (1:1000; Jackson ImmunoResearch, 711-565-152)
2. Incubate sections for 5 hours at room temperature, maintaining gentle agitation on orbital shaker.
3. Following secondary incubation, wash sections 5 times in fresh TBS, for 5 mins

Mounting and storage

4. Mount sections onto glass slides.
5. Allow excess buffer to drain without drying tissue.
6. Coverslip using glycerol-based antifade mounting medium and #1.5 glass coverslips.
7. Store slides at 4°C protected from light.
8. Image slides within 2 weeks of cover slipping.

cFos / MOR Imaging in striatum

1. Perform imaging using a Zeiss LSM 900 confocal microscope.
2. Acquire tiled images at 10x magnification to capture the full striatal region of interest.
3. Use a sampling rate of 1.0 and 4x line averaging to improve signal-to-noise ratio.
4. Perform an initial low-magnification preview scan to identify the region of interest prior to acquisition.
5. Acquire tiled images covering the full striatal region and fuse tiles using microscope software to remove stitching artifacts.

6. Apply minimal and uniform background adjustment across images to improve signal-to-noise ratio
7. Export final images as TIFF files without downsampling.
8. Image processing and analysis described in section 5.3.
9. Multiplex IHC in striatum for cFos, pPDH, MOR, and biotinylated-ghrelin analysis

5.5.4 cFOS, pPDH, BGHR, MOR IN STRIATUM

Experimental procedure for cFos analysis

1. Inject rats with either saline or IBU at 0.5x, 1x, 2x, or 10x doses IP injection (n = 6–8 rats per group).
2. Return rats to their home cage with ad libitum access to food and water.
3. Allow rats to remain undisturbed for 3.5 hours post-injection.
4. Following the 3.5-hour incubation period, perform transcardial perfusion as described in Section 5.5.1.
5. Section brains coronally (30 µm) and store tissue in cryoprotectant at −20°C until processing.

Striatum section selection and washes (5 x 5 min)

1. Remove free-floating sections from cryoprotectant and transfer into 1x TBS
2. Select sections corresponding to anterior dorsal striatum within ±0.5 mm of bregma +1.8 mm.
3. Wash sections 5 times for 5 minutes each in fresh 1x TBS with gentle agitation.

Endogenous biotin blocking kit (Thermo #E21390)

1. Incubate sections in reagent A solution (Thermo Fisher Endogenous Biotin Blocking Kit, #E21390) for 15-30 minutes at room temperature
2. Wash sections 3 x 5 minutes in 1x TBS
3. Incubate sections in reagent B solution for 15-30 minutes at room temperature.
4. Wash sections 3 x 5 minutes in 1x TBS
5. Maintain gentle agitation throughout all incubations

Blocking (2 hours, room temperature)

1. Prepare blocking solution with the following:
    - 1x TBS
    - 0.1% Triton X-100
    - 4% normal donkey serum (NDS)
2. Incubate sections in blocking solution for 2 hours at room temperature.
3. Maintain gentle agitation throughout incubation.

Primary antibody + ligand incubation (48 hours, 4°C)

1. Mix primary antibodies in blocking solution prepared above
    - mouse anti-cFos (1:2000; Santa Cruz, sc-272343)
    - Rabbit anti-pPDH (1:1000; Cell Signaling Technology #E4V9L)
    - Guinea pig anti-MOR (1:1000; Millipore Sigma AB5509)

- Biotinylated-ghrelin (AnaSpec AS-29391; 1:500)

2. Incubate sections in primary antibody solution for 48 hours at 4°C, maintaining gentle agitation on an orbital shaker.
3. Following primary incubation, wash sections 5 x 5 in fresh TBS

Secondary antibody incubation (5 hours, room temperature)

1. Mix secondaries antibodies in blocking solution
   - cFos: donkey anti-mouse Alexa Fluor 555 (1:1000; Jackson ImmunoResearch)
   - pPDH: donkey anti-rabbit Alexa Fluor 647 (1:1000; Jackson ImmunoResearch)
   - MOR: Donkey anti-guinea pig Alexa Fluor 488 (1:1000; Jackson)
   - Streptavidin Alexa Fluor 594 (1:1000; Jackson ImmunoResearch)
2. Incubate sections for 5 hours at room temperature, maintaining gentle agitation on orbital shaker.
3. Following secondary incubation, wash sections 5 times in fresh TBS, for 5 mins

Nissl counterstaining

1. Incubate sections in NT (1:500 in TBS) for 10 minutes at room temperature.
2. Maintain gentle agitation and protect from light during incubation.
3. wash sections 5 times in fresh TBS, for 5 mins

Mounting and storage

1. Mount sections onto glass slides.
2. Allow excess buffer to drain without drying tissue.
3. Coverslip using glycerol-based antifade mounting medium and #1.5 glass coverslips.
4. Store slides at 4°C protected from light.
5. Image slides within 48 hours of coverslipping.

cFos, pPDH, MOR, and Biotin-ghrelin imaging in striatum

1. Perform imaging using a Zeiss LSM 900 confocal microscope.
2. Acquire tiled images at 20x magnification to capture the full striatal region of interest.
3. Use a sampling rate of 0.4 sampling and 4x line averaging to improve signal-to-noise ratio.
4. Perform an initial low-magnification preview scan to identify the region of interest prior to acquisition.
5. Acquire tiled images covering the full striatal region and fuse tiles using microscope software to remove stitching artifacts.
6. Apply minimal and uniform background adjustment across images to improve signal-to-noise ratio
7. Export final images as TIFF files without downsampling.
8. Image processing and analysis described in section 5.3.

5.5.5 IHC FOR GHSR EXPRESSION IN STRIATAL COMPARTMENTS

Experimental procedure

1. Inject rats with saline via IP injection (n = 7 rats).
2. Return rats to their home cage with ad libitum access to food and water.
3. Allow rats to remain undisturbed for 3.5 hours post-injection.
4. Following the 3.5-hour incubation period, perform transcardial perfusion as described in Section 5.5.1.

5. Section brains coronally (30 µm) and store tissue in cryoprotectant at −20°C until processing.

Striatum section selection and washes

1. Remove free-floating sections from cryoprotectant and transfer into 1x TBS
2. Select sections corresponding to anterior dorsal striatum within ±0.5 mm of bregma +1.8 mm.
3. Wash sections 5 times for 5 minutes each in fresh 1x TBS with gentle agitation.

Blocking (2 hours, room temperature)

1. Prepare blocking solution with the following:
    - 1x TBS
    - 0.1% Triton X-100
    - 4% normal donkey serum (NDS)
2. Incubate sections in blocking solution for 2 hours at room temperature.
3. Maintain gentle agitation throughout incubation.

Primary antibody + ligand incubation (48 hours, 4°C)

1. Mix primary antibodies in blocking solution prepared above
    - Rabbit anti-GHSR (1:1000; Alomone Labs, # AGR-031)
    - Guinea pig anti-MOR (1:1000; Millipore Sigma AB5509)
2. Incubate sections in primary antibody solution for 48 hours at 4°C, maintaining gentle agitation on an orbital shaker.
3. Following primary incubation, wash sections 5 x 5 in fresh TBS

Secondary antibody incubation (5 hours, room temperature)

1. Mix secondaries antibodies in blocking solution
    - GHSR: donkey anti-rabbit Alexa Fluor 647 (1:1000; Jackson ImmunoResearch)
    - MOR: Donkey anti-guinea pig Alexa Fluor 555 (1:1000; Jackson)
2. Incubate sections for 5 hours at room temperature, maintaining gentle agitation on orbital shaker.
3. Following secondary incubation, wash sections 5 times in fresh TBS, for 5 mins

Nissl counterstaining

1. Incubate sections in NT (1:500 in TBS) for 10 minutes at room temperature.
2. Maintain gentle agitation and protect from light during incubation.
3. wash sections 5 times in fresh TBS, for 5 mins

Mounting and storage

1. Mount sections onto glass slides.
2. Allow excess buffer to drain without drying tissue.
3. Coverslip using glycerol-based antifade mounting medium and #1.5 glass coverslips.
4. Store slides at 4°C protected from light.
5. Image slides within 48 hours of coverslipping.

GHSR and MOR imaging in striatum

1. Perform imaging using a Zeiss LSM 900.
2. Perform an initial 2.5x preview scan, followed by 10x imaging to identify striosomal regions using the MOR (A555) channel.
3. Following region identification, remove the slide, apply immersion oil, and reload the slide for high-magnification imaging.
4. Acquire tiled images at 63x magnification (oil immersion, 1.4 NA) with a sampling rate of 0.6 and 4x line averaging to capture high-resolution images of GHSR expression within striosomes.
5. Acquire tiled images of the dorsal striatum in 16-bit format, and fuse tiles using microscope software to remove stitching artifacts.
6. Export final images as BigTIFF files with 80% downsampling.
7. Image processing and analysis described in section 5.3.

5.5.6 GHSR AND BIOTINYLATED-GHRELIN LOCALIZATION IN STRIOSOMES

Experimental procedure

1. Inject rats with saline via IP injection (n = 6 rats).
2. Return rats to their home cage with ad libitum access to food and water.
3. Allow rats to remain undisturbed for 3.5 hours post-injection.
4. Following the 3.5-hour incubation period, perform transcardial perfusion as described in Section 5.5.1.
5. Section brains coronally (30 µm) and store tissue in cryoprotectant at −20°C until processing.

Striatum section selection and washes

1. Remove free-floating sections from cryoprotectant and transfer into 1x TBS
2. Select sections corresponding to anterior dorsal striatum within ±0.5 mm of bregma +1.8 mm.
3. Wash sections 5 times for 5 minutes each in fresh 1x TBS with gentle agitation.

Endogenous biotin blocking kit (Thermo #E21390)

1. Incubate sections in reagent A solution (Thermo Fisher Endogenous Biotin Blocking Kit, #E21390) for 15-30 minutes at room temperature
2. Wash sections 3 x 5 minutes in 1x TBS
3. Incubate sections in reagent B solution for 15-30 minutes at room temperature
4. Wash sections 3 x 5 minutes in 1x TBS
5. Maintain gentle agitation throughout all incubations

Blocking (2 hours, room temperature)

1. Prepare blocking solution with the following:
    - 1x TBS
    - 0.1% Triton X-100
    - 4% normal donkey serum (NDS)
2. Incubate sections in blocking solution for 2 hours at room temperature.
3. Maintain gentle agitation throughout incubation.

Primary antibody incubation (48 hours, 4°C)

1. Mix primary antibodies in blocking solution prepared above

- Rabbit anti-GHSR (1:1000; Alomone Labs, # AGR-031)
- Guinea pig anti-MOR (1:1000; Millipore Sigma AB5509)
- Biotinylated-ghrelin (AnaSpec AS-29391; 1:500)

2. Incubate sections in primary antibody solution for 48 hours at 4°C, maintaining gentle agitation on an orbital shaker.
3. Following primary incubation, wash sections 5 x 5 in fresh TBS

Secondary antibody incubation (5 hours, room temperature)

1. Mix secondaries antibodies in blocking solution
   - GHSR: donkey anti-rabbit Alexa Fluor 647 (1:1000; Jackson ImmunoResearch)
   - MOR: Donkey anti-guinea pig Alexa Fluor 555 (1:1000; Jackson)
   - Streptavidin Alexa Fluor 594 (1:1000; Jackson ImmunoResearch)
1. Incubate sections for 5 hours at room temperature, maintaining gentle agitation on orbital shaker.
2. Following secondary incubation, wash sections 5 times in fresh TBS, for 5 mins

Nissl counterstaining

1. Incubate sections in NT (1:500 in TBS) for 10 minutes at room temperature.
2. Maintain gentle agitation and protect from light during incubation.
3. wash sections 5 times in fresh TBS, for 5 mins

Mounting and storage

1. Mount sections onto glass slides.
2. Allow excess buffer to drain without drying tissue.
3. Coverslip using glycerol-based antifade mounting medium and #1.5 glass coverslips.
4. Store slides at 4°C protected from light.
5. Image slides within 48 hours of coverslipping.

GHSR, MOR, and biotin-ghrelin imaging in striatum

1. Perform imaging using a Zeiss LSM 900 confocal microscope.
2. Acquire tiled images at 20x magnification to capture the full striatal region of interest.
3. Use a sampling rate of 0.4 sampling and 4x line averaging to improve signal-to-noise ratio.
4. Perform an initial low-magnification preview scan to identify the region of interest prior to acquisition.
5. Acquire tiled images covering the full striatal region and fuse tiles using microscope software to remove stitching artifacts.
6. Apply minimal and uniform background adjustment across images to improve signal-to-noise ratio
7. Export final images as TIFF files without downsampling.
8. Image processing and analysis described in section 5.3.

5.5.7 cFOS IN LHB, ARC

Experimental procedure

1. Inject rats with either saline or IBU at 0.5x, 1x, 2x, or 10x doses IP injection (n = 6–8 rats per group).
2. Return rats to their home cage with ad libitum access to food and water.
3. Allow rats to remain undisturbed for 3.5 hours post-injection.

4. Following the 3.5-hour incubation period, perform transcardial perfusion as described in Section 5.5.1.
5. Section brains coronally (30 µm) and store tissue in cryoprotectant at −20°C until processing.

Section selection and washes (5 x 5 min

1. Remove free-floating sections from cryoprotectant and transfer into 1x TBS saline (TBS).
2. Select sections corresponding to the lateral habenula (LHb) and arcuate nucleus (ARC) around 1mm from bregma -3.0mm coordinate.
3. Wash sections 5 times for 5 minutes each in fresh 1x TBS with gentle agitation.

Blocking (2 hours, room temperature)

1. Prepare blocking solution with the following:
    - 1x TBS
    - 0.1% Triton X-100
    - 4% normal donkey serum (NDS)
2. Incubate sections in blocking solution for 2 hours at room temperature.
3. Maintain gentle agitation throughout incubation.

cFos Primary antibody incubation (48 hours, 4°C)

1. Mix primary antibodies in blocking solution prepared above
    - mouse anti-cFos (1:2000; Santa Cruz, sc-272343)
2. Incubate sections in primary antibody solution for 48 hours at 4°C, maintaining gentle agitation on an orbital shaker.
3. Following primary incubation, wash sections 5 x 5 in fresh TBS

Secondary antibody incubation (5 hours, room temperature)

1. Mix secondaries antibodies in blocking solution
    - cFos: donkey anti-mouse Alexa Fluor 647 (1:1000; Jackson ImmunoResearch)
1. Incubate sections for 5 hours at room temperature, maintaining gentle agitation on orbital shaker.
2. Following secondary incubation, wash sections 5 times in fresh TBS, for 5 mins

Striatum section selection and washes

Nissl counterstaining

1. Incubate sections in NT (1:500 in TBS) for 10 minutes at room temperature.
2. Maintain gentle agitation and protect from light during incubation.
3. wash sections 5 times in fresh TBS, for 5 mins

Mounting and storage

1. Mount sections onto glass slides.
2. Allow excess buffer to drain without drying tissue.
3. Coverslip using glycerol-based antifade mounting medium and #1.5 glass coverslips.
4. Store slides at 4°C protected from light.
5. Image slides within 48 hours of coverslipping.

cFos Imaging

1. Perform imaging using a Zeiss LSM 900 confocal microscope.
2. Acquire tiled images at **20x magnification** to capture the full LHb and ARC region of interest.
3. Use 4x line averaging to improve signal-to-noise ratio.
4. Acquire tiled images and fuse tiles using microscope software to remove stitching artifacts.
5. Export final images as TIFF files without downsampling.
6. Image processing and analysis described in section 5.3.

5.5.8 IHC OF CFOS AND PPDH IN DOPAMINERGIC NEURONS OF SNC

Experimental procedure

1. Inject rats with either saline or IBU at 0.5x, 1x, 2x, or 10x doses IP injection (n = 6-8 rats per group).
2. Return rats to their home cage with ad libitum access to food and water.
3. Allow rats to remain undisturbed for 3.5 hours post-injection.
4. Following the 3.5-hour incubation period, perform transcardial perfusion as described in Section 5.5.1.
5. Section brains coronally (30 µm) and store tissue in cryoprotectant at −20°C until processing.

SNc section selection and washes

1. Remove free-floating sections from cryoprotectant and transfer into 1x Tris-buffered saline (TBS).
2. Select sections corresponding to the dopaminergic substantia nigra pars compacta (daSNc) within ±0.5 mm of bregma −5.16 mm**.**
3. Wash sections 5 times for 5 minutes each in fresh 1x TBS with gentle agitation.

Blocking (2 hours, room temperature)

1. Prepare blocking solution with the following:
    - 1x TBS
    - 0.1% Triton X-100
    - 4% normal donkey serum (NDS)
2. Incubate sections in blocking solution for 2 hours at room temperature.
3. Maintain gentle agitation throughout incubation.

Primary antibody incubation (48 hours, 4°C)

1. Mix primary antibodies in blocking solution prepared above
    - Mouse anti-c-Fos (1:2000; Santa Cruz, sc-271243)
    - Rabbit anti-pPDH (1:1000; Cell Signaling Technology #E4V9L)
    - Sheep anti-TH (1:1000; GeneTex, GTX82570)
2. Incubate sections in primary antibody solution for 48 hours at 4°C, maintaining gentle agitation on an orbital shaker.
3. Following primary incubation, wash sections 5 x 5 in fresh TBS

Secondary antibody incubation (5 hours, room temperature)

1. Mix secondaries antibodies in blocking solution

- cFos: donkey anti-mouse Alexa Fluor 555 (1:1000; Jackson ImmunoResearch)
- pPDH: donkey anti-rabbit Alexa Fluor 647 (1:1000; Jackson ImmunoResearch)
- TH: Donkey anti-shee Alexa Fluor 488 (1:1000; Jackson)

1. Incubate sections for 5 hours at room temperature, maintaining gentle agitation on orbital shaker.
2. Following secondary incubation, wash sections 5 times in fresh TBS, for 5 mins

Nissl counterstaining

1. Incubate sections in NT (1:500 in TBS) for 10 minutes at room temperature.
2. Maintain gentle agitation and protect from light during incubation.
3. wash sections 5 times in fresh TBS, for 5 mins

Mounting and storage

1. Mount sections onto glass slides.
2. Allow excess buffer to drain without drying tissue.
3. Coverslip using glycerol-based antifade mounting medium and #1.5 glass coverslips.
4. Store slides at 4°C protected from light.
5. Image slides within 48 hours of coverslipping.

cFos, pPDH, TH imaging in SNc

1. Perform imaging using a Zeiss LSM 900 confocal microscope.
2. Acquire tiled images at 20x magnification to capture the full region of interest.
3. Use a sampling rate of 0.4 sampling and 4x line averaging to improve signal-to-noise ratio.
4. Perform an initial low-magnification preview scan to identify the region of interest prior to acquisition.
5. Acquire tiled images covering the SNc region and fuse tiles using microscope software to remove stitching artifacts.
6. Apply minimal and uniform background adjustment across images to improve signal-to-noise ratio.
7. Export final images as TIFF files without downsampling.
8. Image processing and analysis described in sectio 5.3.

5.5.9 GCAMP IN STRIATUM

Experimental procedure for cFos analysis

1. Oprm1-Cre rats injected with Cre-dependent GCaMP were injected as described in section 2.3.
2. To optimize virus tither, rats were euthanized 4 weeks later with perfusion as described in Section 5.5.1.
3. Section brains coronally (30 µm) and store tissue in cryoprotectant at −20°C until processing.

Striatum section selection and washes

1. TBS
2. To localize the viral injection site, briefly screen sections under a brightfield microscope at low magnification (5x).

3. Identify sections corresponding to injection site based on the needle track and tissue landmarks within the anterior dorsal striatum.
4. Select three sections per animal centered on the injection site for IHC processing
5. Wash sections 5 times for 5 minutes each in fresh 1x TBS with gentle agitation.

Blocking (2 hours, room temperature)

1. Prepare blocking solution with the following:
    - 1x TBS
    - 0.1% Triton X-100
    - 4% normal donkey serum (NDS)
2. Incubate sections in blocking solution for 2 hours at room temperature.
3. Maintain gentle agitation throughout incubation.

Primary antibody incubation (48 hours, 4°C)

1. Mix primary antibodies in blocking solution prepared above
    - Chicken anti-GFP (1:2000; GFP1020)
    - Guinea pig anti-MOR (1:1000; Millipore Sigma AB5509)
2. Incubate sections in primary antibody solution for 48 hours at 4°C, maintaining gentle agitation on an orbital shaker.
3. Following primary incubation, wash sections 5 x 5 in fresh TBS

Secondary antibody incubation (5 hours, room temperature)

1. Mix secondaries antibodies in blocking solution
    - GFP: donkey anti-chicken Alexa Fluor 488 (1:1000; Jackson)
    - MOR: Donkey anti-guinea pig Alexa Fluor 555 (1:1000; Jackson)
1. Incubate sections for 5 hours at room temperature, maintaining gentle agitation on orbital shaker.
2. Following secondary incubation, wash sections 5 times in fresh TBS, for 5 mins

Nissl counterstaining

1. Incubate sections in NT (1:500 in TBS) for 10 minutes at room temperature.
2. Maintain gentle agitation and protect from light during incubation.
3. wash sections 5 times in fresh TBS, for 5 mins

Mounting and storage

1. Mount sections onto glass slides.
2. Allow excess buffer to drain without drying tissue.
3. Coverslip using glycerol-based antifade mounting medium and #1.5 glass coverslips.
4. Store slides at 4°C protected from light.
5. Image slides within 48 hours of coverslipping.

GCaMP and MOR imaging in striatum

1. Perform imaging using a Zeiss LSM 900 confocal microscope.
2. Acquire tiled images at 20x magnification to capture the full striatal region of interest.
3. Use a sampling rate of 0.4 sampling and 4x line averaging to improve signal-to-noise ratio.

4. Perform an initial low-magnification preview scan to identify the region of interest prior to acquisition.
5. Acquire tiled images covering the full striatal region and fuse tiles using microscope software to remove stitching artifacts.
6. Apply minimal and uniform background adjustment across images to improve signal-to-noise ratio
7. Export final images as TIFF files without downsampling.
8. Image processing and analysis described in section 5.3

5.5.10 OPRM1-CRE INHIBITORY DREADD IHC

Experimental procedure for cFos analysis

4. Oprm1-Cre rats injected with Cre-dependent inhibitory DREADD virus (AAV-hSyn-DIO-HA-hM4D(Gi)-IRES-mCitrine) were assigned to experimental groups receiving saline or Ibutamoren (IBU; 2x) in combination with clozapine-N-oxide (CNO), as described above. To maintain DREADD activation across the experimental window, rats received two CNO injections: an initial injection concurrent with saline or IBU administration, followed by a second injection 1.5 hours later. A third group did not receive any injections, and was used for validation of the virus.
5. Return rats to their home cage with ad libitum access to food and water.
6. Allow rats to remain undisturbed for 3.5 hours following the initial injection.
7. Following the 3.5-hour incubation period, perform transcardial perfusion as described in Section 5.5.1.
8. Section brains coronally (30 µm) and store tissue in cryoprotectant at −20°C until processing.

Striatum section selection and washes

6. TBS
7. To localize the viral injection site, briefly screen sections under a brightfield microscope at low magnification (5x).
8. Identify sections corresponding to injection site based on the needle track and tissue landmarks within the anterior dorsal striatum.
9. Select three sections per animal centered on the injection site for IHC processing.
10. Wash sections 5 times for 5 minutes each in fresh 1x TBS with gentle agitation.

Blocking (2 hours, room temperature)

4. Prepare blocking solution with the following:
    - 1x TBS
    - 0.1% Triton X-100
    - 4% normal donkey serum (NDS)
5. Incubate sections in blocking solution for 2 hours at room temperature.
6. Maintain gentle agitation throughout incubation.

Primary antibody incubation (48 hours, 4°C)

4. Mix primary antibodies in blocking solution prepared above.
    - mouse anti-cFos (1:2000; Santa Cruz, sc-272343)
    - Rabbit anti-pPDH (1:1000; Cell Signaling Technology #E4V9L)
    - Guinea pig anti-MOR (1:1000; Millipore Sigma AB5509)
    - Goat anti-HA (1:1000; Cell Signaling Technology)

5. Incubate sections in primary antibody solution for 48 hours at 4°C, maintaining gentle agitation on an orbital shaker.
6. Following primary incubation, wash sections 5 x 5 in fresh TBS

Secondary antibody incubation (5 hours, room temperature)

2. Mix secondaries antibodies in blocking solution
    - cFos: donkey anti-mouse Alexa Fluor 594 (2 drops per mL; Invitrogen)
    - pPDH: donkey anti-rabbit Alexa Fluor 647 (1:1000; Jackson ImmunoResearch)
    - MOR: Donkey anti-guinea pig Alexa Fluor 555 (1:1000; Jackson ImmunoResearch)
    - HA: Donkey anti-goat Alexa Fluor 488 (1:1000; Jackson ImmunoResearch)
3. Incubate sections for 5 hours at room temperature, maintaining gentle agitation on orbital shaker.
4. Following secondary incubation, wash sections 5 times in fresh TBS, for 5 mins

Nissl counterstaining

4. Incubate sections in NT (1:500 in TBS) for 10 minutes at room temperature.
5. Maintain gentle agitation and protect from light during incubation.
6. wash sections 5 times in fresh TBS, for 5 mins

Mounting and storage

6. Mount sections onto glass slides.
7. Allow excess buffer to drain without drying tissue.
8. Coverslip using glycerol-based antifade mounting medium and #1.5 glass coverslips.
9. Store slides at 4°C protected from light.
10. Image slides within 48 hours of coverslipping.

cFos, pPDH, MOR, and inhibitory DREADD imaging in striatum

9. Perform imaging using a Zeiss LSM 900 confocal microscope.
10. Acquire tiled images at 20x magnification to capture the full striatal region of interest.
11. Use a sampling rate of 0.4 sampling and 4x line averaging to improve signal-to-noise ratio.
12. Perform an initial low-magnification preview scan to identify the region of interest prior to acquisition.
13. Acquire tiled images covering the full striatal region and fuse tiles using microscope software to remove stitching artifacts.
14. Apply minimal and uniform background adjustment across images to improve signal-to-noise ratio
15. Export final images as TIFF files without downsampling.
16. Image processing and analysis described in section 5.3.

5.5.11 Oprm1-Cre excitatory DREADD

Experimental procedure

1. Oprm1-Cre rats injected with Cre-dependent excitatory (AAV-hSyn-DIO-hM3D(Gq)-mCherry) DREADD viruses and were assigned to experimental groups receiving saline or Ibutamoren (IBU; 2x) in combination with clozapine-N-oxide (CNO), as described above. To maintain DREADD activation across the experimental window, rats received two CNO

injections: an initial injection concurrent with saline or IBU administration, followed by a second injection 1.5 hours later
2. Return rats to their home cage with ad libitum access to food and water.
3. Allow rats to remain undisturbed for 3.5 hours following the initial injection.
4. Following the 3.5-hour incubation period, perform transcardial perfusion as described in Section 5.5.1.
5. Section brains coronally (30 µm) and store tissue in cryoprotectant at −20°C until processing.

Striatum section selection and washes

1. Remove free-floating sections from cryoprotectant and transfer into 1x TBS
2. To localize the viral injection site, briefly screen sections under a brightfield microscope at low magnification (5x).
3. Identify sections corresponding to injection site based on the needle track and tissue landmarks within the anterior dorsal striatum.
4. Select three sections per animal centered on the injection site for IHC processing
5. Wash sections 5 times for 5 minutes each in fresh 1x TBS with gentle agitation.

Blocking (2 hours, room temperature)

1. Prepare blocking solution with the following:
    - 1x TBS
    - 0.1% Triton X-100
    - 4% normal donkey serum (NDS)
2. Incubate sections in blocking solution for 2 hours at room temperature.
3. Maintain gentle agitation throughout incubation.

Primary antibody incubation (48 hours, 4°C)

1. Mix primary antibodies in blocking solution prepared above
    - mouse anti-cFos (1:2000; Santa Cruz, sc-272343)
    - Rabbit anti-pPDH (1:1000; Cell Signaling Technology #E4V9L)
    - Guinea pig anti-MOR (1:1000; Millipore Sigma AB5509)
2. Incubate sections in primary antibody solution for 48 hours at 4°C, maintaining gentle agitation on an orbital shaker.
3. Following primary incubation, wash sections 5 x 5 in fresh TBS

Secondary antibody incubation (5 hours, room temperature)

1. Mix secondaries antibodies in blocking solution
    - cFos: donkey anti-mouse Alexa Fluor 555 (1:1000; Jackson ImmunoResearch)
    - pPDH: donkey anti-rabbit Alexa Fluor 647 (1:1000; Jackson ImmunoResearch)
    - MOR: Donkey anti-guinea pig Alexa Fluor 488 (1:1000; Jackson)
    - FRP: 594
1. Incubate sections for 5 hours at room temperature, maintaining gentle agitation on orbital shaker.
2. Following secondary incubation, wash sections 5 times in fresh TBS, for 5 mins

Nissl counterstaining

1. Incubate sections in NT (1:500 in TBS) for 10 minutes at room temperature.
2. Maintain gentle agitation and protect from light during incubation.

3. wash sections 5 times in fresh TBS, for 5 mins

Mounting and storage

1. Mount sections onto glass slides.
2. Allow excess buffer to drain without drying tissue.
3. Coverslip using glycerol-based antifade mounting medium and #1.5 glass coverslips.
4. Store slides at 4°C protected from light.
5. Image slides within 48 hours of coverslipping.

cFos, pPDH, MOR, and excitatory DREADD imaging in striatum

1. Perform imaging using a Zeiss LSM 900 confocal microscope.
2. Acquire tiled images at 20x magnification to capture the full striatal region of interest.
3. Use a sampling rate of 0.4 sampling and 4x line averaging to improve signal-to-noise ratio.
4. Perform an initial low-magnification preview scan to identify the region of interest prior to acquisition.
5. Acquire tiled images covering the full striatal region and fuse tiles using microscope software to remove stitching artifacts.
6. Apply minimal and uniform background adjustment across images to improve signal-to-noise ratio
7. Export final images as TIFF files without downsampling.
8. Image processing and analysis described in section 5.3.

6 IN VIVO CALCIUM IMAGING

6.1 Optimization of Cre-dependent GCaMP expression

To validate Cre-dependent GCaMP expression and optimize viral dosing for calcium imaging, initial dilution studies were performed. In a test group (n = 3), each hemisphere received a different viral titer of pGP-AAV-syn-FLEX-GCaMP7f-WPRE-GCaMP7f (Addgene #104492). Rats were allowed 4–6 weeks for viral expression prior to perfusion and histological analysis. Brain sections were examined to identify a dilution that provided the best cellular labeling without signal over-saturation or evidence of tissue damage, and this optimized titer (1:8) was used for all calcium imaging behavior imaging experiments.

6.2 Calcium imaging experimental set up

Calcium imaging recordings were conducted beginning approximately 6 to 8 weeks following viral injection and GRIN lens implantation, as described in section 2.4. Neuronal activity was recorded using a miniaturized epifluorescence microscope (nVoke 2.0 system; Inscopix) coupled to a baseplate-integrated GRIN lens. The miniscope was connected to a commutator system to allow unrestricted movement and prevent cable entanglement, and signals were transmitted to the Inscopix data acquisition system (DAQ).

Rats were briefly handled to remove the baseplate cover, then the miniscope was docked and secured to the baseplate by tightening the side screw. Following attachment, rats were returned to their home cage for recording. Imaging parameters were controlled using the online Inscopix Data Acquisition Software (IDAS). Recordings were performed at a frame rate of 20 Hz, while LED power, sensor gain, and electronic focus were adjusted on per each animal to optimize signal quality. Once optimal parameters were established for an individual animal, they were held as

constant as possible across all subsequent recording sessions to ensure consistent imaging of the same neuronal population. Field of view alignment was maintained across sessions using vasculature.

6.3 Calcium imaging recording sessions following GHSR activation

Baseline recordings were obtained once rats reached approximately 7 weeks post-surgery. Prior to this, rats were recorded every few days beginning ~4 weeks post-surgery to monitor viral expression and confirm the presence of stable, active cells.

For experimental sessions, a baseline recording (3 min) was first obtained. Rats were then briefly anesthetized to allow for IP injection of saline, IBU, or acyl-ghrelin, and were returned to their home cage for imaging. Recordings were conducted at time points corresponding to the established pharmacokinetics of each compound, with IBU recordings performed approximately 2 hours post-injection and acyl-ghrelin recordings performed ~15 minutes post-injection. In vivo calcium imaging revealed that intermediate-dose IBU produced peak striosomal activation approximately 2 hr following administration. Therefore, behavioral testing was initiated 2 hr post-injection, while tissue collection for cFos analysis was performed 3.5 hr post-injection to account for both peak IBU activity and the delayed kinetics of cFos protein expression.

For time-curve experiments, rats were recorded immediately following injection and then other time points. For IBU, recordings were obtained at 30 minutes post-injection and then hourly for up to 5 hours. For acyl-ghrelin, recordings were obtained immediately, and at 10 minutes, 30 minutes, 1 hour, and 2 hours post-injection. A minimum washout period of 2 days was allowed between IBU administrations to ensure complete clearance prior to recordings. Feeding in home cage was monitored for 4 hours during IBU and acyl-ghrelin conditions, as described in section 4.4.

6.4 Calcium imaging recording processing

All recordings were processed using Inscopix Data Processing Software (IDPS) and ImageJ. Preprocessing steps included pixel correction, cropping of the field of view (FOV), and spatial downsampling (2x) to reduce data size while maintaining sufficient resolution. A bandpass Gaussian filter (low: 0.005 $pixel^{-1}$; high: 0.5 $pixel^{-1}$) was applied, followed by motion correction using a reference frame to minimize movement-related artifacts. Neuronal activity was quantified by manually identifying and counting cells exhibiting visually detectable increases in fluorescence intensity, with analyses focused on the number of active neurons per session.

The nVoke miniscope permits adjustment of the focal plane along the z-axis, enabling recordings at multiple depths. In some rats, distinct neuronal populations were observed at separate focal planes (e.g., 600 and 950 z-plane units). Experiments were repeated at each depth to capture these populations, thereby increasing overall sampling. For longitudinal tracking, recordings were aligned to a reference cell map to enable tracking of neurons across sessions when the same FOV was maintained.

6.5 Exp 10: Calcium imaging of GHSR activation after IBU and aGHR administration

Statistical comparisons of activity across concentrations were performed using one-way ANOVA with appropriate post hoc tests under a within-subject design (**Fig. 3E**). All cell count data tables are publicly available (DOI: https://doi.org/10.7910/DVN/US8QTS).

To confirm targeting specificity and implant placement, rats that underwent Inscopix calcium imaging experiments were maintained for up to 6 months and then euthanized for histological validation. Brain tissue was processed for immunohistochemistry as described in 5.5. Sections were labeled for mu-opioid receptor (MOR) to define striosomal compartments, and GCaMP fluorescence was used to identify virus-expressing cells.

7 RABIES-ASSISTED MONOSYNAPTIC TRACING

We used a TRIO (tracing the relationship between input and output) strategy[4] to selectively trace monosynaptic inputs to LHb-projecting GPi neurons using procedures recommended by[5,6]. In a different cohort of rats, we used a standard helper virus and RVΔG injection procedure to achieve Cre-dependent tracing of SNc neurons using *Th-Cre* transgenic rats [7].

7.1 Intracranial surgery and tissue preparation

7.1.1 HELPER VIRUS INJECTION FOR TRIO STRATEGY

We anesthetized wildtype male and female Sprague-Dawley rats (300-350g) with 5% isoflurane. We administered 2.5 mg/kg ketoprofen for analgesia, shaved the rats to expose the head incision area, and secured rats on a stereotaxic frame and maintained thereafter with 2-3% isoflurane. After treating the incision area with Betadine and 70% ethanol, we made a midline incision large enough to reveal the bregma and lambda landmarks. We used a metal spatula to expose the skull surface and we placed alligator clips to secure the skull surface for craniotomy. We achieved a flat-skull position by adjusting the incisor bar height until the bregma and lambda landmarks were at the same depth, and the incisor bar height was recorded to assist in skull positioning for the second surgery. We used a round burr drill bit to perform craniotomy at the injection sites above the LHb and GPi. After gently removing the dura mater with a syringe tip, we lowered syringes (10 µl Hamilton syringe, 33-gauge blunt tips) to inject the viruses. Virus injections targeted AP −3.4 mm, ML ±0.8 mm, DV −5.0 mm for LHb and AP −2.2 mm, ML ±2.8 mm, DV −7.8 for GPi of the same hemisphere. We injected 500 nl of AAVrg-EF1a-Cre (Addgene, cat# 55636-AAVrg; titer: 2.6×10^{13}) into LHb. We injected 500 nl of a mixture containing AAV1-syn-FLEX-splitTVA-EGFP-tTA (Addgene, cat# 100798-AAV1; titer: 8.5×1010 gc) and TREtight-mTagBFP2-B19G (Addgene, cat# 100799-AAV1; titer: 1.6×1012 GC/ml) into GPi. Both injections were delivered at 100 nl/min and syringes were withdrawn after a 5 min diffusion period. The incision site was then sutured, and antibiotics were applied to the site. Rats underwent postoperative monitoring for three days.

7.1.2 HELPER VIRUS INJECTION FOR SNC TRACING

Surgical procedures follow those described in section 7.1.1. We used *Th-Cre* Long-Evans rats (300-350g) for the SNc tracing experiments[7]. We injected 500 nl of a mixture containing AAV1-syn-FLEX-splitTVA-EGFP-tTA (Addgene, cat# 100798-AAV1; titer: 8.5x1010 gc) and TREtight-mTagBFP2-B19G (Addgene, cat# 100799-AAV1; titer: 1.6x1012 GC/ml) into SNc. Injections targeted SNc at AP −5.4 mm, ML ±2.2 mm, and DV −7.9 mm.

7.1.3 RVΔG INJECTIONS FOR TRIO EXPERIMENT

After 4 weeks from the initial helper virus injection, we performed IC surgery in a BSL2 setting to inject RVΔG. The initial procedures leading up to skull exposure follow the description outlined in 7.1.1. RVΔG was rapidly thawed in a water bath warmed to 37 ˚C, and was immediately placed into an ice bath until syringe loading. Using the same entry site from the previous craniotomy, we positioned injectors to AP −2.2 mm, ML ±2.8 mm, DV −7.8 to target the GPi. We injected the rats

with 500 nl of RVΔG-mCherry (Wickersham Lab, 8.7x109 gc/ml) at a 100 nl/min flow rate and 5 min diffusion period. Wound closure and postoperative care procedures follow those described in 7.1.1. All materials that directly contacted RVΔG were treated with 10% bleach and then discarded. Rats were maintained for 7 days before perfusion to allow virus infection.

7.1.4 RVΔG INJECTIONS FOR SNC TRACING EXPERIMENT

Procedures are identical to 7.1.3 except for the injection target. We targeted SNc at AP −5.4 mm, ML ±2.2 mm, and DV −7.9 mm under the same injection parameters.

7.1.5 TRANSCARDIAL PERFUSION FIXATION

Following a 7 d incubation period, rats were lightly anesthetized and injected with IBU (1 mg/kg, IP) 4 h prior to perfusion. We then deeply anesthetized the rats in isoflurane, and performed transcardial perfusion to circulate 200 ml of isotonic PBS at a flow rate of 60 ml/min. Next, we infused 350 ml of 4% PFA mixed in PBS and brains were carefully removed. We left the brains in the PFA mixture overnight and then transferred them into a 30% sucrose solution in PBS until brains lost buoyancy.

7.1.6 CRYOSTAT SECTIONING

We first blocked the brains by removing half of the cerebellum, we then secured brains onto cryostat pedestals using Leica Cryo-Gel. We used crushed dry ice to rapidly freeze brains. 30 min later, we positioned them on the specimen head of a Leica cryostat and maintained chamber and object temperatures at −16 ºC for 15 min prior to cutting. The cutting angle was adjusted to 5 º and we collected 40 µm sections into four series. Cryopreserving was made by mixing isotonic PBS containing 30% ethylene glycol and 20% glycerol. We stored sections at −20 ºC in light-protected conditions until further processing.

7.2 Histological analysis for retrograde tracing

7.2.1 STRIATAL IMMUNOHISTOCHEMISTRY

Tissue sections were shielded from light as much as possible through each of the following IHC steps. We transferred striatal sections from one series into mesh trays containing isotonic PBS and washed them for 10 min with 3 changes (10x3) under gentle agitation to remove cryopreservant. Next, we transferred the well trays into a blocking solution made of PBS containing 0.3% Triton X-100, 2% normal donkey serum. After a 2 h incubation period, we transferred tissues into primary antiserum containing antibodies raised against c-Fos (Host: Mouse, 1:500; Santa Cruz Biotechnology Cat# sc-271243, RRID:AB_10610067) and the c-terminal of the MOR (Host: Rabbit, 1:1,000; Abcam Cat# ab134054, RRID:AB_3122135) dissolved in blocking solution. We left tissue sections to incubate for 48 h at 4 ºC.

After a 10×3 wash, we transferred tissues into secondary antiserum containing antibodies raised against mouse IgG (Alexa Fluor 488; Donkey, 1:500; Jackson ImmunoResearch Labs Cat# 715-545-151, RRID:AB_2341099) and rabbit IgG (Alexa Fluor 647; Host: Donkey, 1:500; Jackson ImmunoResearch Labs Cat# 711-605-152, RRID:AB_2492288) dissolved in blocking solution. Tissue sections were left to incubate at room temperature for 5 h and underwent a final 10×3 wash. Free-floating sections were mounted onto glass slides, air-dried, and coverslipped using Dapi-Fluoromount-G (Electron Microscopy Sciences, Cat #17984-24) and sealed with clear nail polish.

7.2.2 HISTOLOGICAL LOCALIZATION OF SITE SECTIONS

Tissue sections were shielded from light as much as possible through each of the following IHC steps. We transferred striatal sections from one series into mesh trays containing isotonic PBS and washed them for 10 min with 3 changes (10x3) under gentle agitation to remove cryopreservant. We directly mount the tissue sections onto glass slides after the washes. Once dry, we coverslip with a Fluoromount-G (Electron Microscopy Sciences, Cat #17984-25) medium that lacks DAPI to allow direct visualization of endogenous mTagBFP2 signal.

7.3 Microscopy, image processing, and analysis

We used an Olympus VS200 slide scanner to capture epifluorescence images from the RVΔG tracing experiments. We obtained three-channel mosaic images for each section using a x10 objective lens and then exported images for the channels separately as grayscale 16-bit PNG-formatted files. We batch-processed image conversion to 8-bit grayscale with Adobe Photoshop by adjusting the *Levels* parameter. Histograms were used to guide the lower and upper bounds to achieve comparable image scaling between subjects. No nonlinear (gamma) transformations were used.

To facilitate analysis of striosomes, we opened the images as different layers on Adobe Illustrator. Bounding boxes were placed around each mCherry-positive neuron, and we toggled between layers to determine whether they colocalized cFos or whether they were in striosomes (determined using the MOR-labeling channel). Bounding boxes were colored and layer-sorted based on cFos colocalization and compartmental membership. We then tabulated the final counts onto excel spreadsheets.

7.4 Exp 11: Monosynaptic tracing of striosomal circuit analysis

RV-mCherry+ striosomal neurons were quantified for both projection pathways and compared using an unpaired t-test (**fig. S9T, top**). To determine pathway-specific activation following GHSR stimulation (1x IBU), colocalization of cFos within RV-mCherry+ striosomal neurons was assessed. Counts were expressed as the percentage of RV-mCherry+ striosomal neurons co-expressing cFos. These percentages were compared between GPi LHb and daSNC pathways using an unpaired t-test (**fig. S9T, bottom**). All statistical analysis were performed using GraphPad Prism.

Raw image datasets are publicly available (DOI: https://doi.org/10.7910/DVN/ZRLRXV).

8 MODELING DECISION-MAKING

8.1 "Decision-space" model

Here, we test the experimental data against the predictions of the "decision-space" model introduced in our previous work[8]. The decision-space model describes how a specific striatal circuit transforms high-dimensional cortical inputs into context-sensitive choices. Physiologically, cortical neurons excite fast-spiking interneurons (FSIs) and two intermingled populations of projection neurons in the striatum: striosomes (sSPNs) and the surrounding matrix (mSPNs). Striosomal neurons in the direct (dsSPNs) and indirect (isSPNs) pathways each gate distinct subpopulations of midbrain dopamine neurons via globus pallidus internus (GPi) → lateral habenula (LHb) → rostromedial tegmental area (RMTg) → globus pallidus externus (GPe) circuits, respectively. The dopamine signals then feed back onto both sSPNs and mSPNs, controlling which streams of information receive gain and are propagated for decision-making.

Geometrically, each sSPN subpopulation encodes one of several orthogonal "decision-dimensions" (e.g. reward-predominant, cost-predominant), equivalent to the leading principal

components of cortical activity. Dopamine gating probabilistically masks a subset of these axes, carving out a lower-dimensional "decision-space" subspace in which the network operates. Mathematically, this is implemented as a diagonal gain matrix whose entries, set by daSNc activity via a logistic function, select which decision-dimensions are retained.

Behaviorally, matrix neurons (dmSPNs/imSPNs) compute action and inaction values by summing cortical inputs along the retained axes. In this way, matrix neurons define choice, given the contextual decision-space. In this framework, simple decisions engage only the most relevant dimension (producing fast, stereotyped choices) and complex trade-offs recruit multiple dimensions (producing nuanced choices).

In summary, the model links physiology to behavior via a geometrically-interpretable decision-space.

8.2 Dimension of the decision-space based on striosome->LHb activity

To model the probability of engaging different numbers of decision-space dimensions, we assumed a total of 10 potential dimensions relevant to the tasks (for details of the model, see **Summary of the "decision-space" model** and our previous work[8]). The probability, p, of successfully activating any single decision-dimension was made dependent on a generic striosome activity level, x, following the sigmoid function $p(x) = 1/(1 + e^{x})$ as in our previous work[8]. For DMS striosome activity in **Fig. 5D and fig. S14l,** we used $x =$ DMS striosome activity and for DLS striosome activity in **fig. S15l,** we using $x = -$ DLS striosome activity. Using the binomial probability mass function, we then calculated the exact probabilities of activating 0, 1, or 2+ dimensions for a range of x values between 0 and 4. These probabilities, representing the likelihood of occupying a 0D, 1D, …, 10D decision-space, were plotted using a stacked area chart to visualize their dependence on the underlying striosome activity.

For code, see
https://github.com/dirkbeck/ghrelin_project/blob/main/dimensionality_by_strio_activity_10_levels.py

Approach/avoid behavior based on the decision-space

To link changes to the striosome->LHb circuit to context-dependent decision-making, we use our decision-space model of the circuit (for details of the model, see **Summary of the "decision-space" model** and our previous work[8]). In the model, when striosome->LHb activity is low, the decision-space is high-dimensional, for instance incorporating environmental information about reward and cost into decisions. A low-dimensional decision-space (high striosome->LHb activity) might either incorporate reward or cost, but not both. Using this decision-space constructed by striosomes, LHb, and connected neurons, matrix neurons compute action values.

Concretely, our model takes as input two continuous variables, the normalized reward magnitude $I_r \in [0,1]$ and the normalized cost magnitude $I_p \in [0,1]$, together with a scalar G encoding various levels of striosome->LHb activity. We evaluate the model on a 200×200 grid of (I_r, I_p) pairs, computing at each point the probability of avoidance both with and without the sigmoid gating term. The single-trial output is the avoidance probability $P_{\text{avoid}}(I_r, I_p; G)$.

Mathematically, we represent striosome->LHb activity by a scalar D and use two sigmoid gates, representing the incorporation of decision-dimensions relevant to the stimuli in the environment (e.g. use a reward-related decision-dimension when reward information is present):

$$g_1 = \frac{1}{1 + e^{-k_{\text{sig}}(D - \theta_{\text{low}})}}, \qquad g_2 = \frac{1}{1 + e^{-k_{\text{sig}}(D - \theta_{\text{high}})}}$$

Where k_{sig} is the steepness of the gating sigmoids, and θ_{low}, θ_{high} are their activation thresholds.

We then define two decision-dimensions:

$$d_1 = I_r, \quad d_2 = I_p$$

and use g_1 and g_2 (above) to gate contributions on a third decision-dimension that scales with both reward and cost, $I_r\, I_p$. We then enforce a relationship where the decision-space grows as striosome->activity reduces:

$$f(D) \;=\; 1 \;-\; \frac{1}{1 + e^{-k_{\text{dim}}(D - D_{\text{mid}})}}$$

where k_{dim} and D_{mid} shape the sigmoidal relationship.

We initialize

$$Q_{\text{avoid}} = w_p\, I_p, \qquad Q_{\text{app}} = w_r\, I_r$$

where w_r and w_p are static weights.

If the dynamic decision-space strategy is used (but not if it is not), we calculate action values given the decision-space:

$$Q_{\text{avoid}} \mathrel{+}= \; f(D)\, \alpha\, g_3\left(I_r I_p\right), \qquad Q_{\text{app}} \mathrel{+}= \; f(D)\, \beta\, g_4\left(I_r\left(1 - I_p\right)\right)$$

where α and β are scaling coefficients adjusting the sensitivity.

Choices then arise from a softmax rule

$$P_{\text{avoid}} = \frac{\exp(\gamma\, Q_{\text{avoid}})}{\exp\left(\gamma\, Q_{\text{app}}\right) + \exp(\gamma\, Q_{\text{avoid}})}$$

where γ is the softmax gain.

To generate **Fig. 5E** and **fig. S10B**, we evaluate P_avoid(D) at D=0, D=1, and D=10 (baseline, low, high), then define:

$$\Delta P_{\text{low}}\left(I_r, I_p\right) = P_{\text{avoid}}\left(I_r, I_p; D = 1\right) - P_{\text{avoid}}\left(I_r, I_p; D = 0\right)$$

$$\Delta P_{\text{high}}\left(I_r, I_p\right) = P_{\text{avoid}}\left(I_r, I_p; D = 10\right) - P_{\text{avoid}}\left(I_r, I_p; D = 0\right)$$

Plotting ΔP over $\left(I_r, I_p\right)$ quantifies the model's prediction about how increasing striosome->LHb activity selectively increases avoidance in the high-reward, high-cost portion of the grid.

For code, see https://github.com/dirkbeck/ghrelin_project/blob/main/decision_making_maps.py

8.3 Context- and task-dependent effects on approach/avoid

Here, we illustrate the model's prediction that different ghrelin doses produce context-dependent shifts in approach/avoid decision-making. We represent the task context as a continuous variable $c \in [0,1]$ (0 = cost only, 0.5 = conflict, 1 = reward only) and IBU dose $D \in [0,10]$ in arbitrary units. Both axes are evaluated on a 200×200 grid.
Because ghrelin hyperactivates the striosome→LHb circuit at moderate doses but not at low or high doses (an inverted-U relationship, consistent with our imaging and cFos data), we model striosome activity as a Gaussian function of dose:

$$s(D) = \exp\left(-\frac{(D-D_{\text{peak}})^2}{2\sigma_D^2}\right)$$

with peak dose $D_{\text{peak}} = 3$ and width $\sigma_D = 1.2$.
A baseline decision variable is defined as a linear function of context, capturing the intuition that cost-only contexts favor avoidance and reward-only contexts favor approach: $Q_{\text{base}}(c) = w_{\text{ctx}}\,(c - 0.5), w_{\text{ctx}} = 6$. The ghrelin-driven modulation of choice is restricted to conflict-like contexts via a Gaussian weighting centered at $c = 0.5$:

$$w_{\text{conflict}}(c) = \exp\left(-\frac{(c-0.5)^2}{2\sigma_c^2}\right), \sigma_c = 0.12$$

This captures the experimental finding that IBU changes behavior only when competing reward and cost signals are present. The full decision variable is then:

$$Q_{\text{total}}(c, D) = Q_{\text{base}}(c) - w_g\, w_{\text{conflict}}(c)\, s(D), w_g = 5$$

where w_g scales the magnitude of the ghrelin effect. The probability of approach is given by a logistic transformation:

$$P_{\text{approach}}(c, D) = \frac{1}{1 + \exp\left[-\beta\, Q_{\text{total}}(c, D)\right]}, \beta = 10$$

To build the phase diagram (**fig. S10C**), we plot $P_{\text{approach}}(c, D)$ on a colormap, with the $P = 0.5$ contour overlaid in black to mark the boundary between net approach and net avoidance. The resulting diagram shows that at low and high doses the boundary sits near $c = 0.5$ (baseline conflict behavior), while at moderate doses (near $D = 3$) the boundary bulges upward, indicating that a more reward-dominant context is required to elicit approach. Away from the conflict region, behavior is unaffected by dose, reproducing the experimental result that IBU leaves pure reward-only and pure cost-only choices unchanged.
For code, see https://github.com/dirkbeck/ghrelin_project/blob/main/phase_plot.py.

8.4 Ability to perform tasks depending on striosome->LHb activity

Task performance was conceptualized as a utility function, $U(x)$, which aimed to maximize the benefit of meeting task requirements while minimizing a cost associated with deviating from a baseline striosome activity level of $x = 0$. We used $n = 4$ potential dimensions and the sigmoid activation probability $p(x) = 1/(1 + e^x)$, where x = DMS striosome activity and $x = -$ DLS striosome activity. The benefit $B(x)$ for a task requiring at least k dimensions ($k \in \{0, 1, 2\}$) was set equal to the cumulative binomial probability $P\big(Y \geq k \big| n = 4, p(x)\big)$. A quadratic cost $C(x) = cx^2$ was subtracted, using a cost factor $c = 0.1$. The resulting utility curves $U(x) = B(x) - C(x)$

for the 0D, 1D, and 2D tasks were plotted over a range of striosome activity x. The optimal activity level for each task, representing the peak of its respective utility curve, was determined numerically and indicated on the plot. The drop in performance was calculated by setting striosome activity to 2 arbitrary units (for higher dorsomedial striosome activity when ghrelin levels are high) and subtracting the new performance from the optimal performance. A floor of performance of 0 was used.

For code, see https://github.com/dirkbeck/ghrelin_project/blob/main/ability_to_perform_tasks.py.

8.5 Computational Modeling Data and Code Availability

The published article includes all datasets and code generated or analyzed during this study. Code generated for this study have been deposited at github at https://github.com/dirkbeck/ghrelin_project.

9 MOTOR ANALYSIS

All functions are submitted under DOI: https://doi.org/10.5281/zenodo.20651417

To point the reader to each specific method and function, we also used:

https://github.com/atanugiri/GhrelinBehaviorQuantification.git

Data is published at DOI: https://doi.org/10.7910/DVN/G8CBKJ.

9.1 Video Acquisition and Preprocessing

Motor behavior was analyzed from behavioral trials described in section 4. A single camera captured four mazes simultaneously and each recording was therefore separated as a single video file containing the activity of rats in four independent separate arenas. The videos can be found at DOI: https://doi.org/10.7910/DVN/G8CBKJ.To enable individual analysis of each maze, videos were automatically split into four quadrants using a custom Python script split_video_quadrants.py (https://github.com/atanugiri/GhrelinBehaviorQuantification/blob/main/scripts/analysis/split_video_quadrants.py). Each split video was stored and processed independently in subsequent steps. The split videos can also be found at the same data deposit. This preprocessing was performed specifically to enable quantitative motor analysis of individual rats.

9.2 Pose Estimation with DeepLabCut

Pose estimation and model training were carried out using **DeepLabCut (v3.0.0rc8)**[9]. Training and inference were executed on a CUDA-enabled laboratory workstation equipped with an NVIDIA T1000 GPU (cuDNN v9.01.00), and PyTorch v2.5.1+cu121 was used for model training. The purpose of this step was to estimate the pose of different body parts from behavioral videos, enabling quantitative analysis of motor features. Video recordings of rats performing the behavioral task were provided as input; the trained DeepLabCut model produced per-frame x–y coordinates and likelihoods for each labeled body part. These pose time series were the primary input for all downstream analyses (feature extraction, summary statistics, and hypothesis testing). To provide a clear overview of the workflow, the major steps in the DeepLabCut pipeline are described below.

a) A DeepLabCut project was first initialized using representative behavioral videos as input. The output of this step was a project directory containing the configuration file and registered video paths. Following project creation, additional recordings were incorporated using the command:

deeplabcut.add_new_videos(config_path, new_videos, copy_videos=True, extract_frames=False)

b) For frame extraction, representative frames were sampled from each video. The input was the set of registered videos, and the output was a collection of still images stored in the labeled-data subdirectory of the project. We extracted five frames per video using automatic uniform sampling. Each frame was then cropped manually to retain only the maze region, thereby excluding irrelevant portions of the field of view. This step was performed with:

```
deeplabcut.extract_frames(
  config_path, mode='automatic',
  algo='uniform',
  crop='GUI',
  userfeedback=True
)
```

c) The extracted frames were then labeled interactively. The input was the set of sampled and cropped frames, and the output consisted of annotation files in .h5/.csv format along with labeled images in the project's labeled-data subdirectory. Labeling was performed using the napari-DeepLabCut GUI, which allowed manual annotation of the predefined body parts specified in the configuration file (Head, Neck, Midback, Lowerback, Tailbase, and four maze corners). This step was initiated with:

```
deeplabcut.label_frames(config_path)
```

d) The annotated frames were subsequently inspected to confirm labeling accuracy. The input was the labeled dataset, and the output was a visual verification of correct placement of body-part labels across frames. This quality-control step was carried out with:

```
deeplabcut.check_labels(config_path)
```

e) Before training, a train/test dataset was generated from the labeled frames. The input was the manually annotated images from the labeled-data subdirectory, and the output was a structured training dataset stored within the project's training-datasets directory. This step was performed with:

```
deeplabcut.create_training_dataset(config_path)
```

f) Network training was then performed using the training dataset as input. The output of this step was a trained ResNet-50–based model capable of predicting body-part positions across video frames. Training was carried out on the laboratory workstation equipped with an NVIDIA T100 GPU, running for 200 epochs. The process was executed with:

```
deeplabcut.train_network(
  config_path,
  shuffle=1,
  trainingsetindex=0,
  device="cuda:0",
  max_snapshots_to_keep=5,
  displayiters=100,
  save_epochs=5,
  epochs=200,
)
```

g) After training, the accuracy of the network was evaluated. The input was the trained model along with the annotated training and test frames, and the outputs were both quantitative error metrics and diagnostic plots that compared manual labels against model-predicted points. This assessment was carried out with:

```
deeplabcut.evaluate_network(config_path, shuffle=1, plotting=True)
```

h) Once satisfactory accuracy was confirmed, the trained network was applied to the full set of behavioral videos. The input was the list of registered videos, and the output consisted

of pose-estimation files (.h5 and .csv) containing x–y coordinates and likelihoods for each labeled body part across all frames. This step was executed with:

```
deeplabcut.analyze_videos(
    config_path,
    videos=videolist,
    shuffle=1,
    gputouse="cuda:0",
    save_as_csv=True
)
```

i) The resulting trajectory files, containing x–y coordinates and likelihood values for each body part across frames, were further refined using the median filter implementation provided by DeepLabCut. The input was the set of raw pose-estimation files, and the output was a set of filtered .csv files with low-confidence detections removed based on a likelihood threshold of 0.05. This filtering was performed with:

```
deeplabcut.filterpredictions(
    config_path,
    videolist,
    shuffle=1,
    filtertype='median',
    p_bound=0.05
)
```

The filtered trajectory files were subsequently used as the input for all downstream feature extraction analyses.

Motor Feature Extraction for Behavioral Tasks Presented Under **fig. S12, S14.**

9.3 **Estimation of trajectory curvature**

Represented in (**fig. S11A, S13**).

9.3.1 CODE LOCATION AND EXECUTION

All analyses were run from the project root https://github.com/atanugiri/GhrelinBehaviorQuantification/blob/main/runme.sh. The DeepLabCut pose-estimation output files (CSV format) are archived at DOI https://doi.org/10.7910/DVN/G8CBKJ. To reproduce the analyses, users should download the Dataverse archive and extract the pose-estimation CSVs into the data directory of the project root (https://github.com/atanugiri/GhrelinBehaviorQuantification/tree/main/data). The database table (dlc_table) containing metadata and trial information is also located in the data directory as CSV files for offline analysis (https://github.com/atanugiri/GhrelinBehaviorQuantification/tree/main/data).

The curvature feature was implemented in trajectory_curvature module (https://github.com/atanugiri/GhrelinBehaviorQuantification/blob/main/scripts/features/trajectory_curvature.py). Figures and statistical reports generated by the runme.sh from the project root and are saved in results directory. Detailed statistical results can be found in the 'Statistical data deposition section'. Source code, notebooks, and environment files are archived at Zenodo: DOI: 10.5281/zenodo.20651417. All computations were performed in Python (NumPy, SciPy, pandas, Matplotlib, seaborn) using Visual Studio Code with Jupyter notebook integration.

9.3.2 INPUT DATA AND NORMALIZATION OF POSE TRAJECTORIES.

For each trial, pose trajectories (DeepLabCut outputs) and frame rate were accessed via CSV metadata table. Body-part coordinates were obtained with

https://github.com/atanugiri/GhrelinBehaviorQuantification/blob/main/scripts/analysis/normalized_bodypart.py, which returns temporally interpolated and spatially min–max normalized coordinates in a fixed, unit-like arena space.

9.3.3 CURVATURE COMPUTATION FOR TRAJECTORIES.

Per-frame curvature was then defined as:

$$\kappa(t) = \frac{|\dot{x}(t)\,\ddot{y}(t) - \dot{y}(t)\,\ddot{x}(t)|}{(\dot{x}(t)^2+\dot{y}(t)^2)^{3/2}} \quad \ldots\ldots (1)$$

Where,

- $x(t)$ and $y(t)$ be the (optionally smoothed) Cartesian coordinates of the tracked body part at frame t.
- $\dot{x}(t)$ and $\dot{y}(t)$ are the first temporal derivatives of $x(t)$ and $y(t)$, respectively.
- $\ddot{x}(t)$ and $\ddot{y}(t)$ are the corresponding second temporal derivatives.

To avoid unstable values at near-zero speeds, frames with speed below a threshold were set to 0. We used speed_thresh = 1e-2 (normalized-units/s) unless stated otherwise. The per-trial summary statistic was the mean of all finite $\kappa(t)$ values.

9.3.4 KEY HYPERPARAMETERS FOR TRAJECTORY CURVATURE FUNCTION.

When smoothing is enabled, $x(t)$ and $y(t)$ are each convolved with a moving-average (boxcar) filter using scipy.ndimage.uniform_filter1d. We used a symmetric window of window = 23 samples (odd length enforced internally); smoothing was applied before derivative estimation. The following parameters were used: bodypart = 'Midback', smooth = True, window = 23 samples, speed_thresh = 1e-2 normalized-units/s, and time_limit = None (full trial). Per-trial frame rate was read from the database and validated to be > 0. Batch processing across multiple trials was performed thereafter, which applies the computation to lists of trial IDs and returns aggregated DataFrames suitable for statistical analysis.

9.4 Quantification of locomotor velocity

Represented in **fig. S11B, S13**

9.4.1 CODE LOCATION AND EXECUTION.

Velocity was analyzed to quantify locomotor activity over time. The velocity feature was implemented in motion_features module (https://github.com/atanugiri/GhrelinBehaviorQuantification/blob/main/scripts/features/motion_features.py). Project structure, data organization, and archival details are as described in section 9.3 of the estimation of trajectory curvature section above.

9.4.2 INPUT DATA AND NORMALIZATION OF POSE TRAJECTORIES.

Input data handling and normalization procedures are identical to those described for trajectory curvature (section 9.3.2).

9.4.3 VELOCITY COMPUTATION.

Let (x_k, y_k) denote the (normalized) body-part coordinates at time $t_k = k/\text{frame\_rate}$. We first compute frame-to-frame displacement

$$d_k = \sqrt{(x_{k+1} - x_k)^2 + (y_{k+1} - y_k)^2}, \ldots\ldots(2)$$

and per-frame speed

$$v_k = \frac{d_k}{t_{k+1}-t_k} = \text{frame\_rate} \cdot d_k \quad \text{(for uniform sampling)}, \ldots\ldots(3)$$

Here,

- x_k, y_k: normalized x- and y-coordinates of the selected body part at frame k,

- t_k: time (in seconds) corresponding to frame k,
- frame_rate: video sampling rate (frames per second),
- d_k: Euclidean distance (displacement) between consecutive frames,
- v_k: instantaneous speed between frame k and $k+1$.

These arrays are produced by the function, compute_motion_features in motion features module. Our scalar velocity metric for each trial is the time-averaged speed expressed in units/min:

$$v_{\text{per min}} = \frac{\sum_k d_k}{t_N - t_0} \times 60 \quad \ldots\ldots(4)$$

Where,

- d_k denotes the frame-to-frame displacement between consecutive positions.
- $t_N - t_0$ represents the total trial duration in seconds.

This summary statistic is computed by compute_motion_features_per_minute function in motion_features module.

9.4.4 KEY HYPERPARAMETERS OF VELOCITY FUNCTION.

Velocity was computed for bodypart = 'Head', with smooth = False (no temporal smoothing), and time_limit = None (full trial). Batch processing across multiple trials was performed thereafter, which applies the computation to lists of trial IDs and returns aggregated DataFrames with per-trial velocity metrics suitable for statistical analysis.

9.5 Quantification of head–body angle (radians)

Represented in **fig. S11C, S13**.

9.5.1 CODE LOCATION AND EXECUTION.

Angle features were implemented in angle_features module (https://github.com/atanugiri/GhrelinBehaviorQuantification/blob/main/Python_scripts/Feature_functions/angle_features.py). Project structure, data organization, and archival details are as described in section 9.3, trajectory curvature section above.

9.5.2 INPUT DATA AND NORMALIZATION OF POSE TRAJECTORIES.

Input data handling and normalization procedures are identical to those described for trajectory curvature (section 9.3.2), with pose coordinates loaded directly from DeepLabCut CSV output files and filtered by likelihood threshold.

9.5.3 COMPUTATION OF HEAD–BODY ANGLE.

We defined two vectors per frame:

$\mathbf{v}_{\text{body}} = \mathbf{h} - \mathbf{t}$ (Tailbase $\rightarrow$ Head), $\mathbf{v}_{\text{head}} = \mathbf{h} - \mathbf{n}$ (Neck $\rightarrow$ Head) ……(5)

Where,

- $\mathbf{h}, \mathbf{n}, \mathbf{t}$ are the Head, Neck, and Tailbase coordinates.

The head–body angle, $\theta_{\text{HB}}(t)$ was defined as the signed angle (in radians) between the instantaneous body and head direction vectors:

The *head–body angle* $\theta_{\text{HB}}(t)$ is the signed angle (radians) between these vectors,

$$\theta_{\text{HB}}(t) = \text{atan2}\big(u_x v_y - u_y v_x,\ \text{u} \cdot \text{v}\big) \quad \ldots\ldots(6)$$

Where,

- $u = v_{\text{body}}$ and $v = v_{\text{head}}$ denote the unit vectors representing the body and head orientations, respectively.

By convention, positive values indicate a counterclockwise rotation of the head relative to the body axis; $\theta_{\text{HB}}(t) \in (-\pi, \pi]$ per frame. These computations are performed by the function angle_features_for_trial in angle_features module, which returns per-frame timeseries data and summary statistics including mean and 95th percentile values for head-body misalignment.

9.5.4 KEY HYPERPARAMETERS OF HEAD–BODY ANGLE FUNCTION.

We used: likelihood_threshold = 0.65 (filtering low-confidence pose estimates), smooth_window = None (no smoothing applied), and body parts Head, Neck, Midback, Lowerback, and Tailbase for feature extraction. Per-trial frame rate was retrieved from the database metadata and validated to be >0. Batch processing across multiple trials was performed thereafter, which applies the computation to lists of trial IDs and returns aggregated DataFrames with per-trial angle metrics suitable for statistical analysis.

9.6 **Analysis of detailed movement metrics**

To test whether the rats moved differently across contexts, we extracted four movement metrics from the x- and y- coordinates of the rats as they performed the tasks. During this process, raw positional records (X_center, Y_center) were first cleansed of missing values and then smoothed in time using a one-frame Gaussian kernel to suppress jitter without altering overall path structure.

From the smoothed coordinates we computed instantaneous displacements

$$d_i = \sqrt{(x_{i+1} - x_i)^2 + (y_{i+1} - y_i)^2}$$

and headings

$$\theta_i = \arctan 2\left(y_{i+1} - y_i,\ x_{i+1} - x_{(i)}\right)$$

Turn angles at each time step were defined as the wrapped difference between successive headings,

$$\Delta\theta_i = \left((\theta_{i+1} - \theta_i + \pi) \bmod 2\pi\right) - \pi$$

yielding the signed change in direction.

From these time series we distilled four session-level metrics (see **fig. 12A** for illustrations). The mean step length is simply the average of all d_i values, reflecting the animal's typical stride. The mean absolute turn-angle is the average of $|\Delta\theta_i|$, capturing the magnitude of directional changes irrespective of sign. Turn frequency quantifies the proportion of frames for which $|\Delta\theta_i|$ exceeds 90°, indexing the rate of sharp reorientations. Finally, the MSD exponent describes how spatial dispersion grows with time: we compute the mean squared displacement for integer lags l,

$$\mathrm{MSD}(l) = \langle (x_{t+l} - x_t)^2 + (y_{t+l} - y_t)^2 \rangle_t$$

then fit a line to $\log(\mathrm{MSD})$ versus $\log(l)$ and take its slope as the exponent. These four metrics together summarize the animal's locomotor scale, turning behavior, reorientation frequency, and exploration-diffusion dynamics.

To create the plots in **fig. S12C,** for each behavioral metric and task in the non-manipulated cohort, we first collated the session-level summaries for rats that underwent both saline and ghrelin treatments. We then performed a two-tailed paired t-test across each metric's saline versus ghrelin values, recording the mean difference and its associated p-value (Food+light mean step length p=0.008, Toy+light average turn angle p=0.011, Toy+light diffusion p=0.006, Toy+light turn frequency p=0.009).

To create the plot in **fig. S12C**, we built a table of (task, metric, p) entries from all paired comparisons. For each cell we computed signed_logp = $-\log_{10}(p)$ multiplied by the sign of the change in the metric, so that positive bars indicate increases under ghrelin and negative bars

indicate decreases. We then arranged these signed_logp values into a matrix with tasks on the x-axis and metrics represented by offset bars at each task position. Horizontal dashed lines at ± – $\log_{10}$ (0.05) and ± – $\log_{10}$ (0.01) delineate significance thresholds, and a central zero line marks the transition between positive and negative effects.

For code, see https://github.com/dirkbeck/ghrelin_project/blob/main/analysis.py. For data preparation, follow the instructions in the project README https://github.com/dirkbeck/ghrelin_project/blob/main/README.md.

In summary, by computing four key session-level summaries, we quantify the rats' locomotor patterns under saline versus ghrelin. Paired comparisons within each task showed that low-dose IBU decreased strides in the Food+light context, increased diffusion in the Toy+light context, and decreased turns there as well. This analysis confirms that ghrelin's modulation of the striosome->LHb circuit produces measurable, task-specific changes in how rats move.

9.6.1 Computational Modeling Data and Code Availability

The published article includes all datasets and code generated or analyzed during this study. Excel tables with the x/y coordinate data over time are deposited in the Harvard database, see https://doi.org/10.7910/DVN/TNT3FV,. Code generated for this study have been deposited at github at https://github.com/dirkbeck/ghrelin_project.

10 DATA DEPOSITION

Fig. 1
C-D) Non-conflict and Conflict 2x IBU Long Evans:
Food alone
https://doi.org/10.7910/DVN/DCB1IH
Toy alone
https://doi.org/10.7910/DVN/YMYXO0
Light alone
https://doi.org/10.7910/DVN/JW2C3Q
Food+light
https://doi.org/10.7910/DVN/0V6WKG
Toy+light
https://doi.org/10.7910/DVN/ZUH9YY

E) Chow in home cage 2x: https://doi.org/10.7910/DVN/GFLZYM

F) Food consumption in Food alone task 2x: https://doi.org/10.7910/DVN/GFLZYM

G) Food consumption in Food+light task 2x: https://doi.org/10.7910/DVN/GFLZYM

H) 10x IBU Non-conflict vs. conflict: https://doi.org/10.7910/DVN/OE73LI

Analysis for Fig.1 C-G: https://doi.org/10.7910/DVN/KJAMMP

Fig. 2
A-C) IHC of DMS striatum for cFos analysis:
Raw Data: https://doi.org/10.7910/DVN/KRAGMO
Analysis: https://doi.org/10.7910/DVN/NEVZXF

D-F) IHC of DMS striatum for GHSR expression:
Raw Data: https://doi.org/10.7910/DVN/UHTDDW
Analysis: https://doi.org/10.7910/DVN/SNSRF4

G-H) IHC of biotinylated-ghrelin in striatum:
Raw Data: https://doi.org/10.7910/DVN/KRAGMO
Analysis: https://doi.org/10.7910/DVN/SNSRF4

J-K) IHC of LHb for cFos analysis after IBU:
Raw Data: https://doi.org/10.7910/DVN/D5BCOY
Analysis: https://doi.org/10.7910/DVN/JWSLB

L-M) IHC of daSNc for pPDH, TH, and cFos analysis after IBU:
Raw Data: https://doi.org/10.7910/DVN/AVMV9E
Analysis: https://doi.org/10.7910/DVN/JWSLB

Fig. 3

A-B) OPRM1-cre DREADD expression:
Raw data: https://doi.org/10.7910/DVN/C9VBK7
Analysis: https://doi.org/10.7910/DVN/QLVA4X

C-E) In-vivo calcium imaging following intermediate doses of IBU or aGHR, including food consumption data:
Raw Data: https://doi.org/10.7910/DVN/US8QTS

Fig. 4

C) IHC of striosomes with DREADD manipulation in cre-OPRM1:
Raw Data: https://doi.org/10.7910/DVN/C9VBK7
Analysis: https://doi.org/10.7910/DVN/QLVA4X

D) Non-conflict Oprm1 2x:
Raw Data: https://doi.org/10.7910/DVN/TNT3FV,
Analysis: https://doi.org/10.7910/DVN/KJAMMP

E) Conflict Oprm1 2x:
Raw Data: https://doi.org/10.7910/DVN/TNT3FV,
Analysis: https://doi.org/10.7910/DVN/KJAMMP

F) IHC of Lateral habenula with DREADD manipulation in cre-OPRM1:
Raw Data: https://doi.org/10.7910/DVN/CT9ATL
Analysis: https://doi.org/10.7910/DVN/QLVA4X

G) IHC of daSNC with DREADD manipulation in cre-OPRM1:
Raw Data: https://doi.org/10.7910/DVN/N7FGMH
Analysis: https://doi.org/10.7910/DVN/QLVA4X

Fig. 5
https://github.com/dirkbeck/ghrelin_project

Supplemental fig. 1

A) Baseline of simple tasks Oprm1 WT: https://doi.org/10.7910/DVN/OE73LI

B, left) Food alone task 2x Long Evans: https://doi.org/10.7910/DVN/DCB1IH

B, right) Food alone task 2x Oprm1 WT: https://doi.org/10.7910/DVN/NTB2PG

C, left) Toy alone task 2x IBU Long Evans: https://doi.org/10.7910/DVN/YMYXO0

C, right) Toy alone task 2x Oprm1 WT: https://doi.org/10.7910/DVN/NTB2PG

D, left) Light alone task 2x IBU Long Evans: https://doi.org/10.7910/DVN/JW2C3Q

D, right) Light alone task 2x Oprm1 WT: https://doi.org/10.7910/DVN/NTB2PG

E, left) Food+light task 2x IBU Long Evans: https://doi.org/10.7910/DVN/0V6WKG

E, right) Food+light alone task 2x Oprm1 WT: https://doi.org/10.7910/DVN/NTB2PG

F, left) Toy+light task 2x IBU Long Evans: https://doi.org/10.7910/DVN/ZUH9YY

F, right) Toy+light alone task 2x Oprm1 WT: https://doi.org/10.7910/DVN/NTB2PG

G) Long Evans and Oprm1-WT performance across all tasks:
Food alone
https://doi.org/10.7910/DVN/DCB1IH
Toy alone
https://doi.org/10.7910/DVN/YMYXO0
Light alone
https://doi.org/10.7910/DVN/JW2C3Q
Food+light
https://doi.org/10.7910/DVN/0V6WKG
Toy+light
https://doi.org/10.7910/DVN/ZUH9YY

Analysis for S1: https://doi.org/10.7910/DVN/KJAMMP

Supplemental fig. 2

A) Non-conflict tasks 10x IBU Oprm1 WT : https://doi.org/10.7910/DVN/OE73LI

B) Food alone task 10x IBU Oprm1 WT: https://doi.org/10.7910/DVN/OE73LI

C) Toy alone task 10x IBU Oprm1 WT: https://doi.org/10.7910/DVN/OE73LI

D) Light alone task 10x IBU Oprm1 WT: https://doi.org/10.7910/DVN/OE73LI

E) Conflict tasks 10x IBU Oprm1 WT: https://doi.org/10.7910/DVN/OE73LI

F) Food+light task 10x IBU Oprm1 WT: https://doi.org/10.7910/DVN/OE73LI

G) Toy+light task 10x IBU Oprm1 WT: https://doi.org/10.7910/DVN/OE73LI

H) Chow in home cage 10x: https://doi.org/10.7910/DVN/GFLZYM

I) Food consumption in Food alone task 10x: https://doi.org/10.7910/DVN/GFLZYM

J) Food consumption in Food+light task 10x: https://doi.org/10.7910/DVN/GFLZYM

Analysis for S2: https://doi.org/10.7910/DVN/KJAMMP

Supplemental fig. 3

A-D) cFOS IHC in 50 brain regions after 1x IBU:
Raw Data/ analysis: https://doi.org/10.7910/DVN/DTXBD5
https://doi.org/10.7910/DVN/EI60AH
https://doi.org/10.7910/DVN/PYW4WW

E-Q): IHC analysis in striatum for cFos and MOR after 1x IBU:
Analysis: https://doi.org/10.7910/DVN/EI60AH

R): IHC across 50 brain regions following IBU:
Raw Data/ analysis: https://doi.org/10.7910/DVN/DTXBD5
https://doi.org/10.7910/DVN/EI60AH
https://doi.org/10.7910/DVN/PYW4WW

S-T): IHC of DMS striatum for cFos analysis after 0.5x and 10x IBU:
Raw Data: https://doi.org/10.7910/DVN/KRAGMO

U-V) IHC of DMS striatum for GHSR expression:
Raw Data: https://doi.org/10.7910/DVN/UHTDDW

W) IHC of BGHR in striatum:
Raw Data: https://doi.org/10.7910/DVN/KRAGMO

Supplemental fig. 4

A) IHC of LHb for cFos analysis after IBU:
Raw Data: https://doi.org/10.7910/DVN/D5BCOY

B-C) IHC of daSNc for pPDH, TH, and cFos analysis after IBU:
Raw Data: https://doi.org/10.7910/DVN/AVMV9E
Analysis: https://doi.org/10.7910/DVN/JWSLB

D) Left: Correlation between DMS strio and LHb fos
DMS striosomes cFos IHC:

Raw Data: https://doi.org/10.7910/DVN/KRAGMO
Analysis: https://doi.org/10.7910/DVN/NEVZXF
LHb cFos IHC
Raw Data: https://doi.org/10.7910/DVN/D5BCOY
Analysis: https://doi.org/10.7910/DVN/JWSLB

Right: Correlation between DMS striosomes cFos and daSNC pPDH:
DMS striosomes cFos IHC:
Raw Data: https://doi.org/10.7910/DVN/KRAGMO
Analysis: https://doi.org/10.7910/DVN/NEVZXF
daSNc pPDH
Raw Data: https://doi.org/10.7910/DVN/AVMV9E
Analysis: https://doi.org/10.7910/DVN/JWSLB

E) Correlation between LHb fos and daSNc pPDH:
LHb cFos IHC:
Raw Data: https://doi.org/10.7910/DVN/D5BCOY
Analysis: https://doi.org/10.7910/DVN/JWSLB
daSNc pPDH:
Raw Data: https://doi.org/10.7910/DVN/AVMV9E
Analysis: https://doi.org/10.7910/DVN/JWSLB

F) Correlation between DMS striosomes cFos and daSNc cFos:
DMS striosomes cFos IHC:
Raw Data: https://doi.org/10.7910/DVN/KRAGMO
Analysis: https://doi.org/10.7910/DVN/NEVZXF
daSNc cFos:
Raw Data: https://doi.org/10.7910/DVN/AVMV9E
Analysis: https://doi.org/10.7910/DVN/JWSLB

G) IHC of Arcuate nucleus for cFos analysis after IBU:
Raw Data: https://doi.org/10.7910/DVN/WANMCY
Analysis: https://doi.org/10.7910/DVN/JWSLB

H) Correlation between DMS striosomes cFos and ARC cFos:
DMS striosomes cFos IHC:
Raw Data: https://doi.org/10.7910/DVN/KRAGMO
Analysis: https://doi.org/10.7910/DVN/NEVZXF
ARC cFos IHC:
Raw Data: https://doi.org/10.7910/DVN/WANMCY
Analysis: https://doi.org/10.7910/DVN/JWSLB

Supplemental fig. 5

A) In-vivo calcium imaging following intermediate doses of IBU and acyl-ghrelin:
Raw data: https://doi.org/10.7910/DVN/US8QTS

B) IPS cell map following 2xIBU injection:
Analysis: https://doi.org/10.7910/DVN/US8QTS

C) In-vivo calcium imaging following high doses of IBU acyl-ghrelin:
Raw data: https://doi.org/10.7910/DVN/US8QTS

D) 2x IBU calcium dynamics time curve:
Analysis: https://doi.org/10.7910/DVN/US8QTS

E, left) In-vivo calcium imaging time curve following 2x and 10x IBU:
Analysis: https://doi.org/10.7910/DVN/US8QTS

E, right) In-vivo calcium imaging time curve following 4.3 and 86 ug/kg acyl-ghrelin:
Analysis: https://doi.org/10.7910/DVN/US8QTS

F) Food consumption following acyl-ghrelin:
Analysis: https://doi.org/10.7910/DVN/US8QTS

G) Food consumption following IBU and acyl-ghrelin in moderate and high doses:
Analysis: https://doi.org/10.7910/DVN/US8QTS

Supplemental fig. 6

A-D) IHC of striosomes with DREADD manipulation in cre-OPRM1:
Raw Data: https://doi.org/10.7910/DVN/C9VBK7

E-I) pPDH IHC of striosomes with DREADD manipulation in cre-OPRM1:
Analysis: https://doi.org/10.7910/DVN/QLVA4X

Supplemental fig. 7

B) Non-conflict tasks:
Food alone task 2X IBU CRE-OPRM1: https://doi.org/10.7910/DVN/NTB2PG

Toy alone task 2X IBU CRE-OPRM1: https://doi.org/10.7910/DVN/NTB2PG

Light alone task 2X IBU CRE-OPRM1: https://doi.org/10.7910/DVN/NTB2PG

Raw Data Analysis: https://doi.org/10.7910/DVN/KJAMMP

C) Conflict tasks:

Food+light task 2X IBU CRE-OPRM1: https://doi.org/10.7910/DVN/NTB2PG

Toy+light task 2X IBU CRE-OPRM1: https://doi.org/10.7910/DVN/NTB2PG

Raw Data Analysis: https://doi.org/10.7910/DVN/KJAMMP

Supplemental fig. 8

B): IHC of Lateral habenula with DREADD manipulation in Oprm1-cre:
Raw Data: https://doi.org/10.7910/DVN/CT9ATL

C: IHC of daSNC with DREADD manipulation in Oprm1-cre:
Raw Data: https://doi.org/10.7910/DVN/N7FGMH

D-G): ANOVA post-hoc values following DREADD manipulation in Oprm1-cre:
Analysis: https://doi.org/10.7910/DVN/QLVA4X

Supplemental fig. 9

A-N) Monosynaptic tracing of striosomes
Raw data and analysis: https://doi.org/10.7910/DVN/ZRLRXV

Supplemental fig. 10

A-C): https://github.com/dirkbeck/ghrelin_project

Supplemental fig. 11

A-E) Motor analysis data and scripts:
Functions: https://doi.org/10.5281/zenodo.17280633
Living Functions: https://github.com/atanugiri/GhrelinBehaviorQuantification.git
Data: https://doi.org/10.7910/DVN/G8CBKJ

Supplemental fig. 12

Motor Analysis: https://github.com/dirkbeck/ghrelin_project

Supplemental fig. 13

A-D)Motor analysis data and scripts:
Functions: https://doi.org/10.5281/zenodo.17280633
Living Functions: https://github.com/atanugiri/GhrelinBehaviorQuantification.git
Data: https://doi.org/10.7910/DVN/G8CBKJ

Supplemental fig. 14

A-B): IHC of BGHR in DLS striosome
Raw Data: https://doi.org/10.7910/DVN/KRAGMO
Analysis: https://doi.org/10.7910/DVN/SNSRF4

C): IHC of DMS and DLS striatum for cFos, MOR, and pPDH analysis after IBU:
Raw Data: https://doi.org/10.7910/DVN/KRAGMO

D): IHC of DMS and DLS striosomes for cFos analysis after IBU:
Raw Data: https://doi.org/10.7910/DVN/KRAGMO
Analysis: https://doi.org/10.7910/DVN/NEVZXF

E): IHC of DMS and DLS striosomes for pPDH analysis after IBU:
Raw Data: https://doi.org/10.7910/DVN/KRAGMO
Analysis: https://doi.org/10.7910/DVN/NEVZXF

F) Correlation between striosomes DMS cFos and DLS pPDH:
DMS striosomes cFos IHC:
Raw Data: https://doi.org/10.7910/DVN/KRAGMO
Analysis: https://doi.org/10.7910/DVN/NEVZXF
DLS striosomes pPDH IHC:
Raw Data: https://doi.org/10.7910/DVN/KRAGMO
Analysis: https://doi.org/10.7910/DVN/NEVZXF

G) Excitation-inhibition balance in DMS and DLS
Analysis: https://doi.org/10.7910/DVN/NEVZXF

H, Left) Striosomal cFos expression in DMS and DLS
Analysis: https://doi.org/10.7910/DVN/NEVZXF

H, right) Striosomal pPDH expression in DMS and DLS
Analysis: https://doi.org/10.7910/DVN/NEVZXF

I-J): https://github.com/dirkbeck/ghrelin_project

11 SUPPLEMENTARY TEXT

11.1 Supplementary note 1: Ghrelin's effect on the decision-space.

Our finding that ghrelin administration selectively increases dorsomedial striatum (DMS) striosome activity and impairs decision-making specifically in tasks requiring the integration of conflicting information provides empirical support for our "decision-space" model of the circuit. This Supplementary Note summarizes this framework, integrates it with the existing literature on ghrelin, and speculates on its broader implications for understanding the neural basis of choice under varying internal states and in neuropsychiatric conditions.

Ghrelin as a regulator of the decision-space

Our computational model, building upon previous work , conceptualizes decision-making as a process occurring within a multi-dimensional space, where each dimension represents a distinct stream of behaviorally relevant information processed by the cortex (e.g., potential reward, associated cost, novelty, social cues). The model posits that DMS striosomes play a critical role in regulating the dimension of this space, that is, determining which factors are actively considered during a given decision.

The modeled circuit involves projections from cortical areas (like orbitofrontal cortex - OFC, prelimbic cortex - PL, infralimbic cortex - IL) to striosomes, which in turn modulate dopaminergic output from the dopamine neurons of the substantia nigra compacta (daSNC), both directly[5,6] and indirectly via pathways involving the globus palidus internus (GPi)[7], lateral habenula (LHb)[7], and rostromedial tegmental area (RMTg)[8]. Within this network, striosomes parse cortical input along these decision-dimensions. The model proposes an inverse relationship between striosome activity and the complexity of the decision-space. Lower striosome activity (associated with difficult, conflict-rich decisions[9]) facilitates the engagement of more decision-dimensions, allowing for nuanced integration of multiple factors. Conversely, higher striosome activity (associated with simpler, less conflicting decisions[9]) leads to the engagement of fewer dimensions, simplifying the decision process (**Fig. 5c-e**).

Our data indicates that ghrelin administration significantly increases DMS striosome activity. The model predicts that this pharmacologically induced hyperactivity forces the circuit to form a lower-dimensional space, even when faced with complex tasks that would normally benefit from integrating multiple factors. Furthermore, LHb activity, which also inhibits daSNC in the model, might be elevated post-ghrelin. If both striosomes and LHb are hyperactive, this would create convergent pressure towards reducing the dimensionality of the decision-space.

Reinterpreting ghrelin's effects through the lens of the decision-space

This model may also explain other context-dependent results in the literature, where it has been found, for instance, to alter impulsivity and reward sensitivity[10,11]. Increased impulsivity (e.g., reduced willingness to wait for larger rewards) is a predicted consequence of a lower-dimensional decision-space. Considering delayed consequences often requires integrating a 'temporal cost' or 'future value' dimension. If striosomal hyperactivity suppresses this dimension, choices become dominated by immediate factors, manifesting as impulsivity. Similarly, heightened reward sensitivity could arise if the 'reward' dimension becomes overwhelmingly prioritized when other competing dimensions are suppressed.

11.2 Supplementary note 2: Movement data supports our policy-IG model of dopamine.

Even in those non-conflict conditions, where place-preference choices remained unchanged, we consistently observed marked alterations in the rats' movement profiles (**fig. S11-13**). These movement changes offer support for the policy-information-gain (policy-IG) model of striosome-dopamine circuit function[12].

The policy-information-gain (policy-IG) model proposes that dopamine release in the striosome->dopamine->matrix circuit does not broadcast reward-prediction errors but instead encodes an information-theoretic measure of how much a new piece of evidence sharpens the animal's action policy. Formally, policy-IG is the drop in Shannon entropy of the action distribution when a cue arrives, that is, how much the cue reduces uncertainty about which action is best. Through this single scalar signal, the circuit simultaneously (1) gates cortical inputs by expanding or contracting its decision-space, (2) drives synaptic updates when information gain outweighs representational cost, and (3) adjusts the moment-to-moment explore-exploit balance by focusing or broadening action probabilities. As a result, dopamine transients reflect not only reward surprises but also novelty, aversiveness, and real-time shifts in movement and decision bias.

Specifically, the model predicts that under control conditions, moment-to-moment bursts in dopamine initiate actions and focus trajectories toward or away from salient cues. On the other hand, baseline dopamine tunes the exploration-exploitation balance. When IBU elevates striosome->LHb inhibition of dopamine, baseline policy-IG decreases. This heightened tonic signal narrows the decision-space dimensionality, gating out peripheral information, and collapses the action policy toward a few favored movements. This could potentially explain why there is significant reduction in movement variability reduction metrics like average turn angle and average step length after ghrelin administration in conflict tasks (**fig. S12**).

11.3 Supplementary note 3: Implications for neuropsychiatric disorders

Our model linking ghrelin to reduced decision-space dimensionality may offer insights into neuropsychiatric disorders where both ghrelin dysregulation and decision-making deficits are implicated, such as stress-related disorders (PTSD) and addiction (**Table 6**). In these conditions, elevated ghrelin levels could contribute to a pathologically constrained decision-making process. Individuals might become overly focused on immediate threats (in PTSD) or drug-related cues (in addiction), effectively filtering out other relevant dimensions like long-term consequences, social costs, or alternative rewards. This reduced dimensionality could manifest as cognitive rigidity, difficulty adapting to changing circumstances, and an inability to effectively resolve conflicting motivations, all hallmarks of these disorders[11,12]. The ghrelin-striosome axis might therefore represent a potential therapeutic target for restoring more flexible, multi-dimensional decision-making in these patient populations.

11.4 Supplementary note 4: Limitations

Ibutamoren is a non-biological agonist for the ghrelin receptor, potentially resulting in ghrelin receptor activation that does not mimic biological levels[13,14] despite our efforts (including the performance of a dose response assay/curve (**Fig. 3**)) to reasonably match what could be biological ranges for IBU and ghrelin receptor activation. We also performed a similar dose response experiment comparing calcium dynamics within the striosomes following IBU or endogenous ghrelin administration and found that striosomes responded similarly to both agonists in a dose-dependent manner. We do not know the reason for the different dose responses to IBU

or where/how the threshold of GHSR stimulation switches from increasing cost-sensitivity to appetitive processing. The rat model used in this study is highly specific; however, there may be some striosomal properties not observed due to some non-expression, and some matrisomalcontributions could potentially be overlooked. The DREADD manipulations were striosome-specific while IBU itself binds to multiple different regions, though this specificity was useful for illustrating the necessity of striosome activity on behavioral effects observed within our paper.

12 SUPPLEMENTARY FIGURES

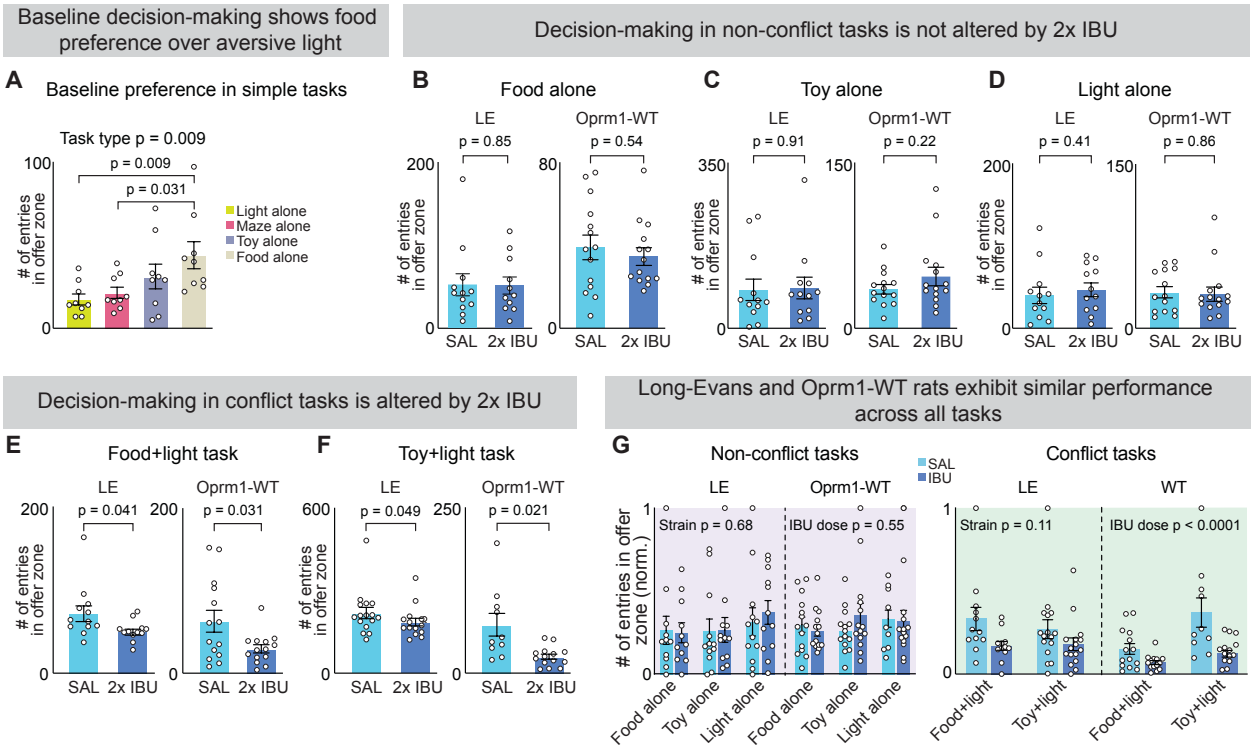

Figure S1: Conflict decision making task impacted by 2x IBU administration.

(A) Baseline entries differed across non-conflict tasks, with rats showing greater approach toward reward-associated zones (Food and Toy) than neutral (Maze alone) or aversive (Light alone) zones (rats=9, repeated-measures one-way ANOVA, p=0.009). **(B-F)** Raw, non-normalized entries into the offer zone are shown for Long-Evans (rats=10-16/group) and Oprm1-WT rats (rats=10-14/group). Consistent with the normalized analyses presented in **Fig. 1C**, 2x IBU did not alter performance in either strain across any non-conflict task (**B**, Food alone; **C**, Toy alone; **D**, Light alone, all p>0.05). But during conflict tasks, in both Long-Evans and Oprm1-WT rats, 2x IBU significantly reduced entries into the reward zone relative to SAL treatment (E, Food+light; F, Toy+light, all p<0.05). (**G**) To determine whether strain contributed to the behavioral effects of IBU, normalized data from both cohorts were analyzed using a three-way ANOVA. No effect of strain was observed in either non-conflict (left; p=0.68) or conflict (right; p = 0.11) tasks. Consistent with the individual task analyses, IBU did not affect non-conflict performance (p=0.55) but significantly altered behavior during conflict tasks (p<0.0001). Mean ± SEM. For additional statistical analyses see table S3.

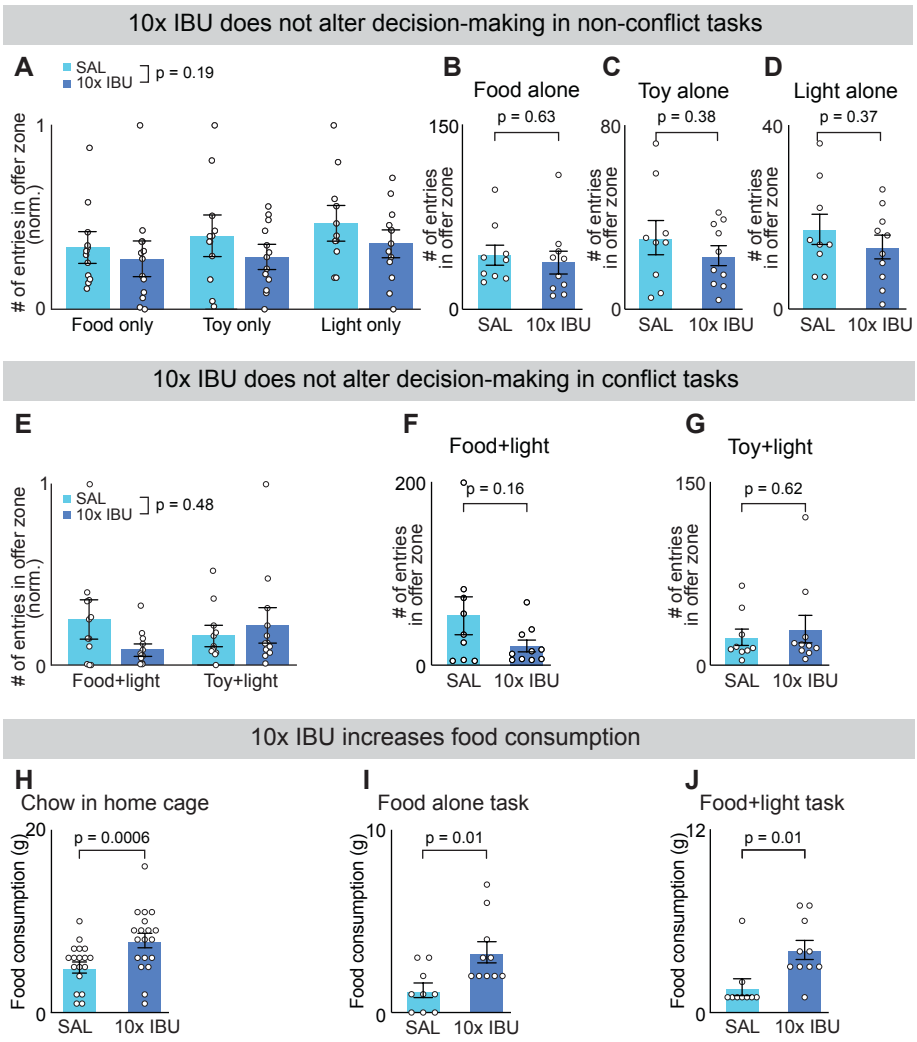

Figure S2: Administration of 10X IBU does not impact decision-making but increases food consumption.

(A-D) High-dose IBU (10x) did not alter performance during non-conflict tasks. No differences were observed between SAL (rats=9) and 10x IBU rats (rats=10) when comparing normalized performance across tasks (**A**; two-way ANOVA, p=0.19) or individual raw task measures (**B**, Food alone, p=0.63; **C**, Toy alone, p=0.38; **D**, Light alone, p=0.37). (**E-G**) Unlike 2x IBU, high-dose IBU did not affect conflict-task performance. No differences were observed between SAL and 10x IBU rats when comparing normalized conflict-task performance (**E**; two-way ANOVA, p=0.48) or individual raw task measures (**F**, Food+light, p=0.16; **G**, Toy+light, p=0.62). **(H-J)** In contrast, high-dose IBU significantly increased food consumption. Food intake was elevated in the home cage (**H**; rats=19, paired t-test, p=0.0006), during the Food-alone task (**I**; p=0.01), and during the Food+light conflict task (**J**; p=0.01). Together, these data demonstrate that high-dose IBU

increases feeding without altering decision-making behavior. Mean ± SEM. For additional statistical analyses, see table S3.

Figure S3

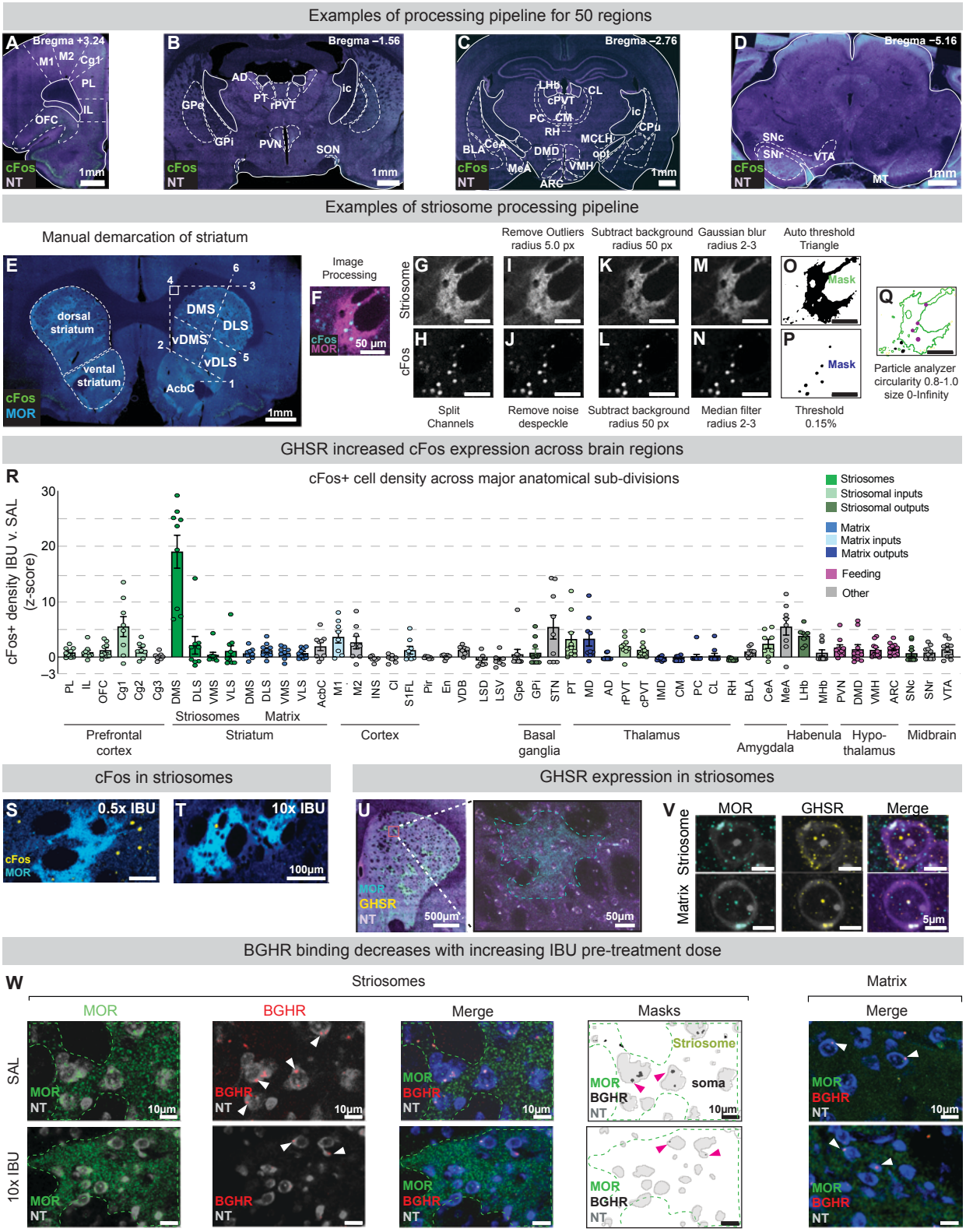
Examples of processing pipeline for 50 regions
Examples of striosome processing pipeline
Manual demarcation of striatum
Image Processing
Remove Outliers radius 5.0 px
Subtract background radius 50 px
Gaussian blur radius 2-3
Auto threshold Triangle
Striosome
cFos
Split Channels
Remove noise despeckle
Subtract background radius 50 px
Median filter radius 2-3
Threshold 0.15%
Particle analyzer circularity 0.8-1.0 size 0-Infinity
GHSR increased cFos expression across brain regions
cFos+ cell density across major anatomical sub-divisions
cFos+ density IBU v. SAL (z-score)
Striosomes
Striosomal inputs
Striosomal outputs
Matrix
Matrix inputs
Matrix outputs
Feeding
Other
Prefrontal cortex
Striatum
Cortex
Basal ganglia
Thalamus
Amygdala
Habenula
Hypo-thalamus
Midbrain
cFos in striosomes
GHSR expression in striosomes
0.5x IBU
10x IBU
MOR
GHSR
Merge
BGHR binding decreases with increasing IBU pre-treatment dose
Striosomes
Matrix
BGHR
Masks
SAL
10x IBU
soma

Figure S3: Striosomal activation by intermediate IBU doses coincides with striosomal enrichment of GHSR signaling.

(A) Representative coronal sections used for whole-brain cFos quantification across 50 brain regions. Section from SAL and 1x IBU rats (rats=7-10/group) were parcellated. Regions were analyzed within 1mm of **(A)** prefrontal cortex, (**B**) rostral thalamus and Gpe/Gpi, (**C)** thalamus, hypothalamus, and amygdala, and (**D**) mid-brain coordinates. See **table S4**. **(E)** Delineation of dorsal striatum into DMS, DLS, vDMS and vDLS. See 5.3.2 of Materials and methods. **(F-Q)** Image processing workflow used for striosomal cFos quantification in ImageJ. (**F**) Merge MOR/cFos images, were split into two channels **(G)** MOR and **(H)** cFos. Overexposed signal was removed **(I-J)**, background signal was subtracted **(K-L)**, and filters were applied **(M-N)** prior to thresholding **(O-P)** to generate binary masks. The MOR mask was converted into a ROI and applied to cFos mask, allowing for particle analysis for cFos-positive cells **(Q)**. **(R)** Z-scored cFos-positive cell densities (cells/mm^2) across anatomical subdivisions following IBU administration. IBU z-scores were calculated relative to SAL controls as:

$$\mathrm{IBUzscore} = \frac{\mathrm{IBU}_{\mathrm{ROI-desnity}} - \mathrm{mean}(\mathrm{SAL}_{\mathrm{group-ROI-density}})}{\mathrm{SD}\ (\mathrm{SAL}_{\mathrm{group-ROI-density}})}$$

(S-W) Additional images corresponding to Fig. 2 showing striosomal cFos following 0.5x **(S)** and 10x IBU **(T)**, GHSR enrichment in striosomes relative to matrix **(U-V**), and reduced BGHR binding following 10x IBU treatment relative to SAL (**W)**. Mean ± SEM.

2767

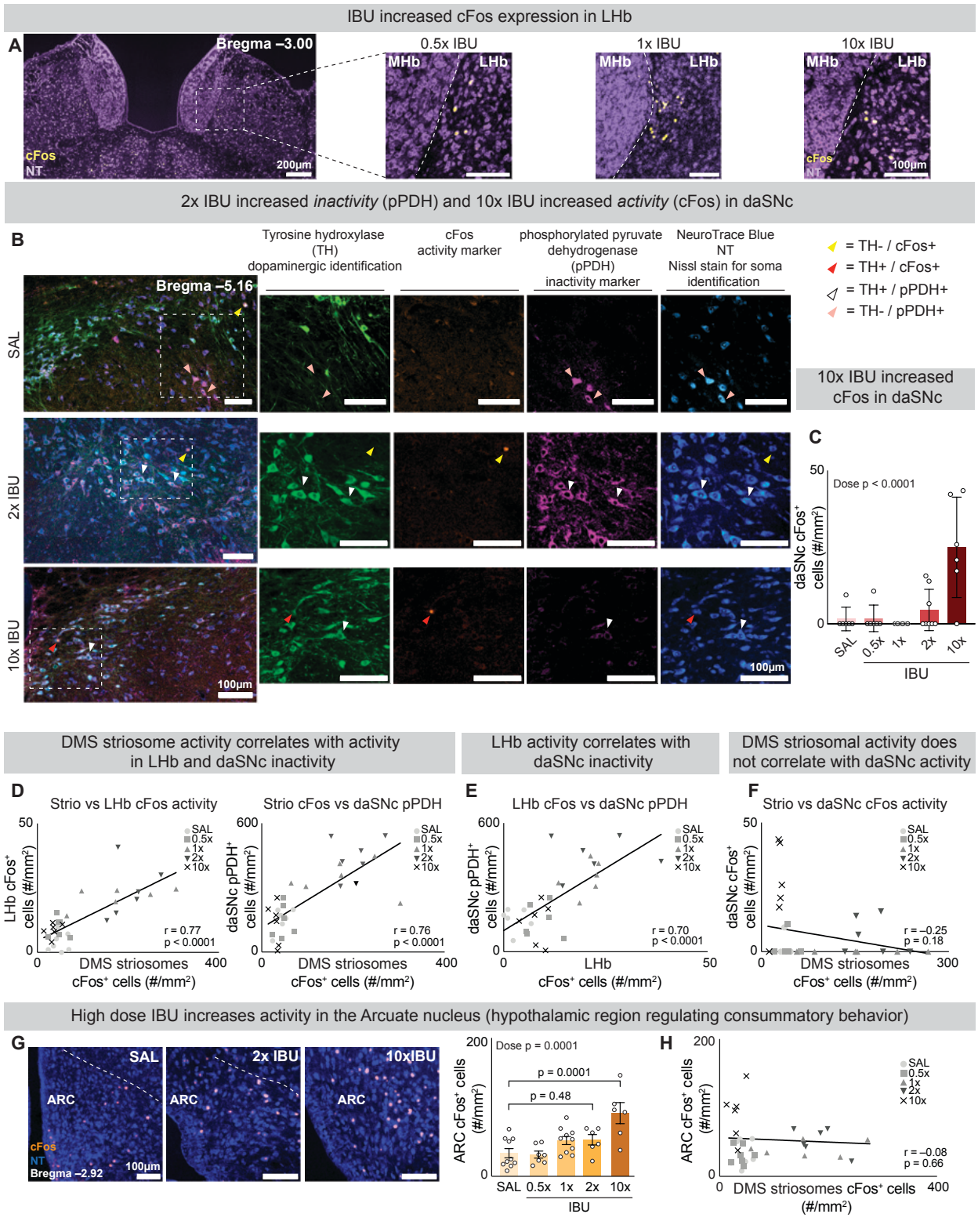

2768
2769

Figure S4: IBU dose-dependently modulate LHb, daSNC, and ARC.

(A) Additional LHb images corresponding to **Fig 2J**. Intermediate IBU doses increase cFos (1x IBU), whereas low (0.5x) and high (10x) doses were comparable to SAL. **(B-C)** 2x IBU increased pPDH expression in daSNc, whereas 10x IBU reduced pPDH and increased cFos expression. cFos expression differed across groups (rats=6-8/group), indicating a dose-dependent effect of IBU on daSNc (**C**, ANOVA, IBU dose, $p<0.0001$). **(D-F)** DMS striosomal cFos (rats=31) positively correlated with LHb activity (**D, left**; $r=0.77$, $p<0.0001$) and daSNc inactivity (**D, right**; $r=0.76$, $p<0.0001$). LHb cFos also correlated with daSNc pPDH (**E**; $r=0.70$, $p<0.0001$). In contrast, DMS striosomal and daSNc cFos were not correlated (**F**; $r=-0.25$, $p=0.18$). **(G-H)** High-dose (10x) selectively increased cFos expression in ARC (**G**, ANOVA, IBU dose, $p=0.0001$) with no differences among lower doses. ARC and DMS striosomal cFos expression did not correlate (**H**; rats=34, $r=-0.08$, $p=0.66$). Mean ± SEM. For additional statistical analyses, see table S3.

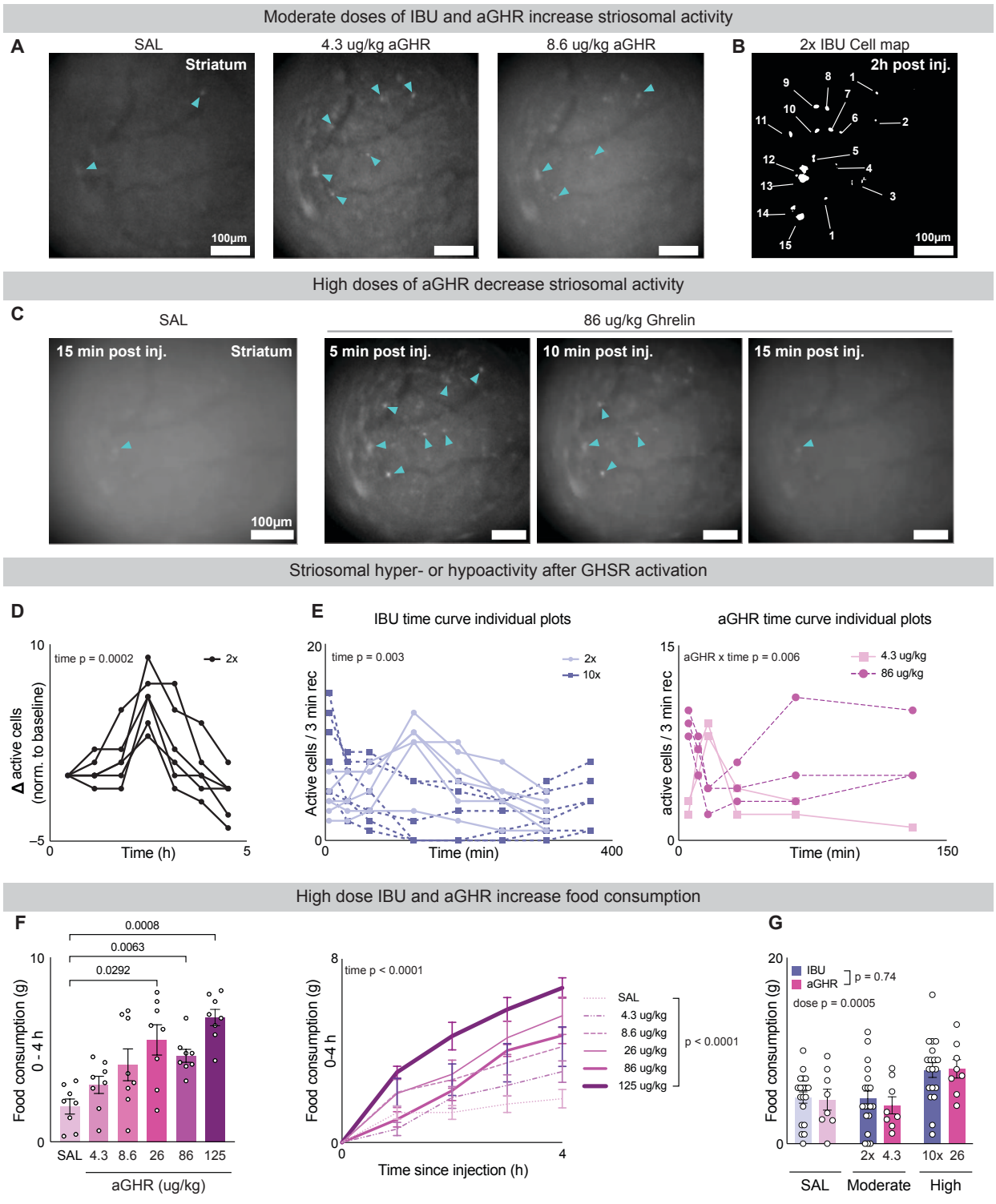
Moderate doses of IBU and aGHR increase striosomal activity
A
SAL
4.3 ug/kg aGHR
8.6 ug/kg aGHR
Striatum
100µm
B
2x IBU Cell map
2h post inj.
High doses of aGHR decrease striosomal activity
C
SAL
86 ug/kg Ghrelin
15 min post inj.
Striatum
5 min post inj.
10 min post inj.
15 min post inj.
Striosomal hyper- or hypoactivity after GHSR activation
D
time p = 0.0002
2x
Δ active cells (norm. to baseline)
Time (h)
E
IBU time curve individual plots
time p = 0.003
2x
10x
Active cells / 3 min rec
Time (min)
aGHR time curve individual plots
aGHR x time p = 0.006
4.3 ug/kg
86 ug/kg
active cells / 3 min rec
Time (min)
High dose IBU and aGHR increase food consumption
F
0.0008
0.0063
0.0292
Food consumption (g) 0 - 4 h
SAL 4.3 8.6 26 86 125
aGHR (ug/kg)
time p < 0.0001
Food consumption (g) 0-4 h
SAL
4.3 ug/kg
8.6 ug/kg
26 ug/kg
86 ug/kg
125 ug/kg
p < 0.0001
Time since injection (h)
G
IBU
aGHR
p = 0.74
dose p = 0.0005
Food consumption (g)
2x 4.3 10x 26
SAL
Moderate
High

2783
2784

Figure S5: IBU or endogenous ghrelin (aGHR) dose-dependently impact striosomal activity and feeding behavior.

(A-C) Maximum projection images illustrating dose-dependent changes in striosomal activity. Compared to SAL (**A, left)**, low/intermediate doses of aGHR (**middle**, 4.3; **right,** 8.6 μg/kg) increased the number of active cells. **(B)** Cell map from 2x IBU recording used in **Fig. 3C**. **(C)** High-doses of aGHR (86 μg/kg) reduced activity. Blue arrows indicate active cells. **(D)** Calcium activity normalized to each animal's baseline showed 2x IBU increased striosomal activity, peaking approximately 2 hours after administration (ANOVA, $p=0.0002$). **(E)** Raw counts of active cells (rats=6, fields of view=7), following IBU (**left**) and aGHR (**right)** demonstrate significant time-dependent effects of GHSR activation (IBU: time, $p=0.003$; aGHR: aGHR x time interaction $p=0.006$). For comparison, cell counts were normalized to baseline in **Fig. 3D**. **(F)** aGHR dose-dependently increased feeding. Total food consumption differed across doses (**left,** ANOVA, $p=0.0009$). Higher GHSR activation (>26 μg/kg) increased food intake and accelerated feeding onset (**right,** effect of time, $p<0.0001$; dose x time $p=0.001$). **(G)** High doses of both IBU (10x) and aGHR (26μg/kg) increased food consumption relative to intermediate doses (2x IBU and 4.3μg/kg aGHR), with no difference between either IBU or aGHR (ANOVA, dose, $p=0.0005$; GHSR activation, $p=0.74$). Mean ± SEM. For additional statistical analyses, see table S3.

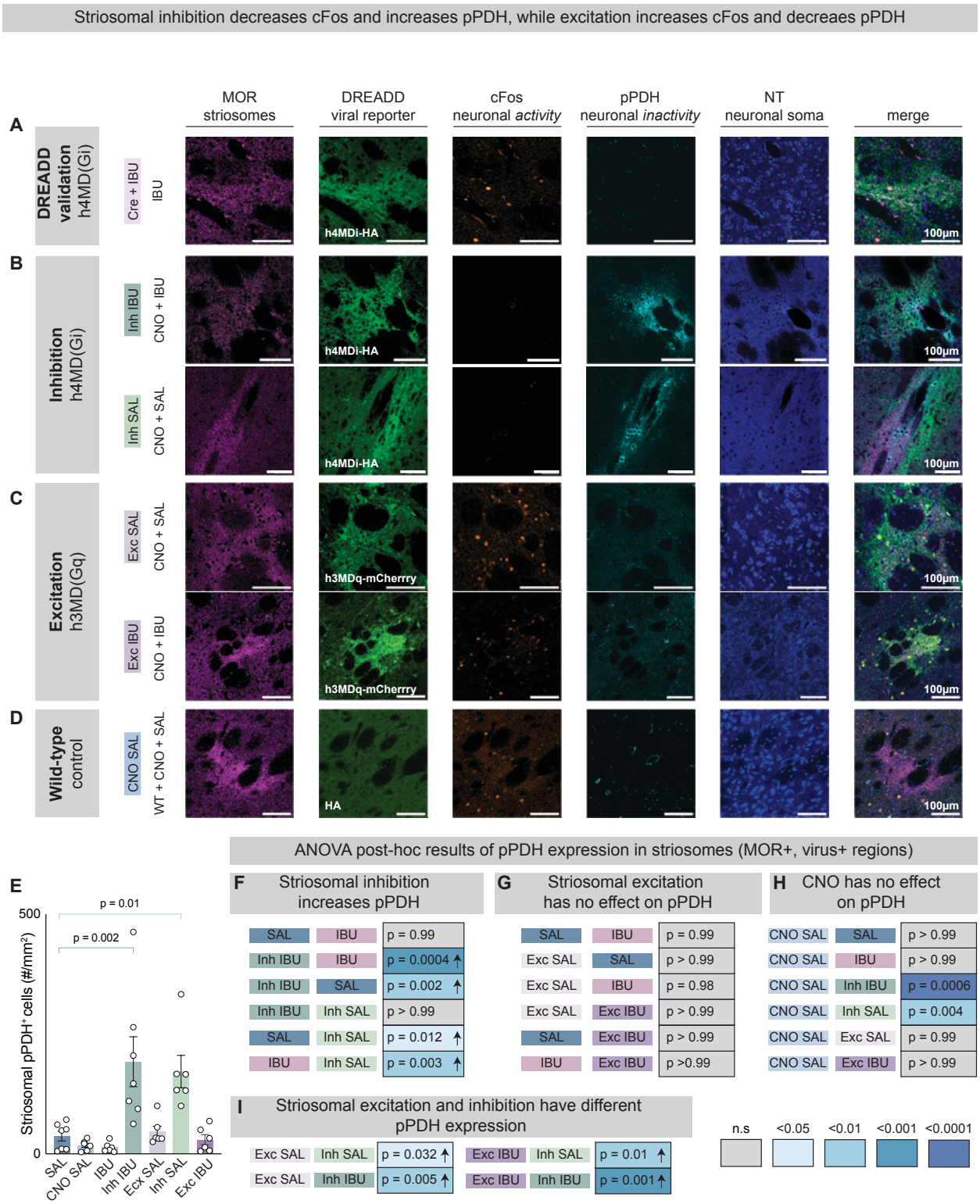
Striosomal inhibition decreases cFos and increases pPDH, while excitation increases cFos and decreaes pPDH
MOR striosomes
DREADD viral reporter
cFos neuronal activity
pPDH neuronal inactivity
NT neuronal soma
merge
A
DREADD validation h4MD(Gi)
Cre + IBU
IBU
B
Inhibition h4MD(Gi)
Inh IBU
CNO + IBU
Inh SAL
CNO + SAL
C
Excitation h3MD(Gq)
Exc SAL
CNO + SAL
Exc IBU
CNO + IBU
D
Wild-type control
CNO SAL
WT + CNO + SAL
h4MDi-HA
h3MDq-mCherrry
HA
100µm
ANOVA post-hoc results of pPDH expression in striosomes (MOR+, virus+ regions)
E
p = 0.01
p = 0.002
500
0
Striosomal pPDH+ cells (#/mm2)
SAL
CNO SAL
IBU
Inh IBU
Exc SAL
Inh SAL
Exc IBU
F Striosomal inhibition increases pPDH
SAL IBU p = 0.99
Inh IBU IBU p = 0.0004
Inh IBU SAL p = 0.002
Inh IBU Inh SAL p > 0.99
SAL Inh SAL p = 0.012
IBU Inh SAL p = 0.003
G Striosomal excitation has no effect on pPDH
SAL IBU p = 0.99
Exc SAL SAL p > 0.99
Exc SAL IBU p = 0.98
Exc SAL Exc IBU p > 0.99
SAL Exc IBU p > 0.99
IBU Exc IBU p >0.99
H CNO has no effect on pPDH
CNO SAL SAL p > 0.99
CNO SAL IBU p > 0.99
CNO SAL Inh IBU p = 0.0006
CNO SAL Inh SAL p = 0.004
CNO SAL Exc SAL p = 0.99
CNO SAL Exc IBU p > 0.99
I Striosomal excitation and inhibition have different pPDH expression
Exc SAL Inh SAL p = 0.032
Exc SAL Inh IBU p = 0.005
Exc IBU Inh SAL p = 0.01
Exc IBU Inh IBU p = 0.001
n.s
<0.05
<0.01
<0.001
<0.0001

Figure S6: Striosomal inhibition decreased cFos and increased pPDH expression, excitation produced the opposite effect.

(A-D) Representative images illustrating DREADD expression and experimental manipulations. Sections were stained for MOR, DREADD reporter (h4MD(Gi)-HA for inhibitory virus and h3MD(Gq)-mCherry for excitatory virus), cFos, pPDH, and NT. Inhibitory manipulations increased pPDH expression and reduced cFos, while excitatory manipulations increased cFos and reproduced effects of IBU. **(A)** Cre+ IBU cFos expression in the absence of CNO. **(B)** Inhibitory DREADD groups (Inh IBU and Inh SAL). **(C)** Excitatory DREADD groups (Exc SAL and Exc IBU). **(D)** CNO SAL control. **(E-I)** Striosomal manipulation altered pPDH expression in striosomes (rats=6-7/group, ANOVA, $p<0.0001$). **(F)** Striosomal inhibition increased pPDH expression regardless of SAL or IBU treatment, indicating reduced striosomal activity. **(G)** In contrast, excitatory manipulations did not significantly alter pPDH expression relative to SAL or IBU controls. **(H)** CNO SAL and SAL groups did not differ in pPDH expression, indicating no detectable effect of CNO alone. **(I)** Inhibitory and excitatory manipulations produced significantly different pPDH levels. Mean ± SEM. For additional statistical analyses, see table S3.

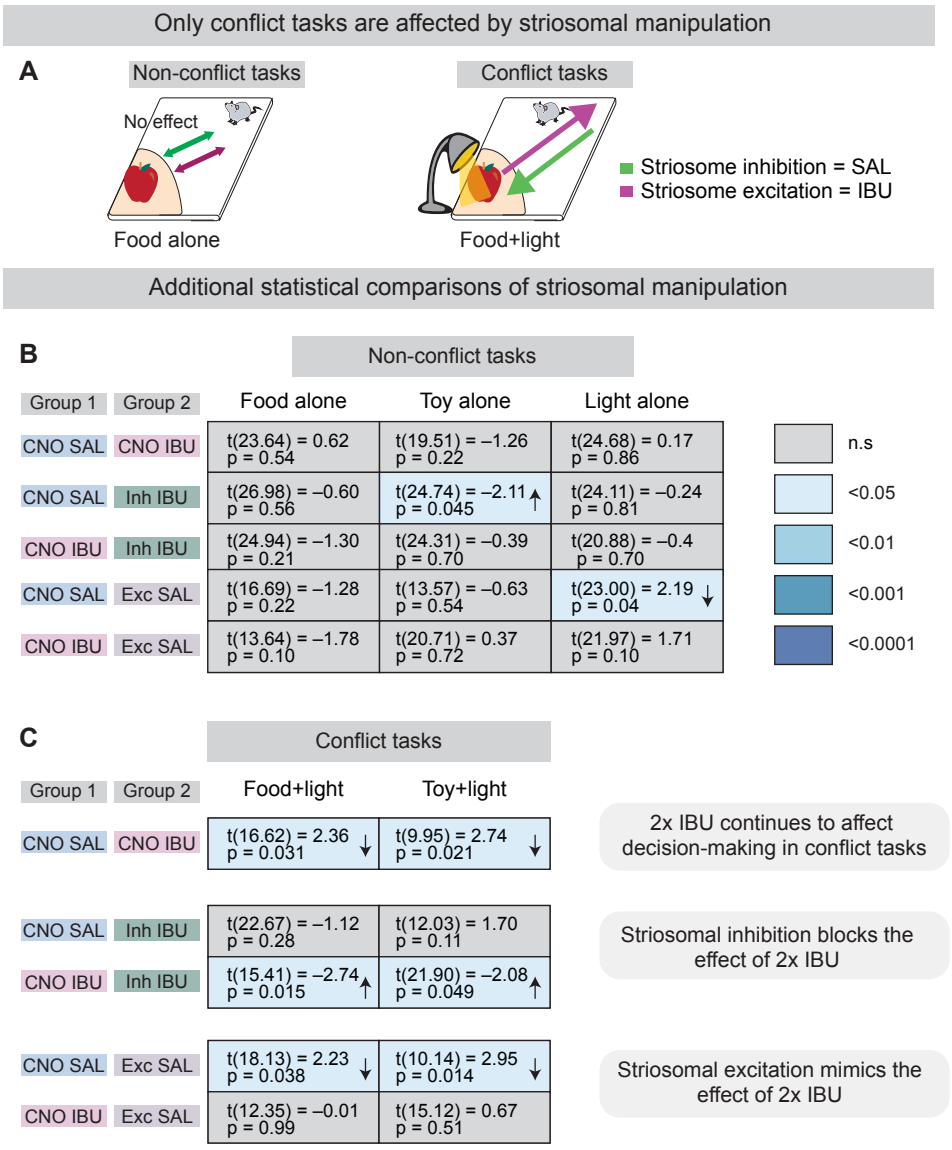

Figure S7: Striosomal inhibition blocks the behavioral effects of 2x IBU during conflict tasks, while striosomal excitation mimics the effects.

(A) Summary diagram of behavioral effects of striosomal inhibition and excitation across non-conflict and conflict tasks. **(B-C)** Individual comparisons of raw behavioral scores across experimental groups during non-conflict **(B)** and conflict **(C)** tasks. Consistent with the normalized analyses presented in **Fig. 4D-E**, striosomal inhibition shifted performance toward CNO SAL-like levels, while excitation reproduced the effects of 2x IBU during conflict tasks, with minimal effects during non-conflict tasks. For additional statistical analyses, see table S3.

Detailed information for each group manipulation

A

					Inhibitory			Excitatory	
Name	SAL	CNO SAL	IBU	CNO IBU	Cre+ IBU	Inh IBU	Inh SAL	Exc SAL	Exc IBU
Strain	WT	WT	WT	WT	Oprm1-Cre	Oprm1-Cre	Oprm1-Cre	Oprm1-Cre	Oprm1-Cre
DREADD virus	None	hM4D(Gi) no expression	None	hM4D(Gi) no expression	hM4D(Gi)	hM4D(Gi)	hM4D(Gi)	hM3D(Gq)	hM3D(Gq)
CNO	None	CNO	None	CNO	None	CNO	CNO	CNO	CNO
Treatment	SAL	SAL	IBU	IBU	IBU	IBU	SAL	SAL	IBU

Striosomal inhibition abolishes cFos in LHb and pPDH in daSNc, while striosomal excitation increase cFos in LHb and pPDH in daSNc

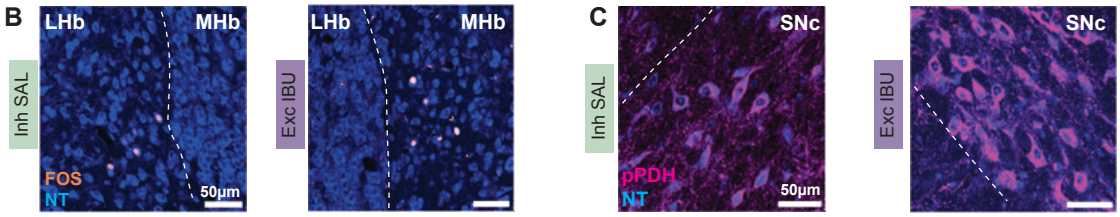

D

	Group 1	Group 2	Striosomes cFos	Group 1	Group 2	LHb cFos	daSNc pPDH	
Inhibition h4MD(Gi)	SAL	Cre + IBU	p < 0.0001 ↑	SAL	IBU	p < 0.0001 ↑	p < 0.0001 ↑	Striosomal inhibition blocks the effects of IBU throughout the circuit
	Cre + IBU	Inh IBU	p < 0.0001 ↓	Inh IBU	IBU	p < 0.0001 ↓	p < 0.0001 ↓	
	SAL	Inh IBU	p > 0.99	Inh IBU	SAL	p > 0.99	p = 0.52	
	Inh IBU	Inh SAL	p > 0.99	Inh IBU	Inh SAL	p > 0.99	p > 0.99	
	SAL	Inh SAL	p > 0.99	SAL	Inh SAL	p > 0.99	p = 0.25	
	Cre + IBU	Inh SAL	p = 0.002 ↓	IBU	Inh SAL	p < 0.0001 ↓	p < 0.0001 ↓	

E

Excitation h3MD(Gq)	SAL	Cre + IBU	p < 0.0001 ↑	SAL	IBU	p < 0.0001 ↑	p < 0.0001 ↑	Striosomal excitation mimics the effects of IBU throughout the circuit
	SAL	Exc SAL	p < 0.0001 ↑	Exc SAL	SAL	p < 0.0001 ↑	p = 0.0005 ↑	
	Cre + IBU	Exc SAL	p = 0.99	Exc SAL	IBU	p > 0.99	p = 0.39	
	Exc SAL	Exc IBU	p = 0.37	Exc SAL	Exc IBU	p = 0.88	p = 0.91	
	SAL	Exc IBU	p = 0.0001 ↑	SAL	Exc IBU	p < 0.0001 ↑	p = 0.012 ↑	
	Cre + IBU	Exc IBU	p = 0.87	IBU	Exc IBU	p = 0.55	p = 0.037 ↓	

F

Inhibitory vs excitatory virus	Exc SAL	Inh SAL	p < 0.0001	Exc SAL	Inh SAL	p = 0.0002	p < 0.0001	Striosomal excitation and inhibition produce opposing circuit effects
	Exc SAL	Inh IBU	p < 0.0001	Exc SAL	Inh IBU	p = 0.0002	p < 0.0001	
	Exc IBU	Inh SAL	p < 0.0001	Exc IBU	Inh SAL	p = 0.012	p < 0.0001	
	Exc IBU	Inh IBU	p < 0.0001	Exc IBU	Inh IBU	p = 0.011	p < 0.0001	

G

Wild-type control	CNO SAL	SAL	p > 0.99	CNO SAL	SAL	p = 0.48	p = 0.97	CNO alone does not alter circuit activity
	CNO SAL	Cre + IBU	p = 0.002 ↑	CNO SAL	IBU	p = 0.005 ↑	p < 0.0001 ↑	
	CNO SAL	Inh IBU	p > 0.99	CNO SAL	Inh IBU	p = 0.79	p = 0.96	
	CNO SAL	Inh SAL	p > 0.99	CNO SAL	Inh SAL	p = 0.84	p = 0.76	
	CNO SAL	Exc SAL	p < 0.0001 ↑	CNO SAL	Exc SAL	p = 0.023 ↑	p < 0.0001 ↑	Viral injection alone does not alter striosomal activity
	CNO SAL	Exc IBU	p < 0.0001 ↑	CNO SAL	Exc IBU	p = 0.33	p = 0.001 ↑	
	Cre + IBU	IBU	p = 0.08					

n.s <0.05 <0.01 <0.001 <0.0001

Figure S8: Striosomal manipulations regulate activity throughout the striosome-LHb-daSNc circuit.

(A) Detailed overview of experimental and control groups used for post hoc comparison from **Fig. 4**. **(B)** LHb sections illustrating reduced cFos expression following striosomal inhibition (left; Inh SAL) and excitation (right; Exc IBU). **(C)** daSNc sections following striosomal inhibition (left; Inh SAL) or striosomal excitation (right; Exc IBU). **(D-G)** Post hoc comparisons corresponding to **Fig. 4C and Fig. 4F-G**. **(D)** Striosomal inhibition reduced cFos expression in both striosomes and LHb and reduced pPDH expression in daSNc, regardless of SAL or IBU treatment, indicating that circuit activity is determined by striosomal state rather than IBU exposure alone. **(E)** Striosomal excitation increased cFos expression in striosomes and LHb and increased pPDH expression in daSNc, independent of IBU treatment. **(F)** Inhibitory and excitatory manipulations produced opposite effects throughout the circuit. **(G)** Control comparisons demonstrated no effect of CNO alone, as CNO SAL and SAL groups did not differ in striosomal or LHb cFos or daSNc expression. Similarly, Cre+IBU and IBU groups did not differ in striosomal cFos expression, indicating that viral expression and surgical procedures did not alter striosomal response to IBU. Mean ± SEM. For additional statistical analyses, see table S3.

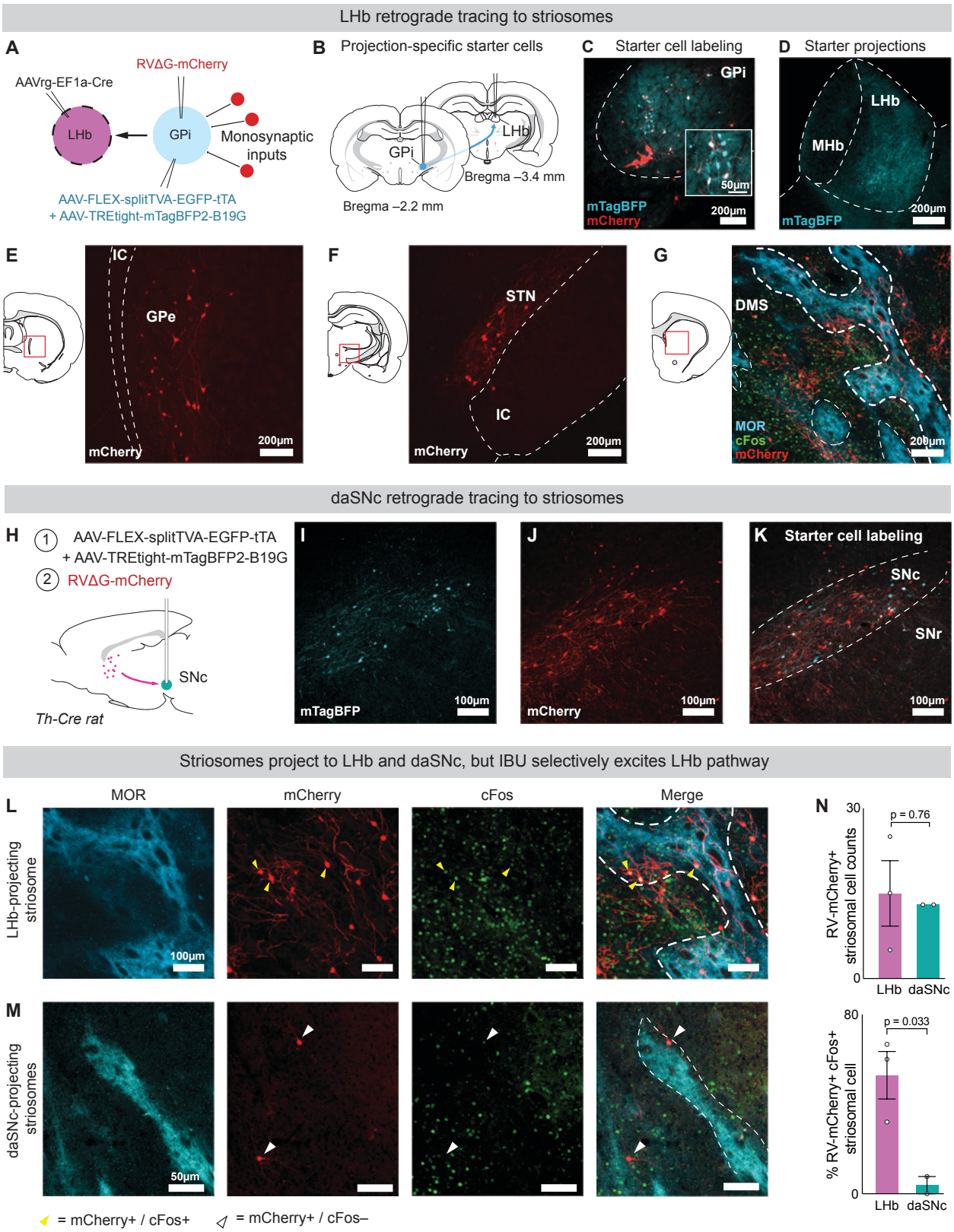
LHb retrograde tracing to striosomes
A
RVΔG-mCherry
AAVrg-EF1a-Cre
LHb
GPi
Monosynaptic inputs
AAV-FLEX-splitTVA-EGFP-tTA
+ AAV-TREtight-mTagBFP2-B19G
B
Projection-specific starter cells
GPi
LHb
Bregma –3.4 mm
Bregma –2.2 mm
C
Starter cell labeling
GPi
50μm
mTagBFP
mCherry
200μm
D
Starter projections
LHb
MHb
200μm
mTagBFP
E
IC
GPe
200μm
mCherry
F
STN
IC
mCherry
200μm
G
DMS
MOR
cFos
mCherry
200μm
daSNc retrograde tracing to striosomes
H
1 AAV-FLEX-splitTVA-EGFP-tTA
+ AAV-TREtight-mTagBFP2-B19G
2 RVΔG-mCherry
SNc
Th-Cre rat
I
mTagBFP
100μm
J
mCherry
100μm
K
Starter cell labeling
SNc
SNr
100μm
Striosomes project to LHb and daSNc, but IBU selectively excites LHb pathway
L
MOR
mCherry
cFos
Merge
LHb-projecting striosome
100μm
M
daSNc-projecting striosomes
50μm
= mCherry+ / cFos+
= mCherry+ / cFos–
N
RV-mCherry+ striosomal cell counts
p = 0.76
30
0
LHb
daSNc
% RV-mCherry+ cFos+ striosomal cell
p = 0.033
80
0
LHb
daSNc

Figure S9: **GHSR stimulation activates striosomal inputs to LHb-projecting GPi neurons, but not to daSNC.**

(A-G) Rabies-assisted monosynaptic retrograde tracing of LHb-projecting GPi neurons. **(A)** Experimental schematic; see Materials and Methods section 7 for details. **(B)** Diagram illustrating projection-defined starter cells and their location within the GPi **(C)**. **(D)** Anterogradely labeled axon terminals from starter cells were observed in LHb. Retrograde mCherry labeling was detected in GPe **(E),** STN **(F)**, and DMS (**G)**. **(H-K)** Monosynaptic retrograde tracing from daSNc neurons. **(H)** Experimental schematic. Starter cells were localized within daSNc and identified by mTagBFP expression **(I**), RV-mCherry labeling **(J)**, and merged signal **(K**). Dashed lines indicate SNc boundaries. **(L-N)** Following 1x IBU administration, DMS sections were stained for MOR, mCherry, and cFos to assess IBU-induced activation of pathway-defined striosomal neurons. LHb-projecting striosomal neurons are shown in **(L)**, and daSNc-projecting striosomal neurons are shown in (**M).** Yellow arrowheads indicate mCherry+/cFos+ neurons; white arrowheads indicate mCherry+/cFos− neurons. **(N)** Similar numbers of RV-mCherry+ striosomal neurons were observed in GPi→LHb and daSNc tracing experiments (**top;** rats=2–3/group; t-test, p=0.76). However, 1x IBU induced a significantly greater proportion of mCherry+/cFos+ neurons in the GPi→LHb pathway compared with the daSNc pathway (**bottom**; p=0.033), indicating preferential recruitment of LHb-projecting striosomal circuits following GHSR activation. Mean ± SEM.

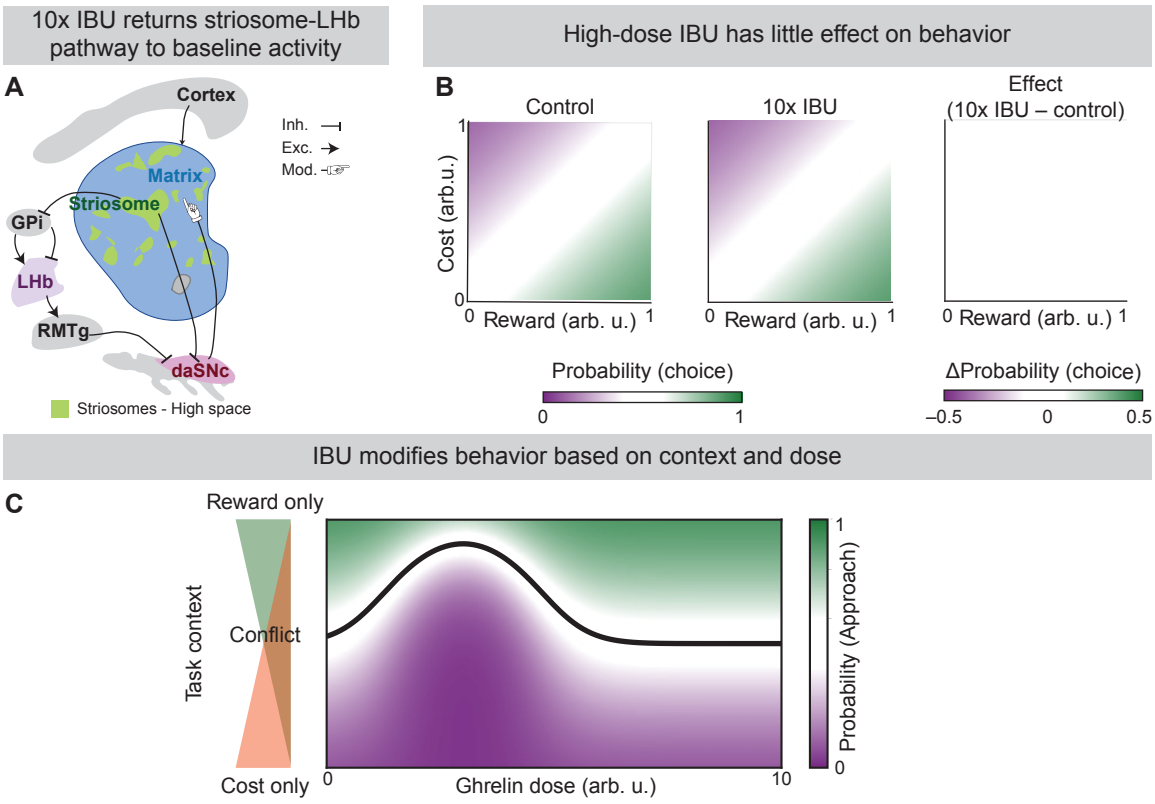

Fig. S10: High-dose ghrelin reversed striosome→LHb activation and restores baseline decision-making.

(A) Model schematic illustrating how high-dose IBU (10x) fails to recruit the striosome→LHb pathway, maintaining circuit activity near baseline levels. **(B)** Model predictions of approach/avoid behavior across reward–cost space following 10x IBU administration. Purple indicates avoidance and green indicates approach. **Left**: baseline (no IBU). **Middle:** 10x IBU condition. **Right**: difference map (baseline minus 10x IBU); white region indicates little to no change in choice probability ($\Delta p(\text{choice})=0$). In contrast to the 2x IBU condition shown in **Fig. 5E**, high-dose IBU produces minimal changes in decision boundaries because circuit is operating near or at baseline activity. **(C)** Phase diagram of the model's approach probability as a function of IBU dosage (x-axis) and task context (y-axis), where 0=cost-only, 0.5=conflict, 1=reward-only. The black contour marks the points at which approach/avoidance becomes greater/less than 50%. This illustrates how IBU guides changes in behavior in a dose-dependent and task-dependent manner. For model details see Context- and task-dependent effects on approach/avoid, section 8.3 of materials and methods.

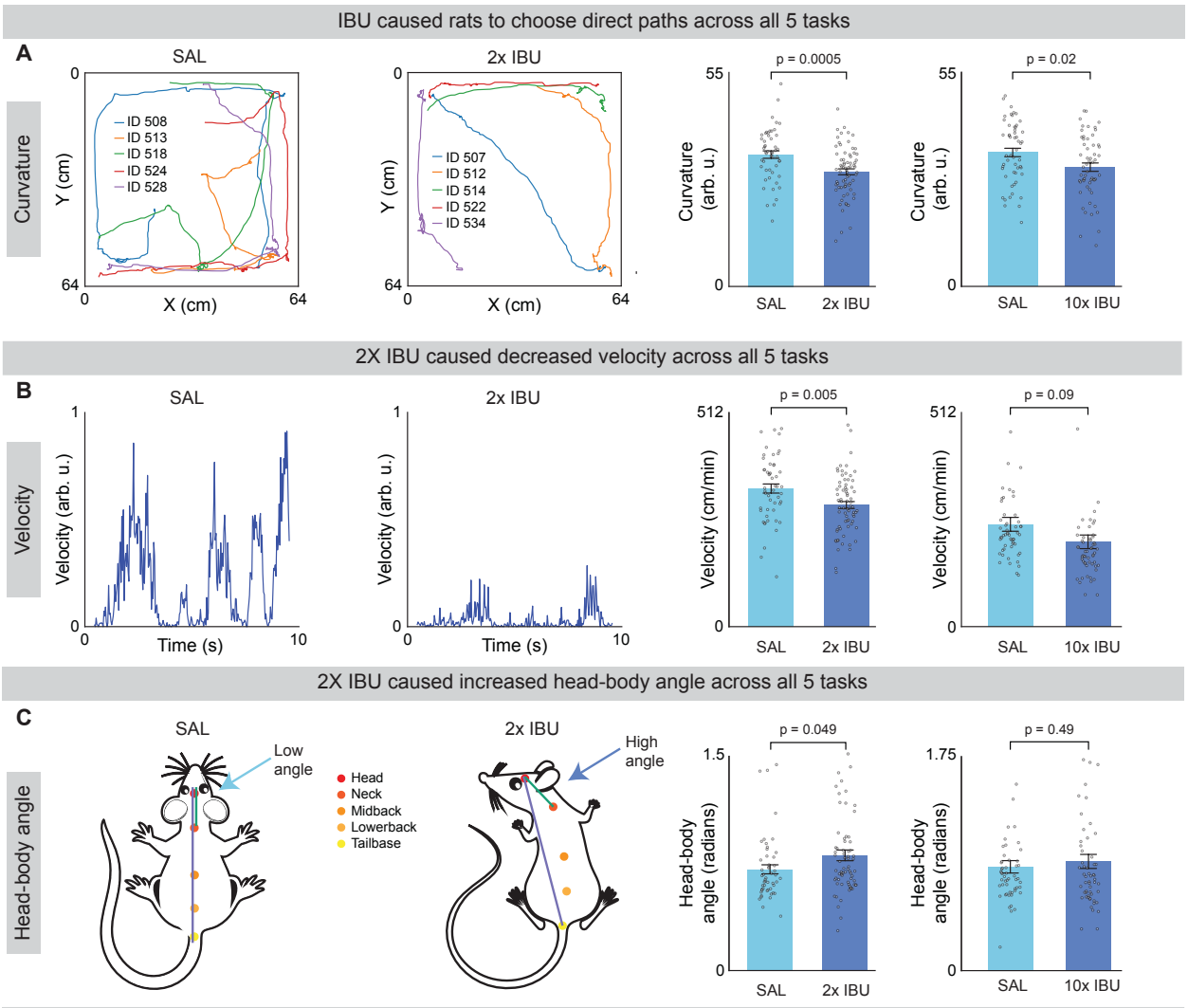
IBU caused rats to choose direct paths across all 5 tasks
A
Curvature
SAL
2x IBU
ID 508
ID 513
ID 518
ID 524
ID 528
ID 507
ID 512
ID 514
ID 522
ID 534
Y (cm)
X (cm)
0
64
p = 0.0005
p = 0.02
Curvature (arb. u.)
55
SAL
2x IBU
10x IBU
2X IBU caused decreased velocity across all 5 tasks
B
Velocity
Velocity (arb. u.)
Time (s)
1
10
p = 0.005
p = 0.09
Velocity (cm/min)
512
2X IBU caused increased head-body angle across all 5 tasks
C
Head-body angle
Low angle
High angle
Head
Neck
Midback
Lowerback
Tailbase
p = 0.049
p = 0.49
Head-body angle (radians)
1.5
1.75
Summary of behavioral feature comparisons between SAL and IBU treatment groups
D
2X IBU
Combined
Food alone
Toy alone
Light alone
Food+light
Toy+light
p = 0.0005
p = 0.005
p = 0.049
SAL = 7 IBU = 16 p = 0.07
p = 0.12
p = 0.06
SAL = 7, IBU = 14 p = 0.019
p = 0.07
p = 0.18
SAL =14, IBU = 14 p = 0.046
p = 0.14
p = 0.58
SAL = 13, IBU = 13 p = 0.55
p = 0.44
p = 0.96
SAL = 10, IBU = 14 p = 0.009
p = 0.003
p = 0.15
Curvature
Velocity
Head-body angle
E
10x IBU
p = 0.02
p = 0.09
p = 0.49
SAL = 9, IBU = 10 p= 0.011
p = 0.002
p = 0.35
SAL = 9, IBU = 10 p = 0.43
p = 0.09
p = 0.85
SAL = 9, IBU = 7 p = 0.99
p = 0.97
p = 0.85
SAL = 9, IBU = 10 p = 0.59
p = 0.11
p = 0.72
SAL = 9, IBU = 10 p = 0.026
p = 0.54
p = 0.33
n.s
<0.05
<0.01
<0.001
<0.0001

Figure S11: IBU administration alters movement features during task performance.
Motor features were extracted from pose-estimation data collected during tasks (section 9, Materials and Methods). Comparisons were performed between SAL and 2x (rats=7-16/group) and between SAL and 10x IBU (rats=7-10/group). **(A)** Example trajectories from SAL and 2x IBU-treated rats. Relative to SAL, IBU reduced trajectory curvature (2x IBU: p=0.0005; 10x IBU, p=0.02). **(B)** Example velocity traces from SAL and 2x IBU-treated rats. 2x IBU reduced velocity (p=0.005), whereas 10x IBU did not (p=0.09). These dose-dependent changes mirror alterations in daSNc pPDH expression, with increased pPDH observed following 2x IBU but not 10x IBU. **(C)** Head-body angle, defined as the difference between the head-vector (green) and body-axis (purple), was increased following 2x IBU (p=0.049) but not 10x IBU (p=0.49). **(G-H)** Motor features were analyzed across individual tasks. Arrows indicate nominal trends (p<0.15). Following 2x IBU **(G)**, curvature and velocity were generally reduced, whereas head-body angle was increased, consistent with the GHSR-mediated striosomal hyperactivity and daSNc inactivity (**Fig. 2C, M).** In contrast, 10x IBU **(H)** produced limited effects, with changes primarily observed during the Food-alone task, consistent with increased food consumption. Mean ± SEM. For additional statistical analyses, see table S3. Icons were generated using Adobe Illustrator generative tool.

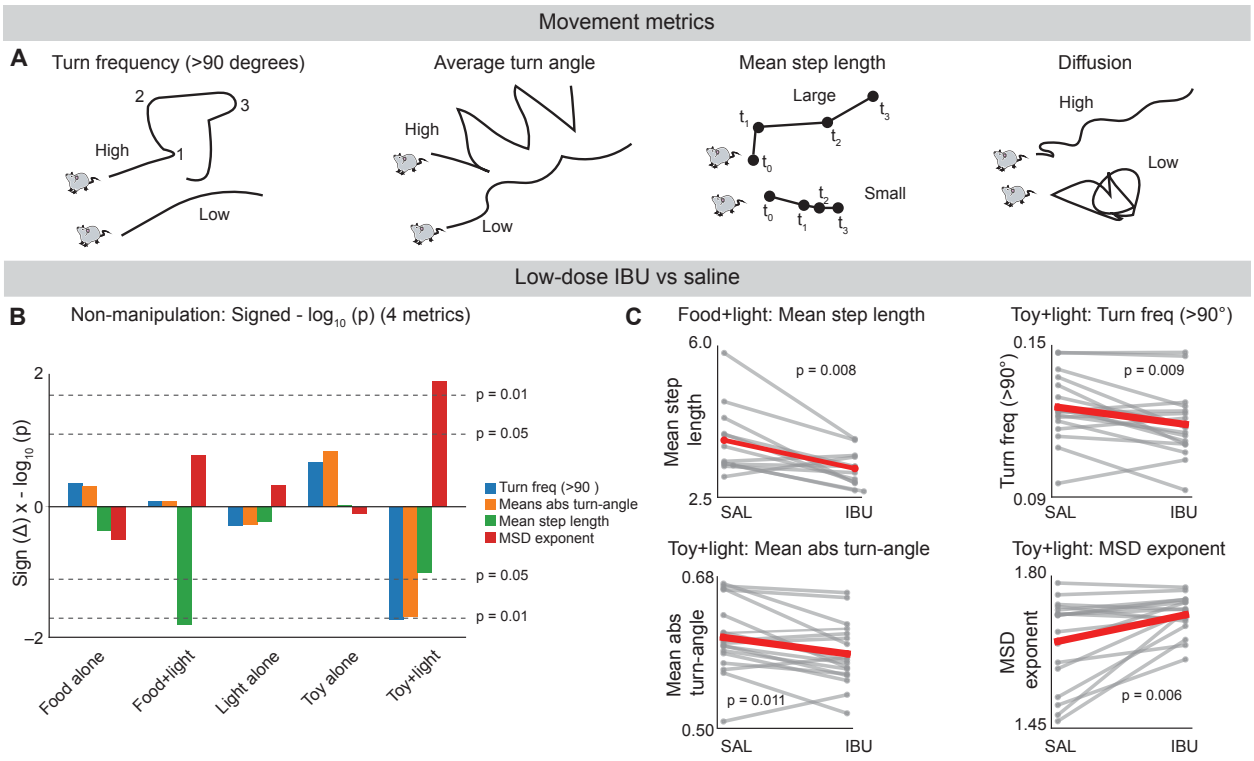

Figure S12: IBU alters movement patterns in a task-dependent manner.

(A) Four additional movement features were quantified during behavior tasks, including the frequency of turns greater than 90 degrees, average turn angle (angle between 0.2 second), mean step length, and diffusion measured from the relationship between mean squared displacement and time (see Materials and Methods section 9.6). **(B-C)** Comparison of movement features across behavioral tasks (rats=12-17/groups). **(B)** The y-axis represents the significance of SAL versus IBU differences, with positive values indicating greater scores in IBU-treated rats and negative values indicating greater scores in SAL-treated rats, dashed lines indicate p-value thresholds (t-test). IBU-induced changes in movement were strongly task-dependent, with the largest effects observed during conflict tasks ($p<0.05$). In contrast to **fig. S11**, where all tasks were impacted in significant or non-significant way. **(C)** Paired line plots showing individual animal differences for the four movement features exhibiting the strongest task-dependent effects identified in panel B (t-test, $p< 0.01$). For additional statistical analyses, see table S3.

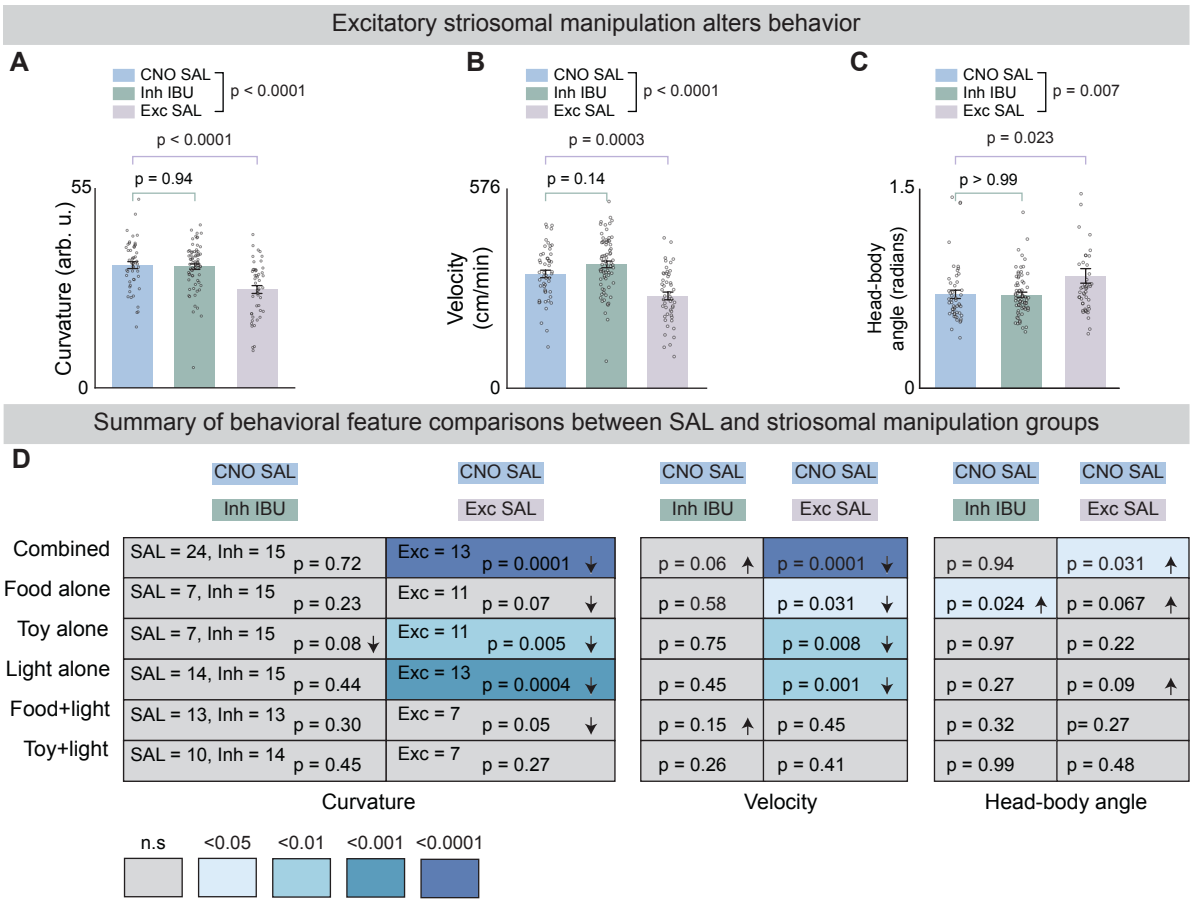

Figure S13: Striosomal manipulations differentially regulate motor dynamics during decision-making.

Movement features were analyzed following DREADD-mediated striosomal manipulation during behavioral tasks (see Materials and Methods sections 9). **(A-C)** Striosomal inhibition abolished the motor effects associated with 2x IBU, restoring trajectory curvature **(A)**, velocity **(B)**, and head-body angle **(C)** to CNO SAL-like levels (rats=7-15/group; ANOVA; post-hoc comparisons: CNO SAL vs Inh IBU: curvature p=0.94, velocity p=0.14, head-body angle p>0.99). Striosomal excitation in the absence of IBU reproduced the motor phenotype associated with GHSR activation, including reduced curvature (p<0.0001), reduced velocity (p=0.0003), and increased head-body angle (p=0.023). These findings indicate that striosomal activity contributes to both choice behavior and movement dynamics during approach–avoid decision-making. **(D)** Task-specific effects of excitatory and inhibitory DREADD manipulations across the five behavioral tasks. Mean ± SEM. Additional statistics see table S3.

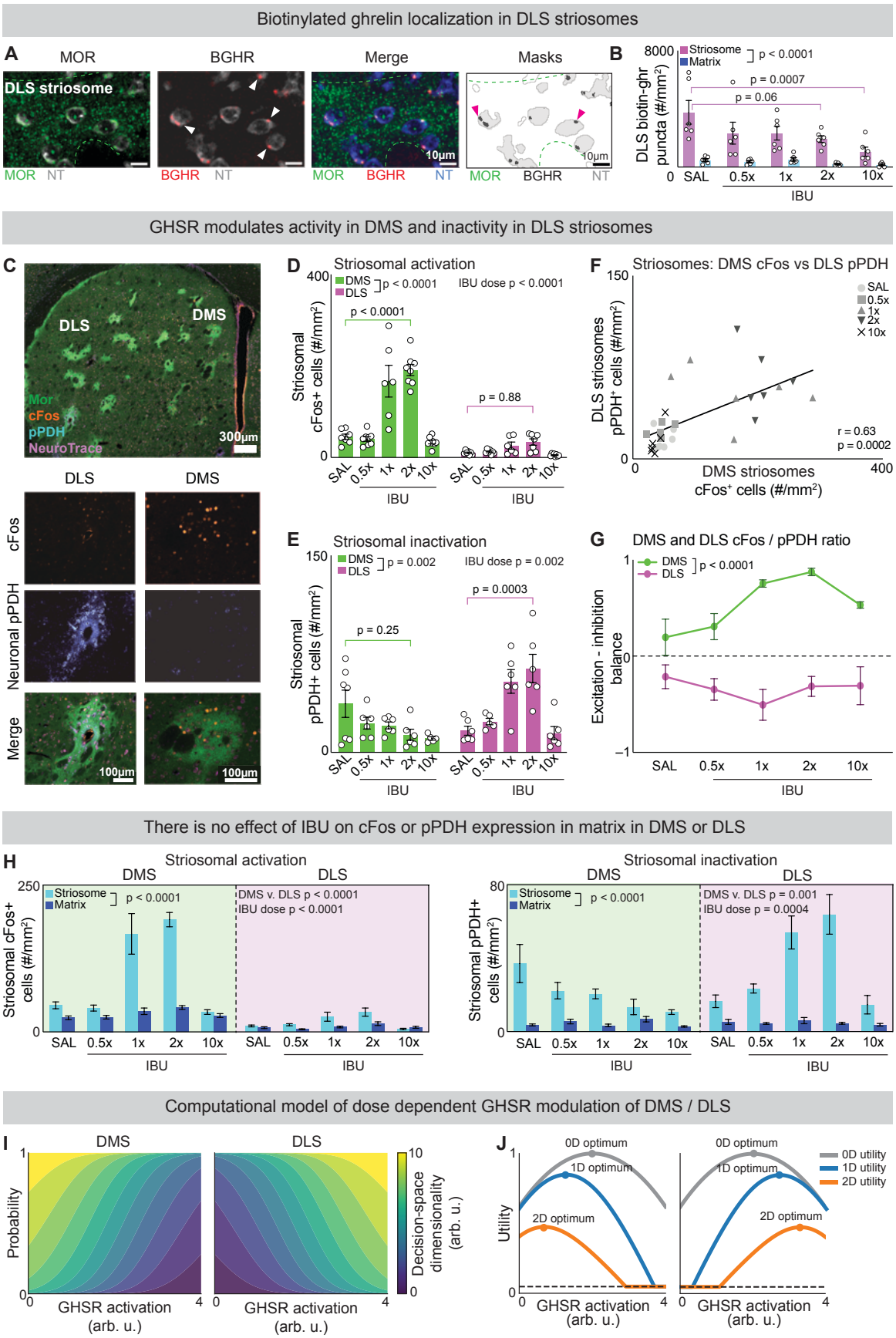
Biotinylated ghrelin localization in DLS striosomes
A
MOR
BGHR
Merge
Masks
DLS striosome
MOR NT
BGHR NT
MOR BGHR NT
MOR BGHR NT
10μm
10μm
B
Striosome
Matrix
p < 0.0001
p = 0.0007
p = 0.06
DLS biotin-ghr puncta (#/mm²)
8000
0
SAL
0.5x
1x
2x
10x
IBU
GHSR modulates activity in DMS and inactivity in DLS striosomes
C
DLS
DMS
Mor
cFos
pPDH
NeuroTrace
300μm
DLS
DMS
cFos
Neuronal pPDH
Merge
100μm
100μm
D
Striosomal activation
DMS
DLS
p < 0.0001
IBU dose p < 0.0001
Striosomal cFos+ cells (#/mm²)
400
p < 0.0001
p = 0.88
SAL
0.5x
1x
2x
10x
IBU
E
Striosomal inactivation
DMS
DLS
p = 0.002
IBU dose p = 0.002
Striosomal pPDH+ cells (#/mm²)
150
p = 0.25
p = 0.0003
F
Striosomes: DMS cFos vs DLS pPDH
SAL
0.5x
1x
2x
10x
DLS striosomes pPDH⁺ cells (#/mm²)
150
r = 0.63
p = 0.0002
DMS striosomes cFos⁺ cells (#/mm²)
400
G
DMS and DLS cFos / pPDH ratio
DMS
DLS
p < 0.0001
Excitation - inhibition balance
1
0
−1
There is no effect of IBU on cFos or pPDH expression in matrix in DMS or DLS
H
Striosomal activation
DMS
DLS
Striosome
Matrix
p < 0.0001
DMS v. DLS p < 0.0001
IBU dose p < 0.0001
Striosomal cFos+ cells (#/mm²)
250
Striosomal inactivation
DMS
DLS
Striosome
Matrix
p < 0.0001
DMS v. DLS p = 0.001
IBU dose p = 0.0004
Striosomal pPDH+ cells (#/mm²)
80
Computational model of dose dependent GHSR modulation of DMS / DLS
I
DMS
DLS
Probability
1
0
GHSR activation (arb. u.)
0
4
Decision-space dimensionality (arb. u.)
10
0
J
0D optimum
1D optimum
2D optimum
Utility
0D utility
1D utility
2D utility
GHSR activation (arb. u.)

Figure S14: GHSR activation increase cFos in DMS and pPDH in DLS striosomes.
(A-B) Similar to DMS, BGHR selectively labeled DLS striosomes **(A)** relative to matrix and decreased with increasing IBU dose (**B**, rats=6/group, ANOVA, striosomes vs matrix, $p<0.0001$; dose $p=0.009$). **(C-G)** IBU produced opposing effects across DMS and DLS striosomes (**C,** rats=5-8/group). IBU increased cFos expression in DMS but not DLS striosomes (**D**, $p<0.0001$), while increasing pPDH in DLS but not DMS striosomes (**E,** $p=0.002$; SAL vs 2x IBU in DLS $p=0.0003$). **(F)** DMS striosomal activity correlated with DLS inactivity across IBU doses ($r=0.63$, $p=0.0002$). **(G)** Excitation-inhibition balance shifted toward excitation in DMS and inhibition in DLS ($p<0.0001$). **(H)** No significant effects of IBU were observed in matrix compartments, indicating striosome-specific responses (**left**, activity, $p<0.0001$; **right**, inactivity, $p<0.0001$). **(I-J)** Model illustrating how opposing DMS and DLS striosomal states may differentially regulate parallel decision-spaces (see Materials and Methods sections 8); showing DMS (**left**, where it reduces the decision-space size) and DLS (**right,** where it increases the decision-space size). **(J)** Increased GHSR activation is predicted to preferentially influence high-dimensional decisions while minimally affecting simple choices. In the simulation, “utility” is calculated from the “optimal” striosomal activity for a decision (given its required decision-space), given GHSR activation.
Mean ± SEM. Additional statistics see table S3.

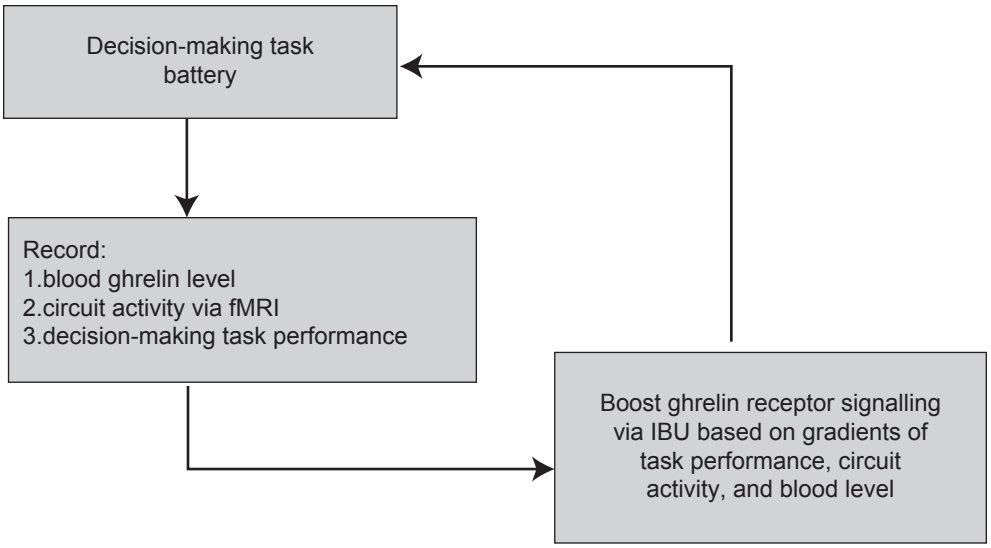

Figure S15: Bioinformed GHSR-based pharmacotherapy framework for treatment of SUD and PTSD.

Flow chart demonstrates potential personalized treatment strategy for substance use disorder (SUD) and post-traumatic stress disorder (PTSD). For each subject, blood ghrelin levels, decision-making performance, and striosomal circuit activity will be assessed. GHSR signaling can then be modulated based on behavioral performance and the striosomal circuit activity, with the goal of “normalizing” the circuit and improving decision-making behaviors.

13 TABLES

13.1 Table S1: Abbreviations

Abbreviations	Full name
GHSR	growth hormone secretagogue receptor
daSNc	dopaminergic neurons of the substantia nigra pars compacta
GPi	Globus Pallidus internus
LHb	Lateral habenula
RMTg	rostral medial tegmental nucleus
pPDH	phosphorylated pyruvate dehydrogenase
DMS	dorsomedial striatum
Oprm1-cre	Opioid Receptor Mu 1 - Cre
IBU	ibutamoren mesylate
SAL	Saline
IP	Intraperitoneal
BGHR	biotinylated acyl-ghrelin
ARC	Arcuate hypothalamic nucleus
MOR	Mu opioid receptor
AAV	Adeno-Associated Virus
GCaMP7f	Genetically encoded calcium indicator
aGHR	acyl-ghrelin
DREADD	Designer Receptors Exclusively Activated by Designer Drugs
CNO	clozapine-N-oxide
TRIO	Tracing Relationship between Input and Output
TH	Tyrosine Hydroxylase
RV	Retrovirus

Exc. SAL	Excitatory Oprm1-cre group (hM3D(Gq)) injected with CNO and Saline
Exc. IBU	Excitatory Oprm1-cre group (hM3D(Gq)) injected with CNO and 2x IBU
Inh. SAL	Inhibitory Oprm1-cre group (hM4D(Gi)) injected with CNO and saline
Inh. IBU	Inhibitory Oprm1-cre group (hM4D(Gi)) injected with CNO and 2x IBU
WT SAL	Wild-type Oprm1-cre group (hM4D(Gi)) injected with CNO and saline
WT IBU	Wild-type Oprm1-cre group (hM4D(Gi)) injected with CNO and 2X IBU
DLS	Dorsolateral striatum

2971
2972

2973 **13.2 Table S2: Reagents**

REAGENT or RESOURCE	SOURCE	IDENTIFIER
Antibodies		
Primary Antibodies		
Monoclonal mouse anti-cFos (C-10)	Santa Cruz	sc-271243
Polyclonal rabbit anti-MOR1	ImmunoStar	24216
anti-Mu Opioid Receptor antibody (UMB3) C-terminal Rabbit	Abcam	ab134054
Polyclonal guinea pig anti-MOR1	Millipore Sigma	AB5509
Monoclonal rabbit anti- phosphor-pyruvate dehydrogenase alpha1(Ser293)	Cell signaling technology	E4V9L
Polyclonal rabbit Anti-Ghrelin Receptor (GHSR) (extracellular)	Alomone labs	AGR-031
Sheep anti- Tyrosine Hydroxylase	GeneTex	GTX82570
Ghrelin, human, Biotin-labeled	AnaSpec	AS-29391
Goat anti-HA Tag	Novus Biologicals	NB600-362
Chicken Anti-Green Fluorescent Protein (GFP)	Aves Labs	GFP1020
Secondary Antibodies		
Donkey anti- guinea pig, Alexa Fluor™ 488	Jackson ImmunoResearch	706-545-148

Donkey anti- guinea pig, Alexa Fluor™ 555	Jackson ImmunoResearch	706-565-148
Donkey anti- mouse, Alexa Fluor™ 555	Jackson ImmunoResearch	715-565-151
Donkey anti- mouse, Alexa Fluor™ 594	Invitrogen	R37115
Donkey anti- mouse, Alexa Fluor™ 647	Jackson ImmunoResearch	715-605-151
Donkey anti- mouse, Alexa Fluor™ 488	Jackson ImmunoResearch	715-545-151
Donkey anti- rabbit, Alexa Fluor™ 647	Jackson ImmunoResearch	711-605-152
Donkey anti- sheep, Alexa Fluor™ 488	Jackson ImmunoResearch	713-545-003
Donkey anti- goat, Alexa Fluor™ 488	Jackson ImmunoResearch	705-545-147
Alexa Fluor™ 594-Streptavidin	Jackson ImmunoResearch	016-580-084
Donkey anti- chicken IgY, Alexa Fluor™ 488	Jackson ImmunoResearch	703-545-155
NeuroTrace™ 435/455 Blue Fluorescent Nissl Stain	Invitrogen	N21479
Other reagents		
Ibutamoren (IBU)	Medchem	HY-50844
Clozapine N-oxide (CNO)	Medchem	HY-17366
GLP-1 (7-36) amide	Bachem	4030663
DMSO	Sigma	D8418
Isoflurane	MWI	502017

0.9% sterile saline	MWI	510223
Enrosite Enroflox 2.2 7%	MWI	502017
Ostilox 5mg/ml	MWI	501080
ketamine 100mg/ml	MWI	501072
Revertidine (Atipamezole)	MWI	503012
Optixcare eye lube	MWI	065441
Lactated Ringer	MWI	501033
Bupivicaine 0.5%	MWI	65627
Metabond quick base	Patterson Dental Company C&B	75533492
Metabond gold quick catalyst	Patterson Dental Company C&B	75533500
Metabond tooth powder	Patterson Dental Company C&B	75533559
Ortho Jet liquid resin	Patterson Dental Company C&B	4594750
silicone elastomer (Kwik-Sil™)	World Precision Instruments	KWIK-SIL
Hamilton 70 microliter syringes: N Termination	Hamilton	80383
TBS	VWR	76371-738
PBS	VWR	76371-734
Triton-x 100	Sigma	T8787
Donkey Serum	Sigma	s30-100mL

Biotin Blocking Kit	Fisher Thermo labs	e21390
Glass slides	Fisher Scientific	22-034486
Coverslips	VWR	16004-312
Dapi-Fluoromount-G	Electron Microscopy Sciences	17984-24
Fluoromount-G	Electron Microscopy Sciences	7984-25
Teklad Global Irradiated 18% protein rodent diet	Laboratory Animal Resources Center	
Bacterial and Virus Strains		
pGP-AAV-syn-FLEX-**jGCaMP7f**-WPRE (AAV8)	AddGene	104492-AAV8
hSyn-DIO-**hM3D(Gq)**-mCherry (AAV8)	AddGene	50454-AAV8
pAAV-hSyn-DIO-HA-**hM4D(Gi)**-IRES-mCitrine (AAV8)	AddGene	50455-AAV8
pAAV-EF1a-Cre	AddGene	55636-AAVrg
TREtight-mTagBFP2-B19G	AddGene	100799-AAV1
AAV1-syn-FLEX-splitTVA-EGFP-tTA	Addgene	100798-AAV1
RVΔG-mCherry	Dr.Wickersham Lab	
Experimental models: Organisms		
Rat: Oprm1-Cre knock-in	Bossert et al.[29]	SD-Tg(Oprm1-icre) 1Ottc (RGD#155641245) (RRRC#975)
Th-Cre Long-Evans	NIH NIDA	N/A

Rat Long-Evans	Envigo	Strain (RRC#)
Rat Sprague Dawley	Charles River Laboratories	#001
Other		
Confocal Ziess LSM 900	Ziess	N/A
ProView Integrated Lens 1.0mm x 9.0mm	Inscopix	1050-004416
Baseplate cover	Inscopix	1050-004639
Olympus VS200 slide scanner	Olympus	N/A
Software and hardware and algorithms		
Autodesk Fusion 360 2022 or later	Autodesk	https://www.autodesk.com/products/fusion-360/personal
MATLAB R2024a	Mathworks	https://www.mathworks.com/products/matlab.html
PuTTY 0.76 or later	PuTTY	https://www.chiark.greenend.org.uk/~sgtatham/putty/latest.html
Ethovision XT16	Noldus	https://www.noldus.com/ethovision-xt
Basler acA1300-60	Basler GenICam	
Bonsai	Open Ephys	https://bonsai-rx.org/
ImageJ 1.53K	NIH	https://imagej.net/ij/,1997-2024

2974
2975

13.3 Table S3: Detailed Statistical Analysis

Figure	Main Effect	Post-hoc/ interpretation
Fig 1C, left Effects of 2x IBU on non-conflict	**Main effects:** To determine whether intermediate GHSR activation alters performance during simple non-conflict behavioral paradigms, behavioral performance was compared between SAL- and 2x IBU-treated rats across three non-conflict tasks: Food alone, Toy alone, and Light alone (rats = 25–26 per group). Because each behavioral tasks measured different baseline values and behavioral ranges, raw behavioral data were min-max normalized prior to cross-task comparisons. Group comparisons were analyzed using a two-way ANOVA followed by Tukey's multiple comparisons test. Analysis revealed no significant interaction between treatment and task ($F=0.5698$, $p=0.6504$), no significant main effect of IBU treatment ($F=0.1328$, $p=0.6545$), and no significant main effect of task ($F=1.531$, $p=0.3166$), indicating that 2x IBU did not alter performance across simple non-conflict behavioral conditions	**Post hoc comparisons:** Tukey's multiple comparisons test revealed no significant differences between SAL and 2x IBU conditions within any individual task (Food alone: $p=0.9984$; Toy alone: $p=0.9451$; Light alone: $p=0.9997$). Similarly, no differences were observed across behavioral tasks within either SAL- or IBU-treated groups (all $p > 0.72$). Together, these findings demonstrate that intermediate-dose GHSR activation does not alter performance during simple non-conflict behavioral paradigms, indicating that the behavioral effects of IBU are selective to tasks requiring conflict-based or higher-order decision-making processes.
Fig. 1 C (right) Effects of 2x IBU across conflict-based behavioral paradigms Main effects	**Main effects:** To determine whether the behavioral effects of intermediate GHSR activation differed across conflict-based paradigms, entries into the reward zone were compared between Food+Light and Toy+Light tasks following SAL or 2x IBU administration. Because behavioral tasks differed in baseline values and behavioral ranges, raw behavioral data were min-max normalized prior to cross-task comparisons. Group comparisons were analyzed using a two-way ANOVA followed by Tukey's multiple comparisons test. Analysis revealed a significant main effect of IBU treatment ($F(1,104) = 16.47$, $p=0.000096$), while no significant main effect of task type was observed ($F(1,104)=2.725$, $p=0.1018$), indicating that behavioral changes were driven primarily by IBU treatment rather than differences between conflict paradigms	**Post hoc comparisons:** Tukey's multiple comparisons test revealed no differences between Food+Light and Toy+Light tasks under SAL conditions ($p=0.4216$) or following 2x IBU administration ($p=0.8594$). In contrast, both conflict paradigms showed significantly altered behavioral performance following 2x IBU administration relative to SAL controls (SAL Toy+Light vs IBU Food+Light, $p=0.00076$; SAL Toy+Light vs IBU Toy+Light, $p=0.0067$). Together, these findings demonstrate that intermediate-dose GHSR activation similarly alters behavior across distinct conflict-based paradigms, indicating that the behavioral effects of IBU are generalized across conflict-related decision-making conditions rather than being task specific.
Fig 1D Effects of 2x IBU on	**Main effects:** To determine whether the behavioral effects of intermediate GHSR activation were selective to conflict-based decision-making paradigms, entries into the reward zone were compared between non-conflict tasks (Food alone,	**Post hoc comparisons:** Tukey's multiple comparisons test revealed no differences between SAL and 2x IBU conditions during non-conflict tasks ($p=0.9580$). In contrast, 2x IBU

conflict versus non-conflict	Toy alone, and Light alone; rats=77) and conflict-based tasks (Food-Light and Toy-Light; rats=52–56) following SAL or 2x IBU administration. Because behavioral tasks differed in baseline values and behavioral ranges, raw behavioral data were min-max normalized prior to cross-task comparisons. Group comparisons were analyzed using a two-way ANOVA followed by Tukey's multiple comparisons test. Analysis revealed a significant interaction between treatment and task type ($F(1,258)=8.891$, $p=0.0031$), a significant main effect of IBU treatment ($F(1,258)=5.451$, $p=0.0203$), and a significant main effect of task type ($F(1,258)=14.30$, $p=0.0002$), indicating that the behavioral effects of IBU differed between conflict and non-conflict paradigms.	significantly altered performance during conflict-based tasks relative to both SAL non-conflict conditions ($p=0.0001$) and SAL conflict conditions ($p=0.0034$). Similarly, within the IBU-treated group, conflict tasks differed significantly from non-conflict tasks ($p<0.0001$), whereas no differences were observed between SAL non-conflict and SAL conflict conditions ($p=0.9440$). Together, these findings demonstrate that intermediate-dose GHSR activation selectively alters behavior during conflict-based decision-making paradigms while sparing performance during simple non-conflict conditions.
Fig. 1E Chow in home cage	Paired t-test found no significant difference in amount of food consumed in the home cage between rats who received low-dose IBU to those that received saline (Paired t-test: $t(18)=0.12$, $p=0.904$). Rats=19.	
Fig. 1F Food alone task feeding	No significant difference in amount of food consumed was found in Food alone task (unpaired t-test ($t(25.87) =1.115$, $p=0.275$) between SAL (rats=14) and 2x IBU treated rats (rats=14).	
Fig. 1G Food+light task feeding	No significant difference in amount of food consumed was found in food-light task (unpaired t- test: $t(17.49) = 0.5388$, $p=0.5968$) between SAL (rats=14) and 2x IBU treated rats (rats=14).	
Fig 1H Effects of 10x IBU on conflict versus non-conflict behavioral performance	**Main effects:** To determine whether high levels of GHSR activation alter performance during conflict-based decision-making paradigms, entries into the reward zone were compared between non-conflict tasks and conflict-based tasks following SAL or 10x IBU administration. Raw behavioral data were min-max normalized prior to cross-task comparisons. Group comparisons were analyzed using a two-way ANOVA followed by Tukey's multiple comparisons test. Analysis revealed no significant interaction between treatment and task type ($F(1,91)=0.1369$, $p=0.7123$) and no significant main effect of IBU treatment ($F(1,91)=2.009$, $p=0.1598$). A significant main effect of conflict condition was observed ($F(1,91)=10.62$, $p=0.0016$), indicating overall differences between conflict and non-conflict behavioral paradigms independent of treatment condition.	**Post hoc comparisons:** Tukey's multiple comparisons test revealed no significant differences between SAL and 10x IBU conditions during either non-conflict tasks ($p=0.4946$) or conflict-based tasks ($p=0.9059$). Similarly, no differences were observed between non-conflict and conflict conditions within the 10x IBU group ($p=0.1612$). Together, these findings demonstrate that high-dose GHSR activation does not significantly alter behavioral performance during either conflict or non-conflict paradigms, further supporting an inverted-U relationship between GHSR activation and conflict-related behavioral modulation.
Fig 2C	**Main effects:** cFos expression was quantified within DMS striosome and matrix compartments following	**Post hoc comparisons:** Post hoc multiple comparisons revealed that the

Striatal cFos expression across IBU doses	SAL (rats=7), 0.5x IBU (rats=8), 1x IBU (rats=6), 2x IBU (rats=8), and 10x IBU (rats=8) administration. A two-way ANOVA revealed a significant main effect of IBU dose ($F(4,64)=32.94$, $p=7.0\times10^{-15}$), a significant main effect of region ($F(1,64)=96.15$, $p=2.3\times10^{-14}$), and a significant interaction between dose and region ($F(4,64)=22.66$, $p=1.09\times10^{-11}$), indicating that IBU modulates cFos expression in a region- and dose-dependent manner.	effects of IBU dose were driven by selective increases in striosomal cFos expression at intermediate doses (Strio: SAL vs 1x, $p=4.18\times10^{-9}$; SAL vs 2x, $p=1.02\times10^{-11}$), while no differences were observed at low or high doses (Strio: SAL vs 0.5x, p=0.9999; SAL vs 10x, p = 0.9986). Within-dose comparisons confirmed significant differences between striosome and matrix compartments only at 1x and 2x IBU doses (1x: Strio vs Matrix, $p=1.07\times10^{-9}$; 2x: Strio vs Matrix, $p=9.67\times10^{-12}$), with no compartment differences observed under SAL, 0.5x, or 10x conditions (SAL: p=0.9209; 0.5x: p=0.9826; 10x: p=0.9999). In contrast, matrix cFos expression did not differ across treatment conditions (Matrix: SAL vs 0.5x, p>0.9999; SAL vs 1x, p=0.9994; SAL vs 2x, p=0.9707; SAL vs 10x, p=0.9999), indicating that IBU selectively recruits striosomal neurons without altering matrix activity. Together, these findings demonstrate an inverted-U relationship between GHSR activation and striosomal recruitment, with selective engagement of DMS striosomes occurring only at intermediate levels of GHSR signaling.
Fig 2F Compartment-specific GHSR expression within the DMS	To determine whether Growth Hormone Secretagogue Receptor (GHSR) expression was enriched within the striosomal compartments of the dorsomedial striatum (DMS), GHSR expression was quantified in striatum (rats=7). A paired t-test comparing GHSR expression between compartments revealed significantly greater GHSR expression within striosomes relative to the surrounding matrix (paired t-test: $t(6)=5.656$, $p=0.0013$), indicating preferential localization of GHSR within striosomal compartments of the DMS.	
Fig 2H BGHR binding across striatum	**Main effects:** To further validate compartment-specific GHSR localization within the striatum and determine whether prior IBU treatment altered subsequent ghrelin ligand binding, biotinylated ghrelin (BGHR) puncta density was quantified within striosome and matrix compartments following administration of SAL (rats=7), 0.5x IBU (rats=6), 1x IBU (rats=6), 2x IBU (rats=6), and 10x IBU (rats=6). Tissue sections were incubated ex vivo with BGHR	**Post hoc comparisons:** Tukey's post hoc multiple comparisons first confirmed significantly greater BGHR puncta density within SAL striosomes relative to SAL matrix compartments ($p=7\times10^{-8}$), a secondary validation that GHSR expression is localized predominantly within striosomal compartments. Comparisons across IBU doses further

	to assess ligand binding density across striatal compartments. A two-way ANOVA revealed a significant interaction between IBU dose and compartment ($F(4, 52)=4.322$, $p=0.0043$), a significant main effect of IBU dose ($F(4, 52)=5.393$, $p=0.0010$), and a significant main effect of compartment ($F(1, 52)=65.50$, $p<0.00000001$), indicating that BGHR binding varied across both compartment and prior IBU exposure conditions.	revealed progressive reductions in striosomal BGHR binding following prior IBU administration, consistent with reduced availability of ghrelin ligand binding sites following in vivo GHSR activation. Relative to SAL striosomes, BGHR puncta density was significantly reduced following 0.5x ($p=0.0179$), 1x ($p=0.0143$), 2x ($p=0.0080$), and 10x IBU ($p=0.00000797$). In contrast, matrix BGHR puncta density did not differ across treatment conditions (all $p>0.99$), indicating that the effects of IBU were largely restricted to striosomal compartments. Within-dose compartment comparisons further demonstrated significant striosomes enrichment under SAL ($p=0.00000007$) and 0.5x IBU conditions ($p=0.0478$), while compartment differences were no longer detected following 1x, 2x, or 10x IBU administration (all $p>0.05$). Together, these findings demonstrate that GHSR expression is enriched within striosomes under baseline conditions and that prior in vivo IBU administration dose-dependently reduces subsequent BGHR binding, consistent with receptor occupancy and/or reduced ligand accessibility following GHSR activation. IBU-induced reductions in BGHR binding may suggest that intermediate levels of GHSR activation selectively recruit striosomal signaling, whereas high levels of GHSR activation disrupt this compartment-specific state. Excessive GHSR activation collapses striosomal-selective signaling within the dorsal striatum.
Fig 2K LHb cFos expression across IBU doses	**Main effects:** cFos expression in the LHb was compared across SAL (rats=10), 0.5x IBU (rats=6), 1x IBU (rats=8), 2x IBU (rats=6), and 10x IBU (rats=6) conditions to determine whether IBU dose-dependently modulates LHb activity. A one-way ANOVA revealed a significant effect of IBU concentration on LHb cFos expression ($F(4,31)=14.52$, $p=8.7 \times 10^{-8}$), indicating a dose-dependent effect of IBU on LHb activation	**Post hoc comparisons:** Tukey post hoc multiple comparisons showed that LHb cFos expression was significantly increased under both 1x and 2x IBU conditions compared to SAL (SAL vs 1x, $p=2.09 \times 10^{-5}$; SAL vs 2x, $p=1.32 \times 10^{-5}$), whereas no differences were observed between SAL and either 0.5x or 10x IBU (SAL vs 0.5x, $p=0.665$; SAL vs 10x, $p=0.823$). Similarly, both 1x and 2x conditions showed significantly greater cFos expression relative to 0.5x IBU

		(0.5x vs 1x, p = 0.0054; 0.5x vs 2x, p=0.0023). No differences were observed between the 1x and 2x IBU groups (p=0.973), indicating similar levels of LHb activation at intermediate doses. In contrast, both intermediate doses showed significantly greater cFos expression than the 10x condition (1x vs 10x, p=0.0026; 2x vs 10x, p=0.0011), further supporting a nonlinear dose-dependent effect of IBU on LHb activity.
Fig 2M daSNc pPDH expression across IBU doses	**Main effects:** pPDH expression in the daSNc was compared across SAL (rats=6), 0.5x IBU (rats=6), 1x IBU (rats=6), 2x IBU (rats=7), and 10x IBU (rats=6) conditions to determine whether IBU dose-dependently modulates neuronal inactivity within dopaminergic SNc regions. A one-way ANOVA revealed a significant main effect of IBU concentration on pPDH expression ($F(4, 26)=17.89$, $p=3.61 \times 10^{-7}$), indicating a dose-dependent effect of IBU on daSNc pPDH levels.	**Post hoc comparisons:** Post hoc multiple comparisons showed that pPDH expression was significantly increased under both 1x and 2x IBU conditions compared to SAL (SAL vs 1x, p=0.0031; SAL vs 2x, $p=1.81 \times 10^{-5}$), whereas no differences were observed between SAL and either 0.5x or 10x IBU (SAL vs 0.5x, p=0.99997; SAL vs 10x, p=0.9970). Similarly, both 1x and 2x IBU conditions showed significantly greater pPDH expression relative to 0.5x IBU (0.5x vs 1x, p=0.0023; 0.5x vs 2x, $p=1.35 \times 10^{-5}$), while no differences were observed between 0.5x and 10x conditions (p=0.9994). No significant differences were detected between the 1x and 2x IBU groups (p=0.373), indicating comparable levels of daSNc pPDH expression at intermediate doses. In contrast, both intermediate doses showed significantly greater pPDH expression than the 10x condition (1x vs 10x, p=0.0013; 2x vs 10x, $p=7.45 \times 10^{-6}$), supporting a nonlinear dose-dependent effect of IBU on daSNc inactivity.
Fig. 3B Striosomal specificity of hM4D(Gi) viral targeting	To determine the compartment-specificity of viral targeting in Oprm1-Cre rat rats, the percentage of hM4D(Gi)-positive cells localized within striosome and matrix compartments was quantified following viral expression. A paired t-test comparing the percentage of virus-positive cells between striosome and matrix compartments revealed a significant enrichment of hM4D(Gi) expression within striosomes (paired t-test: $t(5)=12.27$, $p=6.37 \times 10^{-5}$; rats=6).	Confirming selective striosomal targeting of the inhibitory DREADD virus

Fig. 3D (top) Time-dependent effects of IBU on striosomal activity	**Main effects:** To determine whether intermediate and high IBU doses differentially modulate striosomal activity across time, in vivo calcium imaging was performed following administration of 2x or 10x IBU (rats=4, fields of view=6). Calcium dynamics were monitored longitudinally across multiple time points (0, 30, 60, 120, 180, 240, 300, and 360 min) to assess the temporal effects of IBU-induced striosomal activity. Because individual rats displayed different baseline numbers of active cells, data were normalized to each animal's baseline recording by calculating the change in active cells relative to the 0 min condition at each subsequent time point. Raw non-normalized values are shown in fig. S5E. Data were analyzed using a mixed-effects model with matching time points. Analysis revealed a significant main effect of time ($F(7, 35)=3.562$, $p=0.0054$) and a significant main effect of IBU dose ($F(1, 5)=36.59$, $p=0.0018$), indicating that striosomal activity varies across time and differs between intermediate and high IBU doses.	**Post hoc comparisons:** Post hoc multiple comparisons revealed that 2x IBU results in elevated striosomal activity beginning approximately 30–120 min following administration, consistent with the delayed pharmacokinetics of IBU. 2x IBU produced greater striosomal activity than 10x IBU across matched time points from baseline through 300 min (0 min, $p=0.000034$; 30 min, $p=0.000034$; 60 min, $p=0.000034$; 120 min, $p=0.000034$; 180 min, $p=0.000034$; 240 min, $p=0.000034$; 300 min, $p=0.000034$), indicating prolonged activation under intermediate-dose conditions. Within the 2x IBU condition, striosomal activity remained relatively stable across 30–180 min (all $p>0.88$), suggesting a prolonged plateau of elevated striosomal activity during this interval. In contrast, the 10x IBU dose showed prolonged suppression of striosomal activity relative to baseline conditions. Comparisons between early baseline time points and later 10x recordings demonstrated significantly reduced activity at 300 min (0 vs 300 min, $p=0.019$), with suppressed activity persisting through 360 min, indicating that high-dose IBU inhibited striosomal activity for well over 5 hr following administration. Together, these findings indicate that intermediate IBU doses produce sustained striosomal activation peaking approximately 2–3 hr following administration, whereas high doses suppress striosomal signaling below baseline levels across an extended recording window, supporting an inverted-U relationship between GHSR activation and striosomal calcium dynamics.
Fig 3D (bottom) Time-dependent effects of endogen	**Main effects:** To determine whether aGHR dose differentially modulates striosomal activity across time, in vivo calcium imaging was performed following administration of an intermediate dose (4.3 µg/kg, rats=2) or high dose (86 µg/kg, rats=3) aGHR. Calcium activity was monitored across multiple time points (0, 10, 15, 30, 60, and 120 min) to assess the temporal dynamics of GHSR-mediated striosomal	**Post hoc comparisons:** Post hoc multiple comparisons revealed that both aGHR doses produced peak effects approximately 15 min following administration. Under the high-dose condition (86 µg/kg), striosomal activity was significantly reduced beginning at 10 min (0 vs 10 min, $p=0.0411$), reached

ous acyl-ghrelin (aGHR) on striosomal activity	signaling. Because individual rats displayed different baseline numbers of active cells, data were normalized to each animal's baseline recording by calculating the change in active cells relative to the 0 min condition at each subsequent time point. Raw non-normalized values are shown in fig. S5E. Data were analyzed using a mixed-effects model with matching time points. Analysis revealed a significant main effect of time ($F(5,14)=8.230$, $p=0.00083$), a significant main effect of aGHR concentration ($F(1,3)=34.14$, $p=0.00999$), and a significant interaction between time and aGHR concentration ($F(5,14)=29.16$, $p=0.00000063$), indicating that aGHR dose differentially modulates striosomal activity across time.	maximal effects at 15 min (0 vs 15 min, $p=0.000012$), and remained significantly inhibited through 60 min (0 vs 30 min, $p=0.00011$; 0 vs 60 min, $p=0.0029$), before returning toward baseline levels by 120 min ($p=0.2140$). In contrast, the intermediate dose (4.3 ug/kg) significant increased activity beginning at 10 min (0 vs 10 min, $p=0.0303$), with maximal effects observed at 15 min (0 vs 15 min, $p=0.000063$), followed by rapid normalization by 30–120 min (all $p>0.46$). Comparisons within the 4.3 ug/kg condition further demonstrated that activity significantly declined following the 15 min peak (15 vs 30 min, $p=0.00016$; 15 vs 60 min, $p=0.000026$; 15 vs 120 min, $p=0.000070$). Together, these findings demonstrate that endogenous aGHR rapidly modulates striosomal activity, with peak effects occurring approximately 15 min following administration and largely resolving within 30–120 min depending on dose
Fig 3E (top) In vivo striosomal calcium activity across IBU doses	**Main effects):** In vivo calcium imaging was performed to determine whether IBU dose-dependently modulates striosomal activity. Calcium dynamics were compared across SAL, 1x, 2x, 10x, and 30x IBU conditions using repeated recordings from the same rats (rats=8; fields of view=10). A repeated-measures ANOVA revealed a significant main effect of IBU dose on the number of active striosomal cells ($F(1.904, 17.13)=16.54$, $p=0.000117$), indicating that IBU modulates striosomal activity depending on dose.	**Post hoc comparisons:** Post hoc multiple comparisons revealed that 2x IBU produced prolonged elevations in striosomal activity beginning approximately 30–120 min following administration, consistent with the delayed pharmacokinetics of IBU. Relative to corresponding 10x conditions, 2x IBU produced significantly greater activity at 30 min ($p=0.00031$), 60 min ($p=0.00031$), 120 min ($p=0.00031$), 180 min ($p=0.00031$), 240 min ($p=0.00031$), and 300 min ($p=0.00031$), indicating sustained divergence between intermediate and high IBU doses across the majority of the recording period. Although several within-dose comparisons for the 2x condition did not survive multiple-comparisons correction, striosomal activity remained elevated above baseline-associated levels throughout the 120–300 min interval, consistent with

		a prolonged activation phase peaking approximately 2–3 hr following administration. In contrast, the 10x condition failed to produce sustained activation and instead showed prolonged suppression of striosomal activity. Comparisons within the 10x condition demonstrated significantly reduced activity at 300 min relative to baseline (0 vs 300 min, p=0.0187), with suppressed activity persisting through 360 min, indicating that high-dose IBU inhibited striosomal signaling for well over 5 hr following administration. Together, these findings support a bidirectional dose-dependent effect of IBU on striosomal activity, where intermediate doses induce prolonged activation while high doses suppress activity below baseline levels across an extended temporal window.
Fig 3E (bottom) In vivo striosomal calcium activity across acyl-ghrelin (aGHR) doses	**Main effects:** To determine whether the dose-dependent striosomal activity observed following IBU administration was IBU-specific effect or GHSR activation effect, in vivo calcium imaging was performed administration of increasing doses of endogenous aGHR. Calcium dynamics were compared across SAL, intermediate aGHR doses (4.3 and 8.6 ug/kg), high doses (26 and 86 ug/kg), and an ultra-high dose (125 ug/kg) using repeated recordings from the same rats (rats=8; fields of view=10). A repeated-measures one-way ANOVA revealed a significant main effect of acyl-ghrelin dose on the number of active striosomal cells ($F(2.412, 21.71)=20.89$, $p=0.000004$), indicating that acyl-ghrelin modulates striosomal activity depending on dose.	**Post hoc comparisons:** Tukey's multiple comparisons test showed that intermediate aGHR doses significantly increased the number of active striosomal cells relative to SAL (SAL vs 4.3 ug/kg, p=0.0050; SAL vs 8.6 ug/kg, p=0.0109), whereas higher doses did not differ from SAL (SAL vs 26 ug/kg, p=0.2345; SAL vs 86 ug/kg, p=0.0766). In contrast, the ultra-high 125 ug/kg dose significantly reduced striosomal activity relative to SAL (p=0.0313), indicating suppression of baseline activity at excessive aGHR concentrations. No differences were observed between the two intermediate doses (4.3 vs 8.6 ug/kg, p=0.9344), suggesting comparable increases in striosomal activity. Both intermediate doses also showed significantly greater activity than high and ultra-high doses (4.3 vs 26 ug/kg, p=0.0439; vs 86 ug/kg, p=0.0012; vs 125 ug/kg, p=0.0015; 8.6 vs 86 ug/kg, p=0.0111; vs 125 ug/kg, p=0.0070). Similarly, the 26 ug/kg dose showed

		significantly greater activity than both 86 ug/kg and 125 ug/kg conditions (p=0.0111 and p=0.0434, respectively), while no differences were observed between 86 ug/kg and 125 ug/kg doses (p=0.9601). Together, these findings demonstrate that modulation of striosomal activity is a general feature of GHSR activation and not unique to IBU, supporting an inverted-U relationship between ghrelin signaling and striosomal circuit activity.
Fig 4C Effects of striosomal chemogenetic manipulation on cFos expression	**Main effects:** To determine whether selective manipulation of striosomal neurons altered IBU-induced recruitment of the striosomal circuit, cFos-positive cells were quantified within MOR-positive striosomal ROIs and only in neurons co-expressing the DREADD virus, identified by either HA-tag or mCherry labeling depending on the viral construct. Experimental groups included SAL (rats=7), Cre+IBU (rats=6), Inh IBU (inhibitory hM4Di + CNO + IBU; rats=8), Inh SAL (hM4Di + CNO +SAL; rats=6), Exc SAL (excitatory hM3Dq + CNO +SAL; rats=6), Exc IBU (excitatory + CNO + IBU; rats=6), and WT + CNO saline controls (CNO SAL; rats=6). Group comparisons were analyzed using a one-way ANOVA followed by Tukey's multiple comparisons test. Analysis revealed a significant main effect of treatment group on striosomal cFos expression ($F(6,37)=23.27$, $p<0.000000000035$).	**Post hoc comparisons - inhibitory manipulation:** Tukey's multiple comparisons test revealed that 2x IBU significantly increased striosomal cFos expression relative to SAL conditions (p=0.0000057). Importantly, inhibitory chemogenetic suppression of striosomal neurons abolished the effects of IBU, as the Inh IBU group showed significantly lower striosomal cFos expression relative to the Cre+IBU condition ($p=9.38x10^{-7}$) and was not different from SAL conditions (p=0.996). Similarly, the Inh SAL group was significantly lower than the Cre+IBU condition ($p=3.91x10^{-6}$) and was not different from SAL controls (p = 0.9997). CNO SAL rats that received CNO did not differ from SAL conditions (p=0.9999), indicating that CNO administration alone did not alter striosomal activity in rats lacking DREADD expression. **Post hoc comparisons - excitatory manipulation:** Excitatory chemogenetic activation of striosomal neurons mimicked the effects of IBU, as the Exc SAL group displayed significantly greater striosomal cFos expression relative to SAL controls ($p=4.72x\ 10^{-7}$) and was not different from the Cre+IBU group (p = 0.9851). Similarly, the Exc IBU group was significantly elevated relative to SAL conditions (p=0.000033397) and did not differ from the Cre+IBU condition (p=0.8556). Both excitatory groups also showed significantly greater striosomal cFos

		expression relative to inhibitory manipulation groups and CNO SAL controls (all p<0.00001). Together, these findings demonstrate that inhibitory manipulation blocks IBU-induced striosomal recruitment, whereas excitatory manipulation phenocopies the effects of intermediate-dose GHSR activation on the striosomal circuit.
Fig 4D Effects of striosomal manipulation on non-conflict	**Main Effects:** To determine whether selective manipulation of striosomal neurons altered performance during non-conflict behavioral conditions, behavioral performance was compared across CNO SAL (rats=14), CNO IBU (rats=14), Inh IBU (inhibitory hM4Di + CNO + IBU; rats=15), Inh SAL (hM4Di + CNO +SAL; rats=15), Exc SAL (excitatory hM3Dq + CNO +SAL; rats=11), and Exc IBU (excitatory + CNO + IBU; rats=11). The inhibitory cohort (rats=15) underwent repeated testing under both SAL and IBU conditions, while the excitatory cohort (rats=11) similarly underwent testing under both SAL and IBU conditions. WT rats consisted of separate littermate control groups matched for age and surgical procedures but lacking Cre expression, and therefore did not express DREADD receptors despite receiving identical viral and CNO treatments. Group comparisons were analyzed using a one-way ANOVA followed by Tukey's multiple comparisons test. Analysis revealed a main effect of treatment group ($F(5, 234)=3.085$, $p=0.0102$)	**Post hoc comparisons:** Despite the overall main effect, post hoc multiple comparisons revealed no significant differences between CNO SAL and CNO IBU groups (p=0.9989), reproducing our earlier findings that intermediate-dose IBU does not significantly alter performance during simple, non-conflict behavioral tasks. Similarly, no significant differences were observed between WT controls and either inhibitory or excitatory chemogenetic manipulation groups (all p>0.19), suggesting that neither activation nor inhibition of striosomal neurons substantially altered performance during non-conflict behavioral conditions. The only significant post hoc comparison observed was between the Inh IBU and Exc IBU groups (p=0.0032), indicating that inhibitory and excitatory manipulations produced opposing behavioral effects under IBU conditions. However, because neither group differed significantly from WT controls or saline conditions individually, these findings overall suggest that striosomal recruitment does not strongly influence performance during simple non-conflict behaviors.
Fig 4E Effects of striosomal chemogenetic manipulation on conflict-task	**Main effects:** To determine whether recruitment of the striosomal circuit mediates the behavioral effects of intermediate-dose IBU during conflict-based decision-making, behavioral performance was compared across CNO SAL (rats=12), CNO IBU (rats=14), Inh IBU (inhibitory hM4Di + CNO + IBU; rats=15), Inh SAL (hM4Di + CNO +SAL; rats=15), Exc SAL (excitatory hM3Dq + CNO +SAL; rats=7), and Exc IBU (excitatory + CNO + IBU; rats=13) groups. Group comparisons were analyzed using an ordinary one-way ANOVA followed by Tukey's multiple comparisons test. Analysis revealed a	**Post hoc comparisons:** Tukey's multiple comparisons test first reconfirmed our earlier findings that 2x IBU significantly alters performance during conflict-based tasks (CNO IBU vs CNO SAL, p=0.0067). These experiments were performed in an independent cohort of rats and reproduced the same behavioral phenotype observed previously, demonstrating that the behavioral effects of 2x IBU remain intact following viral

perform ance	significant main effect of treatment group on conflict-task performance ($F(5,146)=6.668$, $p=1.27 \times 10^{-5}$).	surgery, CNO administration, and other experimental manipulations. Inhibitory chemogenetic suppression of striosomal neurons blocked the behavioral effects of IBU. The Inh IBU group differed significantly from CNO IBU rats ($p=0.0320$) but not from CNO SAL controls ($p=0.9834$), indicating that striosomal inhibition returned behavior to baseline levels. No differences were observed between inhibitory groups (Inh IBU vs Inh SAL, $p=0.7269$), further supporting that blockade of the IBU behavioral phenotype was specifically caused by striosomal inhibition rather than nonspecific surgical or treatment-related effects. In contrast, excitatory chemogenetic activation of striosomal neurons, even in the absence of IBU, was sufficient to mimic the behavioral effects of IBU (CNO IBU vs Exc SAL, $p=0.0245$), yield behavioral patterns significantly different form CNO SAL control ($p=0.9999$). Similarly, the Exc IBU group differed significantly from CNO SAL controls ($p=0.00014$) but not from CNO IBU rats ($p=0.8638$). No differences were observed between both excitatory groups (Exc SAL vs Exc IBU, $p=0.9776$), indicating that excitatory manipulation alone was sufficient to reproduce the behavioral phenotype associated with GHSR activation. Finally, inhibitory and excitatory manipulation of striosomal neurons produced significantly different behavioral outcomes under identical IBU conditions, (Inh IBU vs Exc IBU, $p=0.00079$). Together, these findings demonstrate that striosomal recruitment is necessary for mediating the behavioral effects of intermediate-dose GHSR activation during conflict-based decision-making tasks.
Fig 4F Effects of striosom al manipul	**Main effects:** To determine whether GHSR-induced recruitment of the LHb was dependent on striosomal activity, cFos-positive cells were quantified within the LHb following chemogenetic manipulation of striosomal neurons using Cre-dependent DREADD expression. Experimental groups included SAL	**Post hoc comparisons - inhibitory manipulation:** Tukey's multiple comparisons test confirmed that IBU significantly increased LHb cFos expression relative to SAL conditions ($p=0.0000024$). Inhibitory chemogenetic

ation on LHb cFos	(rats=10), IBU (rats=6), Inh IBU (inhibitory hM4Di + CNO + IBU; rats=7), Inh SAL (hM4Di + CNO + SAL; rats=8), Exc SAL (excitatory hM3Dq + CNO + SAL; rats=6), Exc IBU (excitatory + CNO + IBU; rats=6), and WT + CNO saline controls (CNO SAL; rats=6). Group comparisons were analyzed using a one-way ANOVA followed by Tukey's multiple comparisons test. Analysis revealed a significant main effect of treatment group on LHb cFos expression ($F(6,42)=13.25$, $p=2.34 \times 10^{-8}$).	suppression of striosomal neurons abolished the effects of IBU (IBU vs Inh IBU, p=0.000036), returning LHb cFos levels similar to SAL controls (p=0.9995). Similarly, the Inh SAL group differed significantly from the IBU condition (p=0.000032) but was not different from SAL controls (p=0.9968). The Inh IBU and Inh SAL groups also did not differ from one another (p=0.9999), indicating that IBU administration did not increase LHb cFos expression when striosomal neurons were inhibited. WT SAL rats that received CNO alone did not differ from SAL controls (p=0.4761), confirming that CNO administration alone did not alter LHb cFos expression in the absence of DREADD expression. **Post hoc comparisons - excitatory manipulation:** Excitatory chemogenetic activation of striosomal neurons mimicked the effects of IBU, resulting in significantly greater LHb cFos expression relative to SAL controls (p=0.000019) and levels that were not different from the IBU condition (p=0.9973). Similarly, the Exc IBU group showed significantly greater LHb cFos expression relative to SAL conditions (p=0.0015) and did not differ from the IBU group (p=0.5529). Both excitatory groups also showed significantly greater LHb cFos expression relative to inhibitory manipulation groups (all p<0.012). Exc SAL and Exc IBU groups did not differ from one another (p=0.8778), indicating that excitatory manipulation alone was sufficient to recapitulate the effects of intermediate-dose GHSR activation on LHb recruitment. Together, these findings demonstrate that GHSR-induced LHb activation is dependent on striosomal activity and that selective excitation of striosomal neurons is sufficient to

		phenocopy the effects of IBU on downstream circuit recruitment.
Fig 4G Effects of striosomal chemogenetic manipulation on daSNc pPDH	**Main effects:** To determine whether the GHSR-induced inactivity-associated pPDH expression observed in daSNc was dependent on striosomal activity, pPDH-positive cells were quantified within the daSNc following chemogenetic manipulation of striosomal neurons using Cre-dependent DREADD expression. Quantification was restricted to TH-positive dopaminergic neurons co-expressing pPDH. Experimental groups included SAL (rats=7), IBU (rats=7), Inh IBU (inhibitory hM4Di + CNO + IBU; rats=6), Inh SAL (hM4Di + CNO + SAL; rats=6), Exc SAL (excitatory hM3Dq + CNO + SAL; rats=6), CNO SAL (WT + CNO + SAL; rats=6), and Exc IBU (excitatory + CNO + IBU; rats=6). Group comparisons were analyzed using a one-way ANOVA followed by Tukey's multiple comparisons test. Analysis revealed a significant main effect of treatment group on daSNc pPDH expression ($F(6,36)=27.64$, $p=4.384 \times 10^{-12}$).	**Post hoc comparisons - inhibitory manipulation:** Tukey's multiple comparisons test revealed that 2x IBU significantly increased pPDH expression within TH-positive daSNc neurons relative to SAL conditions ($p=0.00000051$). Inhibitory chemogenetic suppression of striosomal neurons abolished the effects of IBU (IBU vs Inh IBU, $p=0.0000000019$), returning pPDH levels similar to SAL controls ($p=0.5231$). Similarly, the Inh SAL group differed significantly from the IBU condition ($p=0.00000000047$) but was not different from SAL controls ($p=0.2522$).The Inh IBU and Inh SAL groups also did not differ from one another ($p=0.9988$), indicating that systemic GHSR activation failed to increase daSNc pPDH expression when striosomal neurons were inhibited. Despite systemic GHSR activation, inhibition of striosomal neurons prevented recruitment of pPDH expression in daSNc, suggesting that at intermediate levels of GHSR signaling, daSNc inactivity occurs downstream of striosomal activation rather than through an independent parallel mechanism. CNO SAL rats that received CNO alone also did not differ from SAL controls ($p=0.9732$), confirming that CNO administration alone did not alter pPDH expression in TH-positive daSNc neurons in the absence of DREADD expression. **Post hoc comparisons - excitatory manipulation:** Excitatory chemogenetic activation of striosomal neurons mimicked the effects of IBU, resulting in significantly greater pPDH expression relative to SAL controls ($p=0.00047$) and levels that were not different from the IBU condition ($p=0.3881$). Similarly, the Exc IBU group showed significantly

		greater pPDH expression relative to SAL conditions (p=0.0116). Although the Exc IBU group remained significantly lower than the IBU condition (p=0.0367), pPDH expression was still significantly elevated relative to inhibitory manipulation groups and CNO SAL controls (all p<0.001). Exc SAL and Exc IBU groups also did not differ from one another (p=0.9140), indicating that excitatory manipulation alone was sufficient to recapitulate the effects of intermediate-dose GHSR activation on the daSNc inactivity profile. Together, these findings demonstrate that GHSR-induced daSNc pPDH recruitment is dependent on striosomal activity and that selective excitation of striosomal neurons is sufficient to phenocopy the effects of IBU on downstream dopaminergic circuit activity.
Fig S1A Baseline decision making of simple tasks	RM one-way ANOVA, significant difference in approach rate between the *Light alone, Maze alone, Toy alone,* and *Food only* tasks (F(3,24)=4.869, p=0.0088). Rats approached the ROI significantly more during the Food only task compared to the *Light alone* (p=0.0092) and *Maze alone* (p=0.0312) tasks, using Tukey post-hoc analysis. Rats = 9. Note: Data shown here are the same saline control values used in **fig. S2**	
Fig S1B (left) Food alone 2x IBU Long Evans	Paired t-test, 2x IBU had no significant effect on approach rate (t(10)=0. 1947, p = 0.8495; rats=11).	
Fig S1B (right) Food alone 2x IBU Oprm1 WT	Using an unpaired t-test we saw that 2x IBU had no significant effect on approach rate (t(23.64)=0.6164, p=0.5435) between SAL (rats=14) and 2x IBU treated rats (rats=14).	
Fig S1C (left) Toy	Paired t-test, 2x IBU had no significant effect on approach rate (t(11)= 0.1199, p=0.9067; rats = 12).	

alone 2x IBU Long Evans		
Fig S1C (right) Toy alone 2x IBU Oprm1 WT	Using an unpaired t-test we saw that 2x IBU had no significant effect on approach rate (t(19.51)=1.255, p=0.2243) between SAL (rats=14) and 2x IBU treated rats (rats=14).	
Fig S1D (left) Light alone 2x IBU Long Evans	Paired t-test, 2x IBU had no significant effect on approach rate (t(11)=0.8633, p=0.4064; rats=12).	
Fig S1D (right) Light alone 2x IBU Oprm1 WT	Using an unpaired t-test we saw that 2x IBU had no significant effect on approach rate (t(24.68)=0.1745, p=0.8629) between SAL (rats=14) and 2x IBU treated rats (rats=14).	
Fig S1E (left) *Food+light 2x IBU Long Evans*	Paired t-test, significant effect on approach rate when comparing 2x IBU and saline rats (t(11)= 2.175, p=0.0407; rats=12).	
Fig S1E (right) *Food+light 2x IBU Oprm1 WT*	Using an unpaired t-test we saw a significant effect on approach rate (t(16.62) =2.363, p=0.0306) between SAL (rats=14) and 2x IBU treated rats (rats=14).	
Fig S1F (left) *Toy+light Task 2X IBU Long Evans*	Paired t-test, significant effect on approach rate when comparing 2x IBU and saline rats (t(15)= 2.146, p =0.0486; rats=16).	
Fig S1F (right) *Toy+ligh*	Using an unpaired t-test we saw a significant effect on approach rate (t(9.953) = 2.742, p=0.0209) between SAL (rats=10) and 2x IBU treated rats (rats=14).	

t 2x IBU Oprm1 WT		
Fig S1G (left) Effects of strain and 2x IBU on non-conflict behavioral tasks	**Main effects:** To determine whether strain differences contributed to behavioral outcomes across simple non-conflict tasks, behavioral performance was compared between Long-Evans and Oprm1-WT rats following SAL or 2x IBU administration. Because individual behavioral tasks measured different parameters with distinct baselines and ranges, raw values were min-max normalized prior to cross-task comparisons. Three non-conflict behavioral tasks were included in the analysis, and data from both strains were combined into a three-way ANOVA comparing non-conflict task type, strain, and IBU treatment. Analysis revealed no significant main effect of non-conflict task ($F(2,71) = 0.8290$, $p=0.4407$), strain ($F(1,71) = 0.1709$, $p=0.6806$), or IBU treatment ($F(1,71) = 0.3568$, $p=0.5522$). Additionally, no significant interactions were observed between task type, strain, or IBU treatment (all $p > 0.46$), indicating that behavioral performance remained consistent across non-conflict paradigms regardless of strain or GHSR activation state. Together, these findings demonstrate that intermediate GHSR activation does not alter performance during non-conflict tasks and that strain differences do not account for the behavioral effects observed in conflict-based paradigms.	
Fig S1G (right) Effects of strain and 2x IBU on conflict-based behavioral tasks	**Main effects:** To determine whether strain differences contributed to behavioral effects observed during conflict-based decision-making tasks, performance across two conflict paradigms was compared between Long-Evans and Oprm1-WT rats following SAL or 2x IBU administration. Because individual behavioral tasks measured different parameters with distinct baselines and ranges, raw values were min-max normalized prior to cross-task comparisons. Data were analyzed using a three-way ANOVA comparing conflict task type, strain, and IBU treatment. Analysis revealed a significant main effect of IBU treatment ($F(1,48) = 28.90$, $p<0.0001$), indicating that 2x IBU significantly altered performance across conflict-based tasks. In contrast, there was no significant main effect of strain ($F(1,52)=2.654$, $p=0.109$), indicating that baseline behavioral performance did not differ between Long-Evans and Oprm1-WT rats. Although significant interactions were observed between conflict task and strain ($F(1,52)=4.423$, $p=0.0403$) and between	

	conflict task, strain, and IBU treatment (F(1,48)=4.665, p=0.0358), no significant interaction was observed between strain and IBU treatment (F(1,48)=0.4195, p=0.520). Together, these findings indicate that the behavioral effects produced by intermediate GHSR activation during conflict-based decision-making are not driven by strain-specific differences, supporting the conclusion that 2x IBU selectively alters conflict-related behavioral processing across both experimental cohorts.	
Fig S2A Non-conflict tasks 10x IBU	A two-way ANOVA (Treatment × Task) revealed no main effect of group, task; and no significant interaction (Effect of IBU: F(1,51)=1.8, p = 0.186; Effect of task: F(2,51)=0.78, p=0.462; effect of group x task: F(2,51)=0.06, p=0.944).	
Fig S2B Food alone task 10X IBU OPRM1 WT	Using an unpaired t-test we saw that high dose IBU had no effect on approach rate (t(16.92) = 0.4868, p=0.6326) between SAL (rats=9) and 10x IBU treated rats (rats=10).	
Fig S2C Toy alone task 10X IBU OPRM1 WT	Using a t-test we saw that high dose IBU had no effect on approach rate (t(13.02)=0.9073, p=0.3808) between SAL (rats=9) and 10x IBU treated rats (rats=10).	
Fig S2D: Light alone task 10X IBU OPRM1 WT	Using an unpaired t-test we saw that high dose IBU (rats=10) had no effect on approach rate relative to SAL (t(15.63) = 0.9182, p=0.3724) between SAL (rats=9) and 10x IBU treated rats (rats=10).	
Fig S2E conflict tasks 10x IBU	A two-way ANOVA (Treatment × Task) revealed no main effect of group, task; and no significant interaction (Effect of IBU: F(1,34)=0.51, p=0.481; Effect of task: F(1,34)=0.08, p=0.782; effect of group x task: F(1,34)=2.09, p=0.158).	
Fig S2F Food+light task 10X IBU OPRM1 WT	Using an unpaired t-test we saw that high dose IBU had no effect on approach rate (t(9.555)=01.517, p=0.1617) between SAL (rats=9) and 10x IBU treated rats (rats=10).	
Fig S2G Toy+ligh	Unpaired T-test reveals high dose IBU did not alter avoidance in Toy+light conflict task (t(14.46)=0.5137,	

t task 10X IBU OPRM1 WT	p=0.6152) between SAL (rats=9) and 10x IBU treated rats (rats=10).	
Fig S2H Chow in home cage 10x IBU	A significant difference in food consumption was found in chow task (paired t-test: t(18) = 4.121, p=0.0006) between SAL and 10x IBU treated rats (rats=19).	
Fig S2I Food alone 10x IBU	A significant difference in food consumption was found in the Food alone task (unpaired t-test: t(15.65)=2.953, p=0.0095) between SAL (rats=9) and 10x IBU treated rats (rats=10).	
Fig S2J Food+light 10x IBU	A significant difference in food consumption was found in the Food+light task (unpaired t: t(16.94)=2.922, p=0.0095) between SAL (rats=9) and 10x IBU treated rats (rats=10).	
Fig S3R Whole-brain z-score analysis of cFos expression across 50 brain regions	To determine how intermediate-dose IBU alters neuronal activity across the brain, cFos expression was quantified in 50 anatomically defined brain regions from SAL and 1x IBU-treated rats (rats = 7-10 per group). To normalize activity differences across regions with different baseline cFos levels, regional cFos expression was converted into z-scores relative to the saline condition. For each brain region, the mean and standard deviation of the SAL group were first calculated. Individual cFos values from IBU-treated rats were then transformed into z-scores using the formula: (IBU value − SAL mean) / SAL standard deviation. The resulting z-scores then represent how many standard deviations cFos expression in an IBU-treated animal deviated from the saline baseline within that same brain region. Positive z-score values indicate greater cFos expression relative to SAL conditions, whereas negative values indicate reduced activity relative to baseline. This approach allowed direct comparison of IBU-induced activity changes across brain regions with different baseline expression levels and variability.	**Regional activity patterns:** Although increased cFos expression was observed across multiple brain regions following 1x IBU administration, the largest increases were observed within DMS striosomes and the LHb. DMS striosomes displayed a z-score of approximately 16, indicating that cFos expression within this compartment was nearly 16 standard deviations greater than saline levels, while LHb cFos expression was approximately 4 standard deviations greater than saline levels following 1x IBU administration. Together, these findings suggest that although GHSR activation broadly alters neuronal activity across the brain, the strongest recruitment occurs within the DMS striosomal and LHb circuitry.
Fig S4C Effects of IBU dose on daSNc cFos expression	**Main effects:** To determine whether increasing IBU doses altered neuronal activity within the dopaminergic neurons of the substantia nigra pars compacta (daSNc), cFos-positive cells were quantified exclusively within TH-positive dopaminergic neurons across SAL (rats=6), 0.5x IBU (rats=6), 1x IBU (rats=6), 2x IBU (rats=8), and 10x IBU (rats=6) conditions. Data was analyzed using an ordinary one-way ANOVA, followed by Tukey's multiple comparisons test. Analysis revealed a	Post hoc comparisons: Tukey's multiple comparisons test revealed significantly greater daSNc cFos expression under the 10x IBU condition relative to SAL (p=0.00034), 0.5x IBU (p=0.00038), 1x IBU (p=0.00014), and 2x IBU (p=0.00079) conditions. No differences were observed between SAL, 0.5x, 1x, or 2x conditions (all p>0.84). Importantly, elevated daSNc cFos expression

	significant main effect of IBU dose on daSNc cFos expression ($F(4, 27)=9.626$, $p=5.7 \times 10^{-5}$), indicating that high levels of GHSR activation alters daSNc activity.	emerged selectively under the highest IBU dose, coinciding with conditions in which striosomal activity was suppressed, suggesting that excessive GHSR activation recruits dopaminergic midbrain circuitry under high-dose conditions distinct from intermediate-dose striosomal activation.
Fig S4D (left) Correlation between DMS striosomal and LHb cFos expression	**Linear regression analysis:** To determine whether activation of DMS striosomes was associated with recruitment of the lateral habenula (LHb), cFos expression within DMS striosomes was correlated with matched LHb cFos counts obtained from the same rats across SAL (rats=7), 0.5x IBU (rats=6), 1x IBU (rats=6), 2x IBU (rats=6), and 10x IBU (rats=6) conditions. Linear regression analysis revealed a significant positive relationship between DMS striosomal and LHb cFos expression ($F(1,29)=42.65$, $p<0.0001$), with an R^2 value of 0.5953, indicating that approximately 60% of the variance in LHb activity could be explained by striosomal cFos expression. The resulting regression equation was $Y=0.09222x + 4.473$.	**Correlation analysis:** Pearson's correlation analysis further confirmed a strong positive correlation between DMS striosomal and LHb cFos expression ($r=0.7715$, $p=3.8 \times 10^{-7}$; XY pairs=31). Together, these findings demonstrate that increased striosomal activation strongly correlates with elevated LHb activity, supporting the recruitment of the striosomes → LHb pathway following intermediate levels of GHSR activation.
Fig S4D (right) Correlation between DMS striosomal cFos expression and daSNc pPDH	**Linear regression analysis:** To determine whether striosomal activation was associated with changes in dopaminergic substantia nigra pars compacta (daSNc) activity, cFos expression within DMS striosomes was correlated with matched daSNc pPDH counts obtained from the same rats across SAL (rats=6), 0.5x IBU (rats=6), 1x IBU (rats=6), 2x IBU (rats=7), and 10x IBU (rats=6) conditions. Linear regression analysis revealed a significant positive relationship between DMS striosomal cFos expression and daSNc pPDH levels ($F(1,29)=39.16$, $p<0.0001$), with an R^2 value of 0.5746, indicating that approximately 57% of the variance in daSNc pPDH expression could be explained by striosomal cFos levels. The resulting regression equation was $y=1.378x + 112.2$.	**Correlation analysis:** Pearson's correlation analysis further confirmed a strong positive correlation between DMS striosomal cFos expression and daSNc pPDH levels ($r=0.7580$, 95% CI: 0.5519–0.8768, $p=7.9 \times 10^{-7}$; XY pairs=31). Together, these findings demonstrate that increased striosomal activation strongly correlates with elevated daSNc pPDH expression, suggesting that increased striosomal activity is associated with reduced activity of dopaminergic neurons in the daSNc.
Fig S4E Correlation between	**Linear regression analysis:** To determine whether activity in LHb was associated with altered daSNc activity, LHb cFos expression was correlated with matched daSNc pPDH counts obtained from the same rats across all IBU dose conditions (rats = 6 per	**Correlation analysis:** Pearson's correlation analysis further confirmed a strong positive correlation between LHb cFos expression and daSNc pPDH levels ($r=0.7033$, 95% CI: 0.4594–0.8485, $p<0.0001$; XY pairs=30).

LHb cFos expression and daSNc pPDH levels	group). Linear regression analysis revealed a significant positive relationship between LHb cFos expression and daSNc pPDH levels ($F(1,28)=27.40$, $p<0.0001$), with an R^2 value of 0.4946, indicating that approximately 49% of the variance in daSNc pPDH expression could be explained by LHb activity. The resulting regression equation was $Y = 10.98x + 98.86$.	Together, these findings suggest that increased LHb recruitment is associated with increased pPDH expression within the daSNc, supporting the striosome → LHb → daSNc pathway following GHSR activation.
Fig S4F Correlation between DMS striosomal and daSNc cFos expression	**Linear regression analysis:** To determine whether activation of DMS striosomes was directly associated with activity in daSNc, cFos expression within DMS striosomes was correlated with matched daSNc cFos counts obtained from the same rats across all IBU dose conditions (rats=6 per group). Linear regression analysis revealed no significant relationship between DMS striosomal and daSNc cFos expression ($F(1,28) = 1.916$, $p=0.1772$). The resulting regression equation was $Y = -0.03816X + 10.47$.	**Correlation analysis:** Pearson's correlation analysis further confirmed the absence of a significant relationship between DMS striosomal and daSNc cFos expression ($r = -0.2531$, 95% CI: -0.5621 to 0.1179, $p = 0.1771$; XY pairs = 30). Together, these data suggest that increased striosomal recruitment is not directly associated with increased daSNc neuronal activation and instead support a model in which elevated GHSR activation suppresses striosomal activity while indirectly recruiting dopaminergic midbrain circuitry through downstream pathways.
Fig S4G Effects of IBU dose on ARC cFos expression	**Main effects:** To determine whether increasing IBU doses altered activation of feeding-related hypothalamic circuitry, cFos-positive cells were quantified within the arcuate nucleus (ARC) across SAL (rats=10), 0.5x IBU (rats=7), 1x IBU (rats=10), 2x IBU (rats=6), and 10x IBU (rats=6) conditions. Group comparisons were analyzed using an ordinary one-way ANOVA followed by Tukey's multiple comparisons test. Analysis revealed a significant main effect of IBU dose on ARC cFos expression ($F(4,34)=7.887$, $p=0.000131$), indicating that high levels of GHSR activation alter recruitment of hypothalamic feeding circuitry	**Post hoc comparisons:** Tukey's multiple comparisons test revealed significantly greater ARC cFos expression under the 10x IBU condition relative to SAL ($p=0.000135$), 0.5x IBU ($p=0.000231$), 1x IBU ($p=0.0121$), and 2x IBU ($p = 0.0329$) conditions. No differences were observed between SAL, 0.5x, 1x, or 2x conditions (all $p>0.36$). Importantly, increased ARC activity was only observed at the highest IBU dose, coinciding with the same high-dose conditions that produced robust feeding behavior in the home cage. Together, these findings suggest that hypothalamic feeding circuits are primarily recruited under high levels of

		GHSR activation associated with increased food consumption.
Fig S4H Correlation between DMS striosomal and ARC cFos expression	**Linear regression analysis:** To determine whether activation of DMS striosomes was associated with recruitment of hypothalamic feeding circuitry, cFos expression within DMS striosomes was correlated with cFos counts in ARC obtained from the same rats across all IBU dose conditions (rats=6 per group). Linear regression analysis revealed no significant relationship between DMS striosomal and ARC cFos expression ($F(1,30)=0.1959$, $p=0.6613$), with an R^2 value of 0.00648. The resulting regression equation was $y = -0.03074x + 51.44$.	**Correlation analysis:** Pearson's correlation analysis further confirmed the absence of a significant relationship between DMS striosomal and ARC cFos expression ($r = -0.0805$, 95% CI: -0.4175 to 0.2759, $p = 0.6613$; XY pairs = 32). Together, these findings suggest that recruitment of DMS striosomal circuitry and hypothalamic feeding circuitry occurs under distinct GHSR activation states and are not directly coupled across individual rats.
Fig S5D Time-dependent effects of 2x IBU on striosomal activity	**Main effects:** To further characterize the temporal dynamics of intermediate-dose Ibutamoren administration, in vivo calcium imaging was analyzed independently within the 2x IBU condition across baseline, 30, 60, 120, 180, 240, and 300 min time points. Recordings were obtained from rats=4 (fields of view=6), and data were analyzed using a repeated-measures one-way ANOVA with Tukey's multiple comparisons test. Because individual rats displayed different baseline numbers of active cells, data were normalized to each recording's baseline activity by calculating the change in active cells relative to the 0 hr condition at each subsequent time point, for non-normalized data see **fig. S5E**. Analysis revealed a significant main effect of time on striosomal activity ($F(2.552, 12.76)=15.52$, $p=0.0002$), indicating that intermediate-dose IBU dynamically modulates striosomal activity across the recording period	**Post hoc comparisons:** Post hoc multiple comparisons revealed that striosomal activity was significantly elevated at 2 hours relative to the baseline (0 vs 2 hr, $p=0.0094$), supporting the conclusion that 2x IBU produces peak striosomal activation approximately 2 hours following administration. Activity at 2 hours was also significantly greater than later time points at 4 hour ($p=0.0001$) and 5 hour ($p=0.0013$), indicating that striosomal activation progressively declined following the 2 hr peak. No differences were observed between baseline and earlier time points at 0.5 or 1 hour (all $p>0.70$), supporting a delayed onset of IBU-mediated striosomal activation consistent with the pharmacokinetic profile of the compound. Together, these findings validate the use of the 2 hr post-injection window for subsequent behavioral experiments and support the later 3.5 hr perfusion time point used for cFos analysis.
Fig S5E (left) Time-dependent effects of IBU dose on	Main effects: To determine how striosomal calcium activity changed over time following IBU administration, in vivo calcium imaging was performed longitudinally following 2x and 10x IBU administration. Calcium dynamics were monitored at baseline, 0.5, 1, 2, 3, 4, 5, and 6 hr post-injection and analyzed using a mixed-effects model. Analysis revealed a significant main effect of time (mixed-	**Post hoc comparisons:** Tukey's multiple-comparisons test revealed that striosomal activity increased during the later recording period relative to baseline. Activity at 4 hr was significantly elevated compared with baseline ($p=0.0172$), and activity at 5 hr remained significantly greater than baseline ($p=0.0037$). In addition, activity at 5 hr

raw striosomal calcium activity	effects model: F(7,71)=3.532, p=0.0026), indicating that striosomal activity changed dynamically across the recording period. In contrast, there was no significant main effect of IBU dose (F(1,10)=0.8866, p=0.3686), suggesting that when averaged across all time points, overall activity did not differ between the 2x and 10x IBU groups. Rats=4, fields of view=6.	was significantly greater than activity at 2 hr (p=0.0276). No other pairwise comparisons reached statistical significance. Together, these findings indicate that striosomal activity gradually increased over time following IBU administration, reaching maximal levels approximately 4–5 hr after injection.
Fig S5E (right) Time-dependent effects of acyl-ghrelin dose on raw striosomal calcium activity	**Main effects:** To determine whether low and high acyl-ghrelin doses differentially modulate raw striosomal calcium activity across time, in vivo calcium imaging was performed following administration of 86 (rats=3) or 4.3 ug/kg (rats=2) acyl-ghrelin. Calcium dynamics were monitored longitudinally across 5, 10, 15, 30, 60, and 120 min time points. Data were analyzed using a mixed-effects model. Analysis revealed a significant interaction between time and ghrelin dose (F(5, 17)=4.927, p=0.0057), indicating that the temporal dynamics of striosomal activity differed between aGHR doses. There was also a significant main effect of ghrelin dose (F(1, 17)=7.187, p=0.0158).	
Fig S5F (left) aGHR-induced feeding in home cage	**Main effects:** To determine whether acyl-ghrelin dose-dependently modulates feeding behavior, food consumption in the home cage was measured 4 hr following administration of increasing aGHR doses. Food intake was compared across SAL, 125 ug/kg, 86 ug/kg, 26 ug/kg, 8.6 ug/kg, and 4.3 ug/kg conditions using a repeated-measures one-way ANOVA. Analysis revealed a significant main effect of aGHR dose on food consumption (F(2.508,17.56)=9.543, p=0.0009), indicating that aGHR dose-dependently increases feeding behavior.	**Post hoc comparisons:** Tukey's multiple comparisons test revealed that food consumption was significantly increased under higher doses 125 ug/kg (p=0.0008), 86 ug/kg (p=0.0063), and 26 ug/kg (p=0.0292) acyl-ghrelin conditions relative to SAL. In contrast, lower doses did not significantly alter feeding behavior (SAL vs 8.6 ug/kg, p=0.3462; SAL vs 4.3 ug/kg, p=0.2732). The highest dose tested (125 ug/kg) also produced significantly greater food intake than the lowest dose condition (4.3 ug/kg, p=0.0087) and modestly greater feeding relative to the 86 ug/kg condition (p=0.0374). No additional differences were observed between intermediate and lower doses (all p>0.10). Together, these findings demonstrate that acyl-ghrelin dose-dependently increases food consumption, with robust effects emerging primarily at moderate-to-high doses.

Fig S5F (right) Time-dependent effects of acyl-ghrelin dose on food consumption	**Main effects:** To determine whether aGHR dose differentially modulates the temporal dynamics of feeding behavior, cumulative food consumption in the home cage was measured hourly for 4 hours following administration of SAL, 4.3 ug/kg, 8.6 ug/kg, 26 ug/kg, 86 ug/kg, or 125 ug/kg aGHR. Because all rats (rats=8) received every dose, data were analyzed using a two-way repeated-measures ANOVA. Analysis revealed a significant main effect of time ($F(1.887,13.21)=98.61$, $p=0.000000014$), indicating that all rats, including saline controls, progressively consumed food across the recording period. There was also a significant main effect of aGHR dose ($F(2.781,19.47)=8.521$, $p=0.00099$), as well as a significant interaction between time and aGHR dose ($F(4.287,30.01)=5.577$, $p=0.00146$), indicating that both the magnitude and temporal dynamics of feeding behavior differed depending on aGHR concentration. Together, these findings demonstrate that food consumption naturally increased across time under all conditions, while higher levels of GHSR activation accelerated and amplified feeding behavior relative to lower doses.	**Post hoc comparisons:** Tukey's post hoc multiple comparisons revealed that feeding behavior differed primarily at higher aGHR doses. At 1 hour following administration, only the highest dose (125 ug/kg) significantly increased food consumption relative to SAL ($p=0.0200$), while all lower doses remained comparable to SAL (all $p>0.50$), indicating a rapid orexigenic effect uniquely at the highest dose. Similarly, at 2 hours, only the 125 ug/kg condition remained significantly elevated relative to SAL ($p=0.0163$). By 3 hours, both high-dose conditions (86 and 125 ug/kg) displayed significantly greater food consumption relative to SAL (86 ug/kg: $p=0.00019$; 125 ug/kg: $p=0.0026$), whereas lower doses remained unchanged (all $p>0.11$). At 4 hours, the three highest doses (26, 86, and 125 ug/kg) significantly increased cumulative food consumption relative to SAL conditions (26 ug/kg: $p=0.0292$; 86 ug/kg: $p=0.0063$;125 ug/kg: $p=0.00080$), while lower doses still failed to alter feeding behavior (all $p>0.27$). Additional comparisons further demonstrated that the highest dose (125 ug/kg) consistently produced greater food consumption than lower doses across multiple time points, including relative to 4.3 ug/kg at 1 hour ($p=0.00024$), 2 hours ($p=0.0146$), 3 hours ($p=0.00020$), and 4 hours ($p=0.0087$). Collectively, these findings indicate that increasing aGHR doses not only increase total food intake, but also accelerate the onset of feeding behavior, with the highest doses producing rapid consummatory responses within the first hour while lower doses produce delayed or minimal effects. Importantly, these findings support previous observations that robust orexigenic effects emerge primarily under high levels of GHSR activation by IBU and activation of ARC.
Fig S5G Effects of GHSR	**Main effects:** To determine whether feeding behavior differed as a function of GHSR activation mode or dose, food consumption in the home cage was compared across SAL, low-dose, and high-dose conditions following either IBU or aGHR	**Post hoc comparisons:** Post hoc multiple comparisons revealed no differences between saline conditions across activation modes (SAL:IBU vs SAL:aGHR, $p>0.9999$), indicating

activation mode and dose on food consumption	administration. Grams of chow consumed were analyzed using a two-way ANOVA with dose and GHSR activation mode as factors. There was a significant main effect of dose ($F(2, 75)=8.460$, $p=0.0005$), whereas no significant main effect of GHSR activation mode was observed ($F(1, 75)=0.1140$, $p=0.7366$), demonstrating that feeding behavior was primarily determined by the magnitude of GHSR activation rather than the specific agonist used	comparable baseline feeding behavior between treatment paradigms. Similarly, no differences were observed between low-dose IBU and low-dose acyl-ghrelin conditions ($p=0.9941$), nor between high-dose IBU and high-dose acyl-ghrelin conditions ($p>0.9999$), further supporting similar feeding responses regardless of GHSR activation mode. Importantly, high-dose IBU significantly increased food consumption relative to low-dose IBU ($p=0.0405$), whereas low-dose conditions did not differ from saline controls (all $p>0.98$). Together, these findings demonstrate that feeding behavior is driven by the magnitude of GHSR activation rather than the agonist used, with robust increases in food intake emerging primarily under high-dose conditions.
Fig S6E Effects of striosomal chemogenetic manipulation on striatal pPDH expression	**Main effects:** To determine whether chemogenetic manipulation of striosomal neurons alters pPDH expression within the dorsal striatum, pPDH-positive cells were quantified following Cre-dependent DREADD manipulation of striosomal neurons. Quantification was restricted to MOR-positive striosomal ROIs and only within neurons expressing the DREADD virus, identified by either HA-tag or mCherry labeling depending on the viral construct. To ensure pPDH signal localization within neuronal somas, only pPDH-positive signal overlapping with the soma marker NeuroTrace was included in the analysis. Experimental groups included SAL (rats=7), IBU (rats=6), Inh IBU (inhibitory hM4Di + CNO + IBU; rats=7), Inh SAL (hM4Di + CNO + SAL; rats=6), Exc SAL (excitatory hM3Dq + CNO + SAL; rats=6), Exc IBU (excitatory + CNO + IBU; rats=6), and WT + CNO saline controls (CNO SAL; rats=6). Group comparisons were analyzed using a one-way ANOVA followed by Tukey's multiple comparisons test. Analysis revealed a significant main effect of treatment group on striatal pPDH expression ($F(6,37)=8.496$, $p=0.0000079$).	
Fig S6F striosomes ppdh inhibition	**Post hoc comparisons: inhibitory manipulation:** Tukey's multiple comparisons test showed that inhibition of striosomal neurons significantly increased pPDH expression relative to SAL controls (SAL vs Inh IBU, $p=0.00159$; SAL vs Inh SAL, $p=0.01225$). Similarly, both inhibitory groups also showed significantly greater pPDH expression relative to the 2x IBU condition (IBU vs Inh IBU, $p=0.00039$; IBU vs Inh SAL, $p=0.00319$). The Inh IBU and Inh SAL groups did not differ from one another ($p=0.9977$), indicating that chemogenetic inhibition of striosomal neurons alone was sufficient to increase pPDH expression independent of IBU administration. Together,	

	these findings are consistent with previous reports demonstrating that DREADD-mediated neuronal inhibition increases pPDH expression, further supporting pPDH as a marker of reduced neuronal activity within the striosomal circuit.	
Fig S6G striosomes ppdh excitation	**Post hoc comparisons: excitatory manipulation:** In contrast to inhibitory manipulation, excitatory chemogenetic activation of striosomal neurons did not alter pPDH expression relative to SAL conditions (Exc SAL vs SAL, p=0.99997; Exc IBU vs SAL, p=0.99999). Similarly, neither excitatory group differed from the 2x IBU condition (IBU vs Exc SAL, p=0.9760; IBU vs Exc IBU, p=0.9995), and Exc SAL and Exc IBU groups did not differ from one another (p = 0.99938). Together, these findings demonstrate that excitatory chemogenetic activation of striosomal neurons does not increase pPDH expression, indicating that pPDH recruitment is selectively associated with neuronal inhibition rather than increased striosomal activity	
Fig S6H WT control comparisons for striosomal pPDH expression	**Post hoc comparisons- WT controls:** CNO SAL rats that received CNO alone did not differ from SAL controls (p=0.9983), confirming that CNO administration alone did not alter pPDH expression in the absence of DREADD expression. In contrast, both inhibitory manipulation groups displayed significantly greater pPDH expression relative to CNO SAL controls (Inh IBU vs CNO SAL, p=0.000565; Inh SAL vs CNO SAL, p=0.00441). Neither excitatory manipulation group differed from CNO SAL controls (Exc SAL vs CNO SAL, p=0.98841; Exc IBU vs CNO SAL, p=0.9999), further supporting that increased pPDH expression was specific to inhibitory chemogenetic manipulation of striosomal neurons.	
Fig S6I striosomes ppdh post hoc	**Post hoc comparisons inhibitory versus excitatory manipulation:** Direct comparisons between inhibitory and excitatory manipulation groups revealed significantly greater pPDH expression following striosomal inhibition relative to excitation (Inh IBU vs Exc SAL, p=0.0053; Inh IBU vs Exc IBU, p=0.0014; Inh SAL vs Exc SAL, p=0.0323; Inh SAL vs Exc IBU, p=0.0103). Together, these findings demonstrate that inhibitory and excitatory manipulation of striosomal neurons produce distinct pPDH expression profiles, with elevated pPDH recruitment occurring selectively following neuronal inhibition.	
Fig S7B-C	Pairwise comparisons between experimental groups were performed using two-sample (unpaired) t-tests for unequal variances. Each column represents a task condition—simple tasks (Food alone, Toy alone, Light alone) on the left and complex tasks (Food+light, Toy+light) on the right. Each row corresponds to a specific group comparison (e.g., CNO Saline vs CNO IBU, CNO Saline vs Inhibitory IBU, etc.). For each cell, t(df) and p-values are shown, with arrows indicating the direction of change relative to the first group in the comparison. Blue shading marks statistically significant effects (p<0.05).	
Fig S8D inhibition post-hocs	**Effects of striosomal inhibition across the striosome→LHb→daSNc circuit** **Post hoc comparisons of inhibitory manipulation:** Across all analyzed regions, striosomal inhibition abolished the effects of 2x IBU administration. Within striosomes, both inhibitory groups displayed significantly reduced cFos expression relative to the 2x IBU condition and returned to SAL-like levels (all p<0.002). Similarly, within the LHb, inhibitory manipulation blocked IBU-induced cFos recruitment, with both inhibitory groups differing significantly from the 2x IBU condition while remaining comparable to SAL controls (all p < 0.0001). In contrast, inhibitory manipulation reduced recruitment of the daSNc pPDH profile, as both inhibitory groups	

	displayed significantly lower pPDH expression relative to the 2x IBU condition (all p<0.0001) and did not differ from SAL conditions. Together, these findings demonstrate that chemogenetic inhibition of striosomal neurons blocks downstream recruitment of the striosome→LHb→daSNc circuit following intermediate GHSR activation.	
Fig S8E striosomal excitation post-hocs	**Effects of excitatory chemogenetic manipulation across the striosome→LHb→daSNc circuit** Striosomal excitaiton phenocopied the effects of intermediate-dose IBU administration across all analyzed regions. Within striosomes, both excitatory groups displayed significantly greater cFos expression relative to SAL controls while remaining comparable to the 2x IBU condition. Similarly, within the LHb, excitatory manipulation increased cFos expression to levels comparable to 2x IBU rats, indicating recruitment of downstream circuit activity. Within the daSNc, both excitatory groups displayed significantly elevated pPDH expression relative to inhibitory manipulation groups and SAL controls, consistent with increased recruitment of the daSNc inactivity profile observed following intermediate-dose GHSR activation. Excitatory groups did not differ from one another across analyzed regions, indicating that chemogenetic excitation alone was sufficient to recapitulate the effects of IBU on downstream circuit recruitment. Together, these findings demonstrate that selective excitation of striosomal neurons is sufficient to mimic intermediate-dose GHSR-mediated activation of the striosome→LHb→daSNc circuit.	
Fig S8F striosomal manipulation post-hocs	**Comparison of inhibitory versus excitatory chemogenetic manipulation across the striosome→LHb→daSNc circuit** **Post hoc comparisons of inhibitory versus excitatory manipulation:** Direct comparisons between inhibitory and excitatory manipulation groups revealed opposing activity profiles across all analyzed regions. Within both striosomes and the LHb, excitatory manipulation produced significantly greater cFos expression relative to inhibitory manipulation groups (all $p < 0.01$). In contrast, within the daSNc, excitatory manipulation resulted in significantly greater pPDH expression relative to inhibitory groups (all p<0.0001), consistent with differential recruitment of downstream dopaminergic activity states. Together, these findings demonstrate that inhibitory and excitatory manipulation of striosomal neurons produce opposing effects across the striosome→LHb→daSNc circuit.	
Fig S8G striosomal manipulation with WT	**WT control comparisons across the striosome→LHb→daSNc circuit** WT SAL rats receiving CNO alone did not differ from SAL controls across striosomal cFos expression, LHb cFos expression, or daSNc pPDH expression (all p>0.48), confirming that CNO administration alone did not alter circuit activity in the absence of DREADD expression. Across all analyzed regions, inhibitory manipulation groups produced activity comparable to WT SAL controls, consistent with suppression of IBU-mediated circuit recruitment. In contrast, both excitatory manipulation groups displayed significantly greater striosomal and LHb cFos expression relative to WT SAL controls while also exhibiting significantly elevated daSNc pPDH expression (all p<0.02). Lastly, there is no significant difference in striosomal cFos between Cre+ IBU and IBU, indicating that viral expression and surgical procedures did not alter striosomal response to IBU. Together, these findings demonstrate that excitatory manipulation mimics intermediate-dose GHSR-mediated recruitment of the striosome→LHb→daSNc circuit, whereas inhibitory manipulation blocks downstream circuit activation and returns activity to WT-like conditions.	
Fig S9N (top)	**Main effects:** To determine whether GHSR-mediated striosomal recruitment preferentially engages specific downstream output pathways,	

Comparison of RV-mCherry labeling across monosynaptic tracing pathways	monosynaptic rabies tracing was performed across two independent tracing paradigms: Strio→daSNc (rats = 2) and Strio→GPi→LHb (rats = 3). The number of RV-mCherry-positive striosomal neurons within MOR-positive ROIs was then quantified across tracing conditions. Group comparisons were analyzed using an unpaired two-tailed t-test. Analysis revealed no significant differences in the number of RV-mCherry-positive striosomal neurons between tracing conditions (t = 0.3464, df=2.000, p=0.7621). Comparable RV-mCherry labeling across tracing paradigms indicates that both monosynaptic tracing experiments produced similar levels of striosomal labeling efficiency. These findings suggest that subsequent differences in pathway-specific cFos recruitment are unlikely to reflect variability in rabies tracing efficiency or preferential labeling between tracing conditions.	
Fig S9N bottom Pathway-specific cFos recruitment across monosynaptic tracing paradigms	**Main effects:** To determine whether GHSR-mediated striosomal recruitment preferentially engages specific downstream output pathways, the percentage of RV-mCherry-positive striosomal neurons co-expressing cFos was quantified following monosynaptic rabies tracing of the Strio→daSNc (rats = 2) and Strio→GPi→LHb (rats = 3) pathways. For each tracing condition, all RV-mCherry-positive striosomal neurons within MOR-positive ROIs were quantified, and the percentage co-expressing cFos was calculated. Group comparisons were analyzed using an unpaired two-tailed t-test. Analysis revealed significantly greater cFos co-labeling within the Strio→GPi→LHb tracing condition relative to the Strio→daSNc pathway (t = 4.339, df = 2.474, p=0.0331). The Strio→GPi→LHb pathway displayed substantially greater recruitment of cFos-positive RV-mCherry-labeled striosomal neurons compared to the direct Strio→daSNc pathway (52.90% vs 3.85%). These findings suggest that intermediate GHSR activation preferentially recruits the indirect Strio→GPi→LHb pathway rather than direct striosomal projections to the daSNc.	
Fig S11A	Trajectory curvature was significantly reduced in the 2x group relative to saline controls (T-test: t(120) = 3.621, p=0.0005), with a smaller but still significant reduction at high-dose IBU (10x) (T-test: t(90) = 2.368, p=0.0200).	
Fig S11B	Velocity also decreased significantly at 2x IBU (T-test: t(120) = 2.891, p=0.0047), but no difference was observed at 10x (T-test: t(90) = 1.723, p=0.0884).	

Fig S11C	Head–body angle was significantly increased at 2x IBU (t-test: t(120) = -1.993, p=0.0485) but unchanged at 10X (T-test: t(90) = -0.686, p=0.4945).	
Fig S11D and E	Pairwise comparisons between saline and IBU groups were performed using independent (unpaired) two-sample t-tests for unequal variances. The figure summarizes treatment effects on three behavioral features—curvature, velocity, and head–body angle—for two IBU doses (2x and 10x). The "Combined" row represents all tasks pooled together, while subsequent rows show results separated by individual task conditions (food alone, toy alone, light alone, food+light, and toy+light). Each cell displays the direction of change (arrow) in the IBU group relative to the saline group. Blue shading denotes statistically significant differences, with color intensity indicating the significance level (p < 0.05 , * * p < 0.01 *, * * * p < 0.001 **, * * * * p < 0.0001 ****); grey shading indicates non-significant comparisons. Sample sizes for each analysis are shown within the matrix as the number of rats (n_S,a, n_IBU,a) and trials (n_S,t, n_IBU,t) included in the saline and IBU groups, respectively.	
Fig S12	To characterize the behavioral effects of ghrelin across different environmental contexts, we analyzed four key movement metrics: turn frequency ($> 90°$), mean absolute turn-angle, mean step length, and the Mean Squared Displacement (MSD) exponent. The integrated effect of ghrelin relative to saline was visualized in **fig. S12B** using a signed $-\log_{10}(p)$ transformation, where the bar height represents the statistical significance (paired t-test) and the sign indicates the direction of change (positive for ghrelin > saline, negative for saline > ghrelin). In **fig. S12C**, the data is visualized using paired line plots to illustrate the degree of consistency across individual subjects within specific task conditions. Ghrelin treatment resulted in a significant reduction in mean step length ($p = 0.008$), indicated by the downward trajectory of the population mean (red line). Significant decreases were observed in both turn frequency ($p = 0.009$) and mean absolute turn-angle ($p = 0.011$). This reduction in turning behavior reflects a smoother, less tortuous path under ghrelin. The MSD exponent showed a significant increase ($p = 0.006$), suggesting that ghrelin shifts the movement dynamics from diffusive or constrained search patterns toward more super-diffusive, exploratory behavior.	

	Paired comparisons between saline and ghrelin sessions were performed using two-tailed paired t-tests. All trajectories were smoothed using a 1D Gaussian filter prior to kinematic feature extraction to minimize tracking noise.	
Fig S13A	Trajectory curvature for Oprm1-cre rats was significantly reduced in the Exc SAL group relative to both saline and Inh IBU (One-way ANOVA: $F(2, 169) = 15.70$, $p=5.5x10^{-7}$; Tukey's HSD: CNO SAL vs Exc SAL $p<0.0001$, Exc SAL vs Inh IBU $p<0.0001$), while, no difference was observed between saline and Inh IBU (Tukey's HSD: CNO SAL vs Inh IBU $p=0.9355$).	
Fig S13B	Velocity was significantly lower in the Exc SAL group relative to both saline and Inh IBU (One-way ANOVA: $F(2, 169) = 19.56$, $p=2.3x10^{-8}$; Tukey's HSD: CNO SAL vs Exc SAL $p=0.0003$, Exc SAL vs Inh IBU $p<0.0001$), while, no difference was observed between saline and Inh IBU (Tukey's HSD: CNO SAL vs Inh IBU $p = 0.1396$).	
Fig S13C	Head–body angle was significantly increased in the excitatory group compared to saline and Inh IBU (One-way ANOVA: $F(2, 169) = 5.0841$, $p= 0.0071$; Tukey's HSD: WT-SAL vs Exc SAL $p=0.0231$, Exc SAL vs Inh IBU $p=0.0106$), but not different from inhibitory (Tukey's HSD: CNO SAL vs Inh IBU $p=0.9981$).	
Fig S13D	Pairwise comparisons were performed using independent (unpaired) two-sample t-tests for unequal variances. The figure summarizes the effects of striatal modulation (inhibitory and excitatory) relative to the saline group on three behavioral features—curvature, velocity, and head–body angle—across different task conditions. Rows represent task types (the top "Combined" row includes all tasks pooled together, followed by individual task conditions: food alone, toy alone, light alone, food+light, and toy+light). Columns at the top indicate group comparisons (e.g., Sal vs Inh and Sal vs Exc) for each feature, while columns at the bottom indicate the features being compared. Vertical solid lines demarcate the boundaries between different features. Within each cell, arrows indicate the direction of change in the modulation group relative to the saline group. Blue shading denotes statistically significant differences, with color intensity reflecting the p-value threshold; grey cells represent non-significant (n.s.) results.	

	Sample sizes are shown within each cell for the number of rats (n_Inh,a, n_Exc,a) and trials (n_Inh,t, n_Exc,t) included in each comparison.	
Fig S14B Biotinylated ghrelin (BGHR) binding across DLS striosome and matrix compartments	**Main effects:** To determine whether prior IBU administration alters subsequent ghrelin ligand binding within DLS striosome and matrix compartments, biotinylated ghrelin (BGHR) puncta density was quantified following administration of SAL (rats = 6), 0.5x IBU (rats = 6), 1x IBU (rats = 6), 2x IBU (rats = 6), and 10x IBU (rats = 6). Tissue sections were incubated ex vivo with BGHR to assess ligand binding density across striatal compartments. Group comparisons were analyzed using a two-way ANOVA followed by Tukey's multiple comparisons test. Analysis revealed a significant main effect of IBU dose ($F(4,50) = 3.766$, $p=0.0094$) and a significant main effect of compartment ($F(1,50) = 57.35$, $p<0.0001$), while the interaction between dose and compartment did not reach significance ($F(4,50) = 2.260$, $p = 0.0757$). These findings indicate that BGHR binding differs across DLS compartments and varies as a function of prior IBU exposure.	**Post hoc comparisons:** Tukey's multiple comparisons test confirmed significantly greater BGHR puncta density within SAL DLS striosomes relative to SAL matrix compartments ($p < 0.0001$), indicating baseline enrichment of GHSR-associated ligand binding within DLS striosomal compartments. Similar compartment enrichment was observed under the 0.5x IBU condition ($p = 0.0368$), whereas compartment differences were no longer detected following 1x, 2x, or 10x IBU administration (all $p > 0.05$). Comparisons across treatment conditions further revealed significantly reduced BGHR puncta density in 10x DLS striosomes relative to SAL striosomes ($p = 0.0007$), while lower IBU doses did not significantly differ from SAL striosomes (all $p > 0.05$). In contrast, DLS matrix BGHR puncta density did not differ across treatment conditions (all $p > 0.99$). Together, these findings demonstrate that DLS striosomes exhibit greater baseline BGHR binding relative to surrounding matrix compartments and that high levels of prior GHSR activation reduce compartment-selective BGHR binding within the DLS.
Fig S14D Striosomal cFos expression across DMS and DLS compartments following IBU administration	**Main effects:** To determine whether different levels of GHSR activation preferentially recruit distinct striosomal subregions, cFos expression was quantified within DMS and DLS striosomal compartments following administration of SAL (rats = 7), 0.5x IBU (rats = 8), 1x IBU (rats = 6), 2x IBU (rats = 8), and 10x IBU (rats = 8). Group comparisons were analyzed using a two-way ANOVA followed by Tukey's multiple comparisons test. Analysis revealed a significant interaction between IBU dose and striatal region ($F(4,62) = 18.04$, $p = 0.00000000072$), a significant main effect of IBU dose ($F(4,62) = 33.45$, $p = 7x10^{-15}$), and a significant main effect of striatal region ($F(1,62) = 128.8$, $p < 0.000000000000001$), indicating that GHSR activation differentially modulates striosomal activity across DMS and DLS compartments.	**Post hoc comparisons:** Tukey's multiple comparisons test revealed that increases in striosomal cFos expression were selectively restricted to the DMS at intermediate IBU doses. Relative to SAL DMS striosomes, both 1x and 2x IBU significantly increased DMS striosomal cFos expression (SAL vs 1x DMS, $p = 0.000000011$; SAL vs 2x DMS, $p = 0.000000000021$), whereas no differences were observed at 0.5x or 10x doses (all $p > 0.99$). Similarly, DMS striosomal activity under 1x and 2x conditions was significantly greater than corresponding DLS striosomal compartments (1x DMS vs 1x DLS, p =

		0.00000000036; 2x DMS vs 2x DLS, p = 0.000000000019). In contrast, DLS striosomal cFos expression did not significantly differ from SAL conditions across any IBU dose (all p > 0.88). Together, these findings demonstrate that intermediate levels of GHSR activation selectively recruit DMS striosomal compartments while sparing DLS striosomes, indicating region-specific recruitment of striosomal circuitry following GHSR activation.
Fig S14E Striosomal pPDH expression across DMS and DLS compartments following IBU administration	**Main effects:** To determine whether different levels of GHSR activation differentially modulate activity states across DMS and DLS striosomal compartments, pPDH expression was quantified within DMS and DLS striosomes following administration of SAL (rats=7), 0.5x IBU (rats=6), 1x IBU (rats=6), 2x IBU (rats=6), and 10x IBU (rats=5). Group comparisons were analyzed using a two-way ANOVA followed by Tukey's multiple comparisons test. Analysis revealed a significant interaction between IBU dose and striatal region ($F(4,49)=9.096$, $p=0.000014$), a significant main effect of IBU dose ($F(4,49)=4.947$, $p=0.00198$), and a significant main effect of striatal region ($F(1,49)=10.33$, $p=0.00231$), indicating that GHSR activation differentially modulates pPDH expression across DMS and DLS striosomal compartments.	**Post hoc comparisons:** Tukey's multiple comparisons test revealed that increases in pPDH expression were selectively restricted to DLS striosomes at intermediate IBU doses. Relative to SAL DLS striosomes, both 1x and 2x IBU significantly increased DLS striosomal pPDH expression (SAL vs 1x DLS, p=0.0079; SAL vs 2x DLS, p=0.0003), whereas no differences were observed within DMS striosomes across treatment conditions (all p>0.17). Within both the 1x and 2x IBU conditions, DLS striosomes displayed significantly greater pPDH expression relative to corresponding DMS striosomal compartments (1x DMS vs 1x DLS, p=0.0267; 2x DMS vs 2x DLS, p<0.0001). In contrast, no DMS versus DLS differences were observed under SAL, 0.5x, or 10x conditions (all p > 0.43). Together, these findings demonstrate that intermediate levels of GHSR activation selectively increase pPDH expression within DLS striosomes while simultaneously increasing cFos recruitment within DMS striosomes, supporting a functional DMS–DLS striosomal seesaw following intermediate GHSR activation.
Fig S14F Correlation between DMS striosomal cFos	**Linear regression analysis:** To determine whether increased activity within DMS striosomes was associated with reduced activity within DLS striosomes across different levels of GHSR activation, correlation analyses were performed comparing DMS striosomal cFos expression with DLS striosomal pPDH expression across all IBU treatment conditions. Linear regression analysis	**Correlation analysis:** Pearson correlation analysis further demonstrated a significant positive correlation between DMS striosomal cFos expression and DLS striosomal pPDH expression ($r = 0.6315$, $p=0.0002$; 95% CI: 0.3447 to 0.8104; $n = 29$). Together, these findings indicate that

expression and DLS striosomal pPDH expression across IBU doses	revealed a significant positive relationship between DMS striosomal cFos expression and DLS striosomal pPDH expression ($F(1,27)=17.91$, $p=0.0002$), with an R^2 value of 0.3988. The resulting regression equation was $Y=0.2032X + 14.09$, with a slope significantly different from zero (95% CI: 0.1047 to 0.3018).	increased recruitment of DMS striosomal activity is associated with increased pPDH expression within DLS striosomes, supporting a functional relationship between DMS striosomal activation and reduced DLS striosomal activity across different levels of GHSR activation.
Fig S14G DMS–DLS activation/inactivity balance across IBU doses	**Main effects:** To determine whether different levels of GHSR activation shift the functional balance between DMS and DLS striosomal activity states, a normalized activation–inactivity index was calculated for each animal by pairing cFos and pPDH values from the same striatal region and applying the formula: (cFos−pPDH)/(cFos+pPDH)(cFos−pPDH)/(cFos+pPDH). Positive values indicate relative activation bias, whereas negative values indicate relative inactivity bias. Separate balance indices were calculated for DMS and DLS striosomes across SAL, 0.5x IBU, 1x IBU, 2x IBU, and 10x IBU conditions (rats = 5–7 per group). Data were analyzed using a two-way ANOVA followed by Tukey's multiple comparisons test. Analysis revealed a significant interaction between IBU dose and striatal region ($F(4,49) = 3.786$, $p = 0.00924$), as well as a significant main effect of striatal region ($F(1,49) = 106.5$, $p < 1 \times 10^{-11}$). In contrast, the main effect of IBU dose did not reach significance ($F(4,49) = 1.701$, $p = 0.165$). Together, these findings indicate that GHSR activation differentially shifts the balance between activation and inactivity across DMS and DLS striosomal compartments.	**Post hoc comparisons:** Tukey's multiple comparisons test revealed that intermediate IBU doses produced the strongest divergence between DMS and DLS activity states. Within the 1x IBU condition, DMS balance values were significantly greater than DLS values ($p = 0.00000065$), indicating increased DMS activation bias relative to DLS. Similarly, within the 2x IBU condition, DMS values remained significantly greater than DLS values ($p = 0.0000026$). Relative to saline DMS values, the 2x DMS condition also showed a significant shift toward activation bias ($p = 0.0142$), whereas DLS values remained comparatively negative across intermediate doses. Additional comparisons further demonstrated that both 1x and 2x DMS balance values differed significantly from multiple DLS conditions (all $p < 0.003$), indicating strong separation between DMS and DLS functional states specifically at intermediate levels of GHSR activation. In contrast, the 10x IBU condition displayed reduced separation between DMS and DLS balance states relative to intermediate doses, consistent with partial loss of the DMS-selective activation state observed at high levels of GHSR activation. Together, these findings support a functional DMS–DLS striosomal seesaw in which intermediate GHSR activation shifts DMS striosomes toward an activated state while simultaneously biasing DLS striosomes toward relative inactivity.

Fig S14H (left) cFos expression across IBU dose, striatal region, and striatal compartment	**Main effects:** To determine whether different levels of GHSR activation differentially recruit striatal subregions and compartments, cFos expression was quantified across IBU dose, striatal region, and striatal compartment. Groups included SAL (rats = 7), 0.5x IBU (rats = 7–8), 1x IBU (rats = 6), 2x IBU (rats = 7–8), and 10x IBU (rats = 8), with cFos quantified in DMS and DLS striosome and matrix compartments. Data were analyzed using a three-way ANOVA followed by Tukey's multiple comparisons test. Analysis revealed significant main effects of IBU dose ($F(4,124) = 38.66$, $p < 1 \times 10^{-15}$), striatal region ($F(1,124) = 198.5$, $p < 1 \times 10^{-15}$), and compartment ($F(1,124) = 107.7$, $p < 1 \times 10^{-15}$). Significant two-way interactions were also observed between IBU dose and striatal region ($F(4,124) = 19.13$, $p = 2.83 \times 10^{-12}$), IBU dose and compartment ($F(4,124) = 24.68$, $p = 5.0 \times 10^{-15}$), and striatal region and compartment ($F(1,124) = 61.34$, $p = 1.84 \times 10^{-12}$). Finally, analysis revealed a significant three-way interaction between IBU dose, striatal region, and compartment ($F(4,124) = 14.68$, $p = 7.59 \times 10^{-10}$), indicating that IBU-induced cFos recruitment depends on both striatal subregion and compartment.	**Post hoc comparisons:** Tukey's multiple comparisons test revealed that intermediate IBU doses selectively increased cFos expression within DMS striosomes. Relative to SAL DMS striosomes, cFos expression was significantly increased following 1x IBU ($p = 1.80 \times 10^{-13}$) and 2x IBU ($p = 9.0 \times 10^{-15}$), but not following 0.5x or 10x IBU (all $p > 0.99$). Within-dose comparisons further showed that DMS striosomes were significantly elevated relative to DMS matrix, DLS striosomes, and DLS matrix at both 1x and 2x IBU doses (all $p < 1 \times 10^{-13}$). In contrast, DLS striosomes did not significantly differ from DLS matrix at any dose, and matrix compartments did not show significant dose-dependent increases relative to saline controls. Together, these findings demonstrate that intermediate levels of GHSR activation selectively recruit DMS striosomes while sparing DLS striosomes and surrounding matrix compartments, supporting compartment- and region-specific engagement of striosomal circuitry following GHSR activation.
Fig S14H (right) pPDH expression across IBU dose, striatal region, and striatal compartment	**Main effects:** To determine whether GHSR activation produced region- and compartment-specific patterns of neuronal inactivity, pPDH expression was quantified across IBU dose, striatal region, and striatal compartment. Groups included SAL (rats = 6–7), 0.5x IBU (rats = 5–6), 1x IBU (rats = 6), 2x IBU (rats = 6), and 10x IBU (rats = 5–6), with pPDH quantified in DMS and DLS striosome and matrix compartments. Data were analyzed using a three-way ANOVA followed by Tukey's multiple comparisons test. Analysis revealed significant main effects of IBU dose ($F(4,99) = 5.551$, $p = 0.00045$), striatal region ($F(1,99) = 10.84$, $p = 0.00138$), and compartment ($F(1,99) = 115.8$, $p < 1 \times 10^{-15}$). Significant two-way interactions were also observed between IBU dose and striatal region ($F(4,99) = 8.651$, $p = 4.97 \times 10^{-6}$), IBU dose and compartment ($F(4,99) = 4.264$, $p = 0.00317$), and striatal region and compartment ($F(1,99) = 9.683$, $p = 0.00243$). Importantly, analysis revealed a significant three-way interaction between IBU dose, striatal region, and compartment ($F(4,99) = 9.639$, $p = 1.26 \times 10^{-6}$),	**Post hoc comparisons:** Tukey's multiple comparisons test revealed that intermediate IBU doses selectively increased pPDH expression within DLS striosomes. Relative to saline DLS striosomes, pPDH expression was significantly elevated following 1x IBU ($p = 3.61 \times 10^{-5}$) and 2x IBU ($p = 4.41 \times 10^{-8}$), while 0.5x and 10x IBU did not significantly differ from saline conditions (all $p > 0.97$). Within-dose comparisons further demonstrated that DLS striosomes exhibited significantly greater pPDH expression relative to DMS striosomes, DMS matrix, and DLS matrix at both 1x and 2x IBU doses (all $p < 5 \times 10^{-4}$). In contrast, matrix compartments did not show significant dose-dependent increases relative to saline controls, and DMS striosomes remained largely unchanged across IBU doses. Together, these findings demonstrate that

	indicating that GHSR-mediated inactivity differed depending on both striatal subregion and compartment.	intermediate levels of GHSR activation selectively increase inactivity within DLS striosomes while not affecting surrounding matrix compartments, supporting a functional DMS/DLS striosomal balance in which activation of DMS striosomes is accompanied by reduced activity within DLS striosomes.

2977
2978

13.4 Table S4: Anatomical Region names and coordinates

Abbreviations	Full Name	Bregma Coordinate
PL	Prelimbic	+3.24
IL	Infralimbic	
OFC	Orbitofrontal	
A24b (Cg1)	Cingulate 1	+1.8
A24a (Cg2)	Cingulate 2	
A33 (Cg3)	Cingulate 3	
DMS	Dorsomedial striatum	
DLS	Dorsolateral striatum	
vDMS	Ventral dorsomedial striatum	
vDLS	Ventral dorsolateral striatum	
AcbC	Nucleus Accumbens	
M1	Motor 1	
M2	Motor 2	
INS	Insular	
Cl	Claustrum	
S1FL	Sensory	
Pir	Piriform	
En	Endoform	
VDB	Diagonal band of Broca, vertical limb	
LSD	Lateral Septal, dorsal	+1.4
LSV	Lateral Septal, ventral	
Gpe	Globus pallidus external	-1.56
Gpi	Globus pallidus internal	

STN	Subthalamic nucleus	-3.60
AD	Anterodorsal thalamic nucleus	-1.56
PT	Paratenial thalamic nucleus	
MD	Mediodorsal thalamic nucleus	
rPVT	rostral Paraventricular thalamic nucleus	
cPVT	caudal Paraventricular thalamic nucleus	-3.24
IMD	Intermediodorsal thalamic nucleus	
CM	Central medial thalamic nucleus	
PC	Paracentral thalamic nucleus	
CL	Central lateral thalamic nucleus	
RH	Rhomboid	
BLA	Basolateral Amygdala	-3.0
CeA	Central Amygdala	
MeA	Medial Amygdala	
LHb	Lateral Habenula	-3.70
MHb	Medial Habenula	
PVN	Paraventricular hypothalamic nucleus	-1.56
DMD	Dorsal medial hypothalamic nucleus	-3.0
VMH	Ventromedial hypothalamic nucleus	
ARC	Arcuate hypothalamic nucleus	
SNr	Substantia nigra pars reticulata	-5.16
daSNc	Substantia nigra pars compacta	
VTA	Ventral Tegmental Area	
Surgical Targeting		
Experiment	Brain region	Surgical Coordinates

GCaMP *in vivo* calcium imaging	DMS	Injection site: AP +1.5 mm, ML ±2.0 mm, DV −3.6 mm Implantation site: AP +1.5 mm, ML ±2.0 mm, DV -3.5mm
DREADD Virus injections		Excitatory (hM3Dq) or Inhibitory (hM4Di): AP +1.28 mm, ML ±1.8 mm, DV −3.7 mm
Rabies Assisted Monosynaptic tracing		
Helper virus injection sites for TRIO strategy	LHb	AP −3.4 mm, ML ±0.8 mm, DV −5.0 mm
	Gpi	AP −2.2 mm, ML ±2.8 mm, DV −7.8
RVΔG injections for TRIO strategy	Gpi	AP −2.2 mm, ML ±2.8 mm, DV −7.8
Helper virus injection for SNc tracing	SNc	AP −5.4 mm, ML ±2.2 mm, and DV −7.9 mm.
RVΔG injections for SNc tracing	SNc	AP −5.4 mm, ML ±2.2 mm, and DV −7.9 mm
Tissue Section Retrieval: Monosynaptic tracing		Bregma Coordinates
	DMS	+2.5 to +0.5 mm
	LHb	-3.4 mm
	Gpi	-2.2 mm

2980

2981

13.5 Table S5: Model Interpretations of selected experimental studies (Related to Note S1)

Paper	Key Finding	Model Interpretation
Pietrzak et al. (2024)[10]	Ghrelin ↓ punishment sensitivity; ↑ prediction error	Reduced weighting of cost dimension; Prediction error reflects space shift
Ralevski et al. (2018)[13]	Higher ghrelin → ↑ reward sensitivity & impulsivity	Ghrelin-induced hyperactivity → ↑ impulsivity & reward focus
Anderberg et al. (2016)[14]	Ghrelin ↑ impulsivity	Reduced dimensionality (via Ghrelin) → ↑ impulsivity
Schéle et al. (2020)[11]	Ghrelin alters social dominance based on baseline tendency	Amplifies focus on individually dominant dimension(s)

13.6 Table S6: Model prediction of disorders coinciding with ghrelin changes (Related to Note S3)

Disorder	Directional Effect	Model Prediction
Stress	↑	Narrowed focus on primary stressor/information
Addiction	↑	Narrowed focus on substance/abuse-related cues

13.7 Table S7: DOIs

Experiment Description	DOI	Notes
Fig. 1B-D.	Food alone https://doi.org/10.7910/DVN/DCB1IH Toy alone https://doi.org/10.7910/DVN/YMYXO0 Light alone https://doi.org/10.7910/DVN/JW2C3Q Food+light https://doi.org/10.7910/DVN/0V6WKG Toy+light https://doi.org/10.7910/DVN/ZUH9YY	Raw Data
Fig. 1E-G.	https://doi.org/10.7910/DVN/GFLZYM https://doi.org/10.7910/DVN/KJAMMP	Raw Data and Analysis
Fig. 1H. 10x behavior	https://doi.org/10.7910/DVN/OE73LI	Raw Data and Analysis
Fig.2A-C. DMS cFos expression across IBU concentrations	https://doi.org/10.7910/DVN/KRAGMO	Raw Data
	https://doi.org/10.7910/DVN/NEVZXF	ImageJ Analysis
Fig. 2D-F. GHSR expression in Striatum (striosomes, matrix)	https://doi.org/10.7910/DVN/UHTDDW	Raw Data
	https://doi.org/10.7910/DVN/SNSRF4	ImageJ Analysis
Fig. 2G-H. BGHR expression in striatum (striosomes, matrix)	https://doi.org/10.7910/DVN/KRAGMO	Raw Data
	https://doi.org/10.7910/DVN/SNSRF4	ImageJ Analysis
Fig. 2J-K. LHb cFos expression across IBU concentrations	https://doi.org/10.7910/DVN/D5BCOY	Raw Data
	https://doi.org/10.7910/DVN/JWSLB	ImageJ Analysis
Fig. 2L-M. daSNC expression of pPDH, TH, and cFOS across IBU concentrations	https://doi.org/10.7910/DVN/AVMV9E	Raw Data
	https://doi.org/10.7910/DVN/JWSLB	ImageJ Analysis
Fig. 3A-B.	https://doi.org/10.7910/DVN/C9VBK7	Raw Data
	https://doi.org/10.7910/DVN/QLVA4X	ImageJ Analysis

hM4Di+ virus expression in striosomes and matrix		
Fig. 3C-E. In-vivo calcium dynamics following 2x and 10X IBU	https://doi.org/10.7910/DVN/US8QTS	Raw Data
Fig. 4C. IHC of Oprm1-cre striosomal manipulation with DREADD	https://doi.org/10.7910/DVN/C9VBK7	Raw Data
	https://doi.org/10.7910/DVN/QLVA4X	ImageJ Analysis
Fig. 4D-E Non-conflict and conflict Oprm1 2x	https://doi.org/10.7910/DVN/TNT3FV https://doi.org/10.7910/DVN/KJAMMP	Raw Data and Analysis
Fig. 4F. cFos expression in LHb after striosomal manipulation with DREADD	https://doi.org/10.7910/DVN/CT9ATL	Raw Data
	https://doi.org/10.7910/DVN/QLVA4X	ImageJ Analysis
Fig. 4G. cFos expression in daSNC after striosomal manipulation with DREADD	https://doi.org/10.7910/DVN/N7FGMH	Raw Data
	https://doi.org/10.7910/DVN/QLVA4X	ImageJ Analysis
Fig. 5 Modeling	https://github.com/dirkbeck/ghrelin_project	Raw Data
Fig. S1A Baseline of simple tasks Oprm1 WT	https://doi.org/10.7910/DVN/OE73LI	Raw Data
Fig. S1 B Food alone 2x	https://doi.org/10.7910/DVN/DCB1IH, left https://doi.org/10.7910/DVN/NTB2PG, right	Raw Data
Fig. S1 C Toy alone 2x	https://doi.org/10.7910/DVN/YMYXO0, eft https://doi.org/10.7910/DVN/NTB2PG, right	Raw Data
Fig. S1 D Light alone 2x	https://doi.org/10.7910/DVN/JW2C3Q, left https://doi.org/10.7910/DVN/NTB2PG, right	Raw Data
Fig. S1 E Food+light 2x	https://doi.org/10.7910/DVN/0V6WKG, left https://doi.org/10.7910/DVN/NTB2PG, right	Raw Data

Fig. S1 F Toy+light 2x	https://doi.org/10.7910/DVN/ZUH9YY, left https://doi.org/10.7910/DVN/NTB2PG, right	Raw Data
Fig.S1 G Long Evans and Oprm1-WT performance across all tasks	Food alone https://doi.org/10.7910/DVN/DCB1IH Toy alone https://doi.org/10.7910/DVN/YMYXO0 Light alone https://doi.org/10.7910/DVN/JW2C3Q Food+light https://doi.org/10.7910/DVN/0V6WKG Toy+light https://doi.org/10.7910/DVN/ZUH9YY Analysis https://doi.org/10.7910/DVN/KJAMMP	Raw data and Analysis
Fig. S2A, E	https://doi.org/10.7910/DVN/TNT3FV	Excel tables with the x/y coordinate data
	https://doi.org/10.7910/DVN/TNT3FV, https://github.com/atanugiri/GhrelinBehaviorQuantification.git	Code generated
Fig. S2 B-D, F-G	https://doi.org/10.7910/DVN/OE73LI https://doi.org/10.7910/DVN/KJAMMP	Raw Data and Analysis
Fig. S2 H-J	https://doi.org/10.7910/DVN/GFLZYM https://doi.org/10.7910/DVN/KJAMMP	Raw Data and Analysis
Fig. S3 A-D. cFOS IHC in 50 brain regions after 1x IBU	https://doi.org/10.7910/DVN/DTXBD5 https://doi.org/10.7910/DVN/EI60AH https://doi.org/10.7910/DVN/PYW4WW	Raw Data/ analysis
Fig. S3E-Q. IHC analysis in striatum for cFos and MOR after 1xIBU	https://doi.org/10.7910/DVN/EI60AH	ImageJ analysis
Fig. S3R IHC across 50 brain regions following IBU	https://doi.org/10.7910/DVN/DTXBD5 https://doi.org/10.7910/DVN/EI60AH https://doi.org/10.7910/DVN/PYW4WW	Raw data
Fig. S3S-T. DMS striatum for cFos analysis after 0.5x and 10xIBU	https://doi.org/10.7910/DVN/KRAGMO	Raw Data
Fig. S3U-V. IHC of DMS striatum for GHSR expression	https://doi.org/10.7910/DVN/UHTDDW	Raw data

Fig. S3W. IHC of BGHR in striatum	https://doi.org/10.7910/DVN/KRAGMO	Raw data
Fig. S4A. IHC of LHb for cFos after IBU	https://doi.org/10.7910/DVN/D5BCOY	Raw data
Fig. S4B-C. IHC of daSNc for pPDH, TH, and cFos analysis after IBU	https://doi.org/10.7910/DVN/AVMV9E	Raw data
	https://doi.org/10.7910/DVN/JWSLB	ImageJ analysis
Fig. S4D. Correlations- (DMS striosomes cFos and LHb cFos) and (DMS striosomes cFos and daSNC pPDH)		
DMS striosomes cFos IHC	https://doi.org/10.7910/DVN/KRAGMO	Raw data
	https://doi.org/10.7910/DVN/NEVZXF	ImageJ analysis
LHb cFos IHC	https://doi.org/10.7910/DVN/D5BCOY	Raw data
	https://doi.org/10.7910/DVN/JWSLB	ImageJ analysis
daSNc pPDH IHC	https://doi.org/10.7910/DVN/AVMV9E	Raw data
	https://doi.org/10.7910/DVN/JWSLB	ImageJ analysis
Fig. S4E. Correlation between LHb fos and daSNc pPDH		
LHb cFos IHC	https://doi.org/10.7910/DVN/D5BCOY	Raw data
	https://doi.org/10.7910/DVN/JWSLB	ImageJ analysis
daSNc pPDH IHC	https://doi.org/10.7910/DVN/AVMV9E	Raw data
	https://doi.org/10.7910/DVN/JWSLB	ImageJ analysis
Fig. S4F. Correlation between DMS striosomes cFos and daSNc cFos		
DMS striosomes cFos IHC	https://doi.org/10.7910/DVN/KRAGMO	Raw data
	https://doi.org/10.7910/DVN/NEVZXF	ImageJ analysis
daSNc cFos IHC	https://doi.org/10.7910/DVN/AVMV9E	Raw data
	https://doi.org/10.7910/DVN/JWSLB	ImageJ analysis
Fig. S4G. IHC of Arcuate nucleus for cFos analysis after IBU	https://doi.org/10.7910/DVN/WANMCY	Raw data
	https://doi.org/10.7910/DVN/JWSLB	ImageJ analysis
Fig. S4H. Correlation between DMS striosomes cFos and ARC cFos		

DMS striosomes cFos IHC	https://doi.org/10.7910/DVN/KRAGMO	Raw data
	https://doi.org/10.7910/DVN/NEVZXF	ImageJ analysis
ARC cFos IHC	https://doi.org/10.7910/DVN/WANMCY	Raw data
	https://doi.org/10.7910/DVN/JWSLB	ImageJ analysis
Fig. S5A. In-vivo calcium imaging and feeding behavior following IBU and aGHR.	https://doi.org/10.7910/DVN/US8QTS	Raw data and analysis
Fig. S5B. IPS cell map following 2xIBU injection	https://doi.org/10.7910/DVN/US8QTS	Analysis
Fig. S5C. In-vivo calcium imaging following high doses of IBU acyl-ghrelin	https://doi.org/10.7910/DVN/US8QTS	Raw data
Fig. S5D. 2x IBU calcium dynamics time curve	https://doi.org/10.7910/DVN/US8QTS	Analysis
Fig. S5E, left *In-vivo calcium imaging time curve following 2x and 10xIBU*	https://doi.org/10.7910/DVN/US8QTS	Analysis
Fig. S5E, right *In-vivo calcium*	https://doi.org/10.7910/DVN/US8QTS	Analysis

imaging time curve following 4.3 and 86ug/kg acyl-ghrelin:		
Fig. S5F. Food consumption following acyl-ghrelin	https://doi.org/10.7910/DVN/US8QTS	Raw data and analysis
Fig. S5G. Food consumption following IBU and acyl-ghrelin in moderate and high doses	https://doi.org/10.7910/DVN/US8QTS	Anlaysis
Fig. S6 A-D. IHC of striosomes with DREADD manipulation in cre-OPRM1	https://doi.org/10.7910/DVN/C9VBK7	Raw data
Fig. S6 E-I. pPDH IHC of striosomes with DREADD manipulation in cre-OPRM1	https://doi.org/10.7910/DVN/QLVA4X	Analysis
Fig. S7B. Non-conflict tasks	*Food alone task 2X IBU CRE-OPRM1*: https://doi.org/10.7910/DVN/NTB2PG *Toy alone task 2X IBU CRE-OPRM1*: https://doi.org/10.7910/DVN/NTB2PG *Light alone task 2X IBU CRE-OPRM1*: https://doi.org/10.7910/DVN/NTB2PG Raw Data Analysis: https://doi.org/10.7910/DVN/KJAMMP	Raw data and analysis
Fig. S7C. Conflict tasks	*Food+light task 2X IBU CRE-OPRM1*: https://doi.org/10.7910/DVN/NTB2PG *Toy+light task 2X IBU CRE-OPRM1*: https://doi.org/10.7910/DVN/NTB2PG	Raw data and analysis

	Raw Data Analysis: https://doi.org/10.7910/DVN/KJAMMP	
Fig. S8B. IHC of Lateral habenula with DREADD manipulation in cre-OPRM1	https://doi.org/10.7910/DVN/CT9ATL	Raw data
Fig. S8C. IHC of daSNC with DREADD manipulation in cre-OPRM1:	https://doi.org/10.7910/DVN/N7FGMH	Raw data
Fig. S8D-G. ANOVA post-hoc values following DREADD manipulation in cre-OPRM1	https://doi.org/10.7910/DVN/QLVA4X	ImageJ analysis
Fig. S9. Monosynaptic tracing of striosomes	https://doi.org/10.7910/DVN/ZRLRXV	Raw Data and analysis
Fig. S10	https://github.com/dirkbeck/ghrelin_project	
Fig.S11 Motor analysis data and scripts	https://doi.org/10.5281/zenodo.17280633	Functions
	https://github.com/atanugiri/GhrelinBehaviorQuantification.git	Living functions
	https://doi.org/10.7910/DVN/G8CBKJ.	data
Fig. S12 Motor analysis	https://github.com/dirkbeck/ghrelin_project	Raw data and analysis
Fig.S13 Motor analysis data and scripts	https://doi.org/10.5281/zenodo.17280633	Functions
	https://github.com/atanugiri/GhrelinBehaviorQuantification.git	Living functions
	https://doi.org/10.7910/DVN/G8CBKJ.	data
Fig. S14 A. IHC of BGHR in DLS striosome	https://doi.org/10.7910/DVN/KRAGMO	Raw data
	https://doi.org/10.7910/DVN/SNSRF4	Analysis
Fig. S14C. IHC of DMS	https://doi.org/10.7910/DVN/KRAGMO	Raw Data

and DLS striatum for cFos, MOR, and pPDH analysis after IBU		
Fig. S14D. *IHC of DMS and DLS striosomes for cFos analysis after IBU*	https://doi.org/10.7910/DVN/KRAGMO	Raw Data
	https://doi.org/10.7910/DVN/NEVZXF	Analysis
Fig. S14E. IHC of DMS and DLS striosomes for pPDH analysis after IBU	https://doi.org/10.7910/DVN/KRAGMO	Raw Data
	https://doi.org/10.7910/DVN/NEVZXF	Analysis
Fig. S14F. Correlation between striosomes DMS cFos and DLS pPDH		
DMS striosomes cFos IHC	https://doi.org/10.7910/DVN/KRAGMO	Raw data
	https://doi.org/10.7910/DVN/NEVZXF	Analysis
DLS striosomes pPDH IHC:	https://doi.org/10.7910/DVN/KRAGMO	Raw data
	https://doi.org/10.7910/DVN/NEVZXF	Analysis
Fig. S14G. Excitation-inhibition balance in DMS and DLS	https://doi.org/10.7910/DVN/NEVZXF	Analysis
Fig. S14H Left *Striosomal cFos expression in DMS and DLS*	https://doi.org/10.7910/DVN/NEVZXF	Analysis
Fig. S14H Right *Striosomal pPDH expression in DMS and DLS*	https://doi.org/10.7910/DVN/NEVZXF	Analysis
Fig. S15 I-J Modeling	https://github.com/dirkbeck/ghrelin_project	

Summary table of behavioral data depositions and processing pipelines	
Raw behavioral videos recorded from rodent decision-making tasks	https://doi.org/10.7910/DVN/SBH3UG
Behavioral videos obtained by splitting each raw recording into four quadrant-specific videos	https://doi.org/10.7910/DVN/F0P2BC
DeepLabCut generated raw pose-estimation data	https://doi.org/10.7910/DVN/CUWGHY
DeepLabCut generated filtered pose-estimation data (input data for motor analysis) (Fig. S12, Fig. S14)	https://doi.org/10.7910/DVN/G8CBKJ
Setting up trial metadata table: dlc_table.csv	https://github.com/atanugiri/DLCDatabaseSetup/tree/main
Data analysis pipeline for processing DeepLabCut pose-estimation data and performing motor-behavior analysis	https://github.com/atanugiri/GhrelinBehaviorQuantification https://doi.org/10.5281/zenodo.17280633
Split videos function	https://github.com/atanugiri/DLCDatabaseSetup/tree/main/scripts
Data deposition for processed behavioral features derived from DeepLabCut pose-estimation outputs	https://doi.org/10.7910/DVN/YNGH9C
Data analysis pipeline for processing behavioral task battery data	https://github.com/atanugiri/Behavioral-task-battery-data-analysis
Processed behavioral datasets prepared for ANOVA statistical analysis	https://doi.org/10.7910/DVN/YNGH9C
RECORD (Ibáñez Alcalá et al., 2024) repository	https://GitHub.com/rjibanezalcala/RECORD
Movement analysis	https://github.com/dirkbeck/ghrelin_project
Decision-space modeling	https://github.com/dirkbeck/ghrelin_project

14 REFERENCES

1. Bossert, J. M. *et al.* Effect of Selective Lesions of Nucleus Accumbens μ-Opioid Receptor-Expressing Cells on Heroin Self-Administration in Male and Female Rats: A Study with Novel *Oprm1-Cre* Knock-in Rats. *J. Neurosci.* **43**, 1692–1713 (2023).
2. Ibáñez Alcalá, R. J. *et al.* RECORD, a high-throughput, customizable system that unveils behavioral strategies leveraged by rodents during foraging-like decision-making. *Commun Biol* **7**, 822 (2024).
3. Morigaki, R. *et al.* Spatiotemporal Up-Regulation of Mu Opioid Receptor 1 in Striatum of Mouse Model of Huntington's Disease Differentially Affecting Caudal and Striosomal Regions. *Front. Neuroanat.* **14**, 608060 (2020).
4. Schwarz, L. A. *et al.* Viral-genetic tracing of the input-output organization of a central noradrenaline circuit. *Nature* **524**, 88–92 (2015).
5. Lavin, T. K., Jin, L. & Wickersham, I. R. Monosynaptic tracing: a step-by-step protocol. *J Chem Neuroanat* **102**, 101661 (2019).
6. Lavin, T. K., Jin, L., Lea, N. E. & Wickersham, I. R. Monosynaptic Tracing Success Depends Critically on Helper Virus Concentrations. *Front Synaptic Neurosci* **12**, 6 (2020).
7. Takahashi, Y. K. *et al.* Dopamine Neurons Respond to Errors in the Prediction of Sensory Features of Expected Rewards. *Neuron* **95**, 1395-1405.e3 (2017).
8. Beck, D. W. *et al.* A decision-space model explains context-specific decision-making. *Nature Communications* **16**, 7437 (2025).
9. Mathis, A. *et al.* DeepLabCut: markerless pose estimation of user-defined body parts with deep learning. *Nat Neurosci* **21**, 1281–1289 (2018).

10. Pietrzak, M. *et al.* Ghrelin decreases sensitivity to negative feedback and increases prediction-error related caudate activity in humans, a randomized controlled trial. *Neuropsychopharmacol.* **49**, 1042–1049 (2024).
11. Schéle, E., Pfabigan, D. M., Simrén, J., Sailer, U. & Dickson, S. L. Ghrelin Induces Place Preference for Social Interaction in the Larger Peer of a Male Rat Pair. *Neuroscience* **447**, 148–154 (2020).
12. Beck, D. & Friedman, A. Striosome-dopamine circuit signals information gain, not prediction error. Preprint at https://doi.org/10.21203/rs.3.rs-7011645/v1 (2025).
13. Ralevski, E. *et al.* Ghrelin is Related to Personality Differences in Reward Sensitivity and Impulsivity. *Alcohol and Alcoholism* **53**, 52–56 (2018).
14. Anderberg, R. H. *et al.* The Stomach-Derived Hormone Ghrelin Increases Impulsive Behavior. *Neuropsychopharmacol* **41**, 1199–1209 (2016).